LONDON'S GLOBAL UNIVERSITY

Neuroimaging of functional and structural alterations in Juvenile Myoclonic Epilepsy and Frontal Lobe Epilepsy

Christian Vollmar

UCL Institute of Neurology

Department of Clinical and Experimental Epilepsy

Queen Square,

London WC1N 3BG

Thesis submitted to University College London

for the degree of Doctor of Philosophy

2015

Declaration

I, Christian Vollmar, confirm that the work presented in this thesis is my own.

Where information has been derived from other sources, I confirm that this has been indicated in the thesis.

This thesis was created during a joint project, carried out by University College London and King's College London. The work presented in this thesis was carried out in cooperation of a team of researchers from both centres. Both centres participated in recruiting patients and most subjects were examined twice, once at each centre. My individual contribution for the scientific studies included in this thesis is outlined below.

I recruited 89% of the patients and 62% of the healthy controls. I acquired the neuroimaging data, comprising conventional structural MRI, five cognitive functional paradigms and diffusion tensor imaging data. I performed complementary neuropsychological testing, including the memory recall test from the fMRI paradigm, the Iowa gambling task and the trail making task. I was responsible for transfer, conversion, processing and archiving of the imaging data. I performed all data analyses described in the thesis, including development and optimisation of parts of the analysis methodology. I have created scripts for batch processing of data and for functional connectivity analyses and I created new templates for spatial normalisation and for data visualisation of functional imaging data. I performed all statistical analyses and produced all the figures and graphical presentation of the data shown in this thesis. All results and interpretations were presented by myself and were developed based on discussions with colleagues and at regular supervision meetings.

Jonathan O'Muircheartaigh recruited the remaining subjects and performed complementary analyses of functional and structural connectivity in JME, focussing on thalamo-cortical connections and investigated morphometric aspects of T1-weighted images in JME. He also carried out neuropsychological assessment of the healthy controls. Serge Vulliemoz performed an intermediate analysis of DTI data from a subgroup of patients. Maria Centeno analysed the memory fMRI and T1 morphometry of FLE patients and has investigated operated FLE patients postoperatively. Clinical neuropsychological assessment of patients was performed by Pamela Thompson. Britta Wandschneider analysed the behavioural data from the Iowa gambling task of JME patients. Clarissa Yasuda analysed the effect of medication on fMRI activation patterns.

12th September 2014,

Abstract

Epilepsy is the commonest neurological disorder and has profound effects on patients, who suffer from epileptic seizures and also from cognitive impairment. The exact mechanisms of cognitive impairment remain unclear. Aim of this study was to analyse in more detail the functional and structural alterations in two different patient groups, juvenile myoclonic epilepsy (JME) and frontal lobe epilepsy (FLE).

We recruited and investigated 26 healthy controls, 30 patients with JME and 67 patients with FLE. All participants underwent magnetic resonance imaging (MRI), including structural imaging, five functional MRI paradigms and diffusion tensor imaging (DTI) as well as neuropsychological assessment.

In patients with JME we could show motor cortex hyperactivity and an increased functional connectivity between the pre-frontal cognitive cortex and the motor system. This correlated with increased structural connectivity, measured by DTI and also with disease severity: patients with more active epilepsy showed a stronger hyperconnectivity.

In FLE, we could show extensive reorganization of cognitive functions, and we could show, that functional MRI can be used as a new diagnostic method, to identify dysfunctional areas, indicative of the seizure onset zone. This is particularly important in patients with nonlesional FLE, where epilepsy surgery may be advisable but is challenged by the absence of a visible surgical target.

The study has provided new insights into pathophysiological mechanisms in JME, specifically explaining the characteristic effect of motor seizures triggered by cognitive effort. It has contributed strong evidence that the observed imaging alterations are the cause and not a consequence of JME, by documenting marked structural changes in seizure free patients.

For patients with FLE the study showed highly individual effects of chronic epilepsy on cognitive processing in the frontal lobe. These alterations are clinically relevant for both, avoiding complications from surgery, but also to identify pathological alterations not visible in conventional MRI.

Table of contents

List of figures

List of tables

List of Abbreviations

ADC	Apparent diffusion coefficient
BOLD	Blood oxygen level dependent
CNS	Central nervous system
CV	Coefficient of variation
DTI	Diffusion tensor imaging
EEG	Electroencephalography
FA	Fractional anisotropy
FC	Functional connectivity
FLAIR	Fluid attenuated inversion recovery
FLE	Frontal lobe epilepsy
fMRI	Functional magnetic resonance imaging
FMRIB	Oxford Centre for Functional Magnetic Resonance Imaging of the Brain
FSL	FMRIB's software library
FWHM	Full width at half maximum
ICA	Independent component analysis
ICC	Intra-class correlation coefficient
IGE	Idiopathic generalised epilepsy
ISI	Inter-stimulus interval
JME	Juvenile myoclonic epilepsy
MD	Mean diffusivity
MRI	Magnetic resonance imaging
PET	Positron emission tomography
ROI	Region(s) of interest
SD	Standard deviation
SMA	Supplementary motor area
SPECT	Single photon emission tomography
SPM	Statistical parametric mapping (software package)
TMS	Transcranial magnetic stimulation

List of Publications

Original articles

- **Vollmar, C**., O'Muircheartaigh, J., Barker, G.J., Symms, M.R., Thompson, P., Kumari, V., Duncan, J.S., Richardson, M.P., Koepp, M.J., 2010. Identical, but not the same: intra-site and inter-site reproducibility of fractional anisotropy measures on two 3.0T scanners. *Neuroimage* 51, 1384–94. doi:10.1016/j.neuroimage.2010.03.046
- **Vollmar, C.**, O'Muircheartaigh, J., Barker, G.J., Symms, M.R., Thompson, P., Kumari, V., Duncan, J.S., Janz, D., Richardson, M.P., Koepp, M.J., 2011. Motor system hyperconnectivity in juvenile myoclonic epilepsy: a cognitive functional magnetic resonance imaging study. *Brain* 134, 1710–9. doi:10.1093/brain/awr098
- **Vollmar, C.**, O'Muircheartaigh, J., Symms, M.R., Barker, G.J., Thompson, P., Kumari, V., Stretton, J., Duncan, J.S., Richardson, M.P., Koepp, M.J., 2012. Altered microstructural connectivity in juvenile myoclonic epilepsy: the missing link. *Neurology* 78, 1555–9. doi:10.1212/WNL.0b013e3182563b44
- Centeno, M.*, **Vollmar, C.***, O'Muircheartaigh, J., Stretton, J., Bonelli, S.B., Symms, M.R., Barker, G.J., Kumari, V., Thompson, P.J., Duncan, J.S., Richardson, M.P., Koepp, M.J., 2012. Memory in frontal lobe epilepsy: an fMRI study. *Epilepsia* 53, 1756–64. doi:10.1111/j.1528-1167.2012.03570.x, *joint first authorship

Original articles as co-author

- Bonelli, S.B., Thompson, P.J., Yogarajah, M., **Vollmar, C.**, Powell, R.H.W., Symms, M.R., McEvoy, A.W., Micallef, C., Koepp, M.J., Duncan, J.S., 2012. Imaging language networks before and after anterior temporal lobe resection: results of a longitudinal fMRI study. *Epilepsia* 53, 639–50. doi:10.1111/j.1528-1167.2012.03433.x
- Centeno, M., **Vollmar, C.**, Stretton, J., Symms, M.R., Thompson, P.J., Richardson, M.P., O'Muircheartaigh, J., Duncan, J.S., Koepp, M.J., 2014.

Structural changes in the temporal lobe and piriform cortex in frontal lobe epilepsy. *Epilepsy Res*. 108, 978–81. doi:10.1016/j.eplepsyres.2014.03.001

- Centeno, M., Koepp, M.J., **Vollmar, C**., Stretton, J., Sidhu, M., Michallef, C., Symms, M.R., Thompson, P.J., Duncan, J.S., 2014. Language dominance assessment in a bilingual population: Validity of fMRI in the second language. *Epilepsia*. In press. doi:10.1111/epi.12757
- Chaudhary, U.J., Centeno, M., Carmichael, D.W., **Vollmar, C.**, Rodionov, R., Bonelli, S., Stretton, J., Pressler, R., Eriksson, S.H., Sisodiya, S., Friston, K., Duncan, J.S., Lemieux, L., Koepp, M., 2013. Imaging the interaction: Epileptic discharges, working memory, and behavior. *Hum. Brain Mapp*. 34, 2910–7. doi:10.1002/hbm.22115
- Feldmann, M., Asselin, M.-C., Liu, J., Wang, S., McMahon, A., Anton-Rodriguez, J., Walker, M., Symms, M., Brown, G., Hinz, R., Matthews, J., Bauer, M., Langer, O., Thom, M., Jones, T., **Vollmar, C.**, Duncan, J.S., Sisodiya, S.M., Koepp, M.J., 2013. P-glycoprotein expression and function in patients with temporal lobe epilepsy: a case-control study. *Lancet Neurol*. 12, 777–85. doi:10.1016/S1474-4422(13)70109-1
- Kovac, S., Scott, C., Rugg-Gunn, F., Miserocchi, A., **Vollmar, C.**, Rodionov, R., McEvoy, A., Diehl, B., 2010. Unusual cortical stimulation findings: connectivity between primary motor and supplementary motor areas. *Epilepsy Behav*. 19, 639–42. doi:10.1016/j.yebeh.2010.09.006
- Laufs, H., Richardson, M.P., Salek-Haddadi, A., **Vollmar, C.**, Duncan, J.S., Gale, K., Lemieux, L., Löscher, W., Koepp, M.J., 2011. Converging PET and fMRI evidence for a common area involved in human focal epilepsies. *Neurology* 77, 904–10. doi:10.1212/WNL.0b013e31822c90f2
- O'Muircheartaigh, J., **Vollmar, C.**, Barker, G.J., Kumari, V., Symms, M.R., Thompson, P., Duncan, J.S., Koepp, M.J., Richardson, M.P., 2011. Focal structural changes and cognitive dysfunction in juvenile myoclonic epilepsy. *Neurology* 76, 34–40. doi:10.1212/WNL.0b013e318203e93d
- O'Muircheartaigh, J., **Vollmar, C.**, Traynor, C., Barker, G.J., Kumari, V., Symms, M.R., Thompson, P., Duncan, J.S., Koepp, M.J., Richardson, M.P., 2011. Clustering probabilistic tractograms using independent component analysis applied to the thalamus. *Neuroimage* 54, 2020–32. doi:10.1016/j.neuroimage.2010.09.054

- O'Muircheartaigh, J., **Vollmar, C.**, Barker, G.J., Kumari, V., Symms, M.R., Thompson, P., Duncan, J.S., Koepp, M.J., Richardson, M.P., 2012. Abnormal thalamo-cortical structural and functional connectivity in juvenile myoclonic epilepsy. *Brain* 135, 3635–44. doi:10.1093/brain/aws296
- Sidhu, M.K., Stretton, J., Winston, G.P., Bonelli, S., Centeno, M., **Vollmar, C.**, Symms, M., Thompson, P.J., Koepp, M.J., Duncan, J.S., 2013. A functional magnetic resonance imaging study mapping the episodic memory-encoding network in temporal lobe epilepsy. *Brain* 136, 1868–88. doi:10.1093/brain/awt099
- Stretton, J., Winston, G., Sidhu, M., Centeno, M., **Vollmar, C.**, Bonelli, S., Symms, M., Koepp, M., Duncan, J.S., Thompson, P.J., 2012. Neural correlates of working memory in Temporal Lobe Epilepsy--an fMRI study. *Neuroimage* 60, 1696–703. doi:10.1016/j.neuroimage.2012.01.126
- Stretton, J., Winston, G.P., Sidhu, M., Bonelli, S., Centeno, M., **Vollmar, C.**, Cleary, R.A., Williams, E., Symms, M.R., Koepp, M.J., Thompson, P.J., Duncan, J.S., 2013. Disrupted segregation of working memory networks in temporal lobe epilepsy. *NeuroImage Clin*. 2, 273–81. doi:10.1016/j.nicl.2013.01.009
- Thornton, R., Vulliemoz, S., Rodionov, R., Carmichael, D.W., Chaudhary, U.J., Diehl, B., Laufs, H., **Vollmar, C.**, McEvoy, A.W., Walker, M.C., Bartolomei, F., Guye, M., Chauvel, P., Duncan, J.S., Lemieux, L., 2011. Epileptic networks in focal cortical dysplasia revealed using electroencephalography-functional magnetic resonance imaging. *Ann. Neurol*. 70, 822–37. doi:10.1002/ana.22535
- Vulliemoz, S., **Vollmar, C.**, Koepp, M.J., Yogarajah, M., O'Muircheartaigh, J., Carmichael, D.W., Stretton, J., Richardson, M.P., Symms, M.R., Duncan, J.S., 2011. Connectivity of the supplementary motor area in juvenile myoclonic epilepsy and frontal lobe epilepsy. *Epilepsia* 52, 507–14. doi:10.1111/j.1528-1167.2010.02770.x
- Wandschneider, B., Centeno, M., **Vollmar, C.**, Stretton, J., O'Muircheartaigh, J., Thompson, P.J., Kumari, V., Symms, M., Barker, G.J., Duncan, J.S., Richardson, M.P., Koepp, M.J., 2013. Risk-taking behavior in juvenile myoclonic epilepsy. *Epilepsia* 54, 2158–65. doi:10.1111/epi.12413
- Wandschneider, B., Centeno, M., **Vollmar, C.**, Symms, M., Thompson, P.J., Duncan, J.S., Koepp, M.J., 2014. Motor co-activation in siblings of patients with

juvenile myoclonic epilepsy: an imaging endophenotype? *Brain* 1–11. doi:10.1093/brain/awu175

- Yasuda, C.L., Centeno, M., **Vollmar, C.**, Stretton, J., Symms, M., Cendes, F., Mehta, M.A., Thompson, P., Duncan, J.S., Koepp, M.J., 2013. The effect of topiramate on cognitive fMRI. *Epilepsy Res*. 105, 250–5. doi:10.1016/j.eplepsyres.2012.12.007

Reviews

- Woermann, F.G., **Vollmar, C.**, 2009. Clinical MRI in children and adults with focal epilepsy: a critical review. *Epilepsy Behav*. 15, 40–9. doi:10.1016/j.yebeh.2009.02.032
- Wandschneider, B., Thompson, P.J., **Vollmar, C.**, Koepp, M.J., 2012. Frontal lobe function and structure in juvenile myoclonic epilepsy: a comprehensive review of neuropsychological and imaging data. *Epilepsia* 53, 2091–8. doi:10.1111/epi.12003

Book chapters

- **Vollmar, C**., Winkler, P., & Noachtar, S. (2008). Multimodal image processing in presurgical planning.. In H. O. Lueders (Ed.), Epilepsy surgery. (pp. 771-778.). London, UK: Informa Healthcare.
- **Vollmar, C**., & Diehl, B. (2011). Diffusion tensor tractography in extratemporal lobe epilepsy.. In M. Z. Koubeissi, & R. J. Maciunas (Eds.), Extratemporal lobe epilepsy surgery. (Vol. 10, pp. 195-202). Esther, Surrey, UK: John Libbey Eurotext.

Acknowledgements

Research is always a team effort, and my years of research and this thesis would not have been possible without the continuous support from a number of people to whom I am grateful for making it such a rewarding experience.

Great thanks go to my principal supervisor Matthias Koepp, who was always available, late night and last minute, for discussion, brainstorming, guidance and encouragement. It was inspiring to see the creative sparks in his ideas and comforting to know his kindness and patience.

I would like to thank my co-supervisor, Mark Symms, who was always of great help tackling the mysteries of MRI physics, image processing or life in Britain, providing expertise and humour, and calmness in times of looming deadlines.

John Duncan was a continuous source of additional direction, stimulating discussion, encouragement - and ample patient referrals throughout the project.

Pam Thompson performed all clinical neuropsychological assessments and was always of great help, explaining the details of her assessments and interpreting our findings.

I am grateful to the consultants, Ley Sander, Sanjay Sisodiya, and Matthew Walker, for referring patients and their interest in the results of this project.

Our cooperation with the team from King's College has been a pleasure and I want to thank Jonathan O'Muircheartaigh, Mark Richardson, Gareth Barker and Veena Kumari for their thoughts, ideas, questions and suggestions throughout the project.

It was a great pleasure to work with the radiographers at the epilepsy society MRI unit, Philippa Bartlett, Jane Burdett, and Elaine Williams, who maintained a great working atmosphere in the MRI unit and were always helpful with the planning of scans, handling of patients and all challenges of daily research life. Peter Gilford was of continuous help in keeping up IT resources, and finding new storage space for our data.

I would like to thank my research fellow colleagues at Chalfont, for the many hours of stimulating discussions on neuroimaging and research, but also on the rest of life. I am grateful for the opportunity to share with them experiences, challenges, worries, ideas and, most importantly, friendship.

I am extremely grateful to all the patients and controls who volunteered to give up their time and spend two tightly packed days of investigations in order to participate in these studies. Without their generous and enthusiastic contribution, this work would not have been possible.

Various funding sources deserve thanks for enabling this project, particularly the Wellcome Trust.

Final thanks go to Claudia for her continuous support and cheerful optimism and to our families for their support, encouragement and understanding of my physical or mental absence for long periods.

1. Introduction

1.1 Epilepsy

1.1.1 Epidemiology and Definition

Epilepsy is the most common serious neurological disease, distributed worldwide and affecting all ages and races. The incidence is about 50 cases per 100,000 persons per year in developed societies and 100-190 per 100,000 in developing countries (Sander and Shorvon, 1996) (MacDonald et al., 2000). The prevalence is estimated at 5-10 cases per 1000 persons, excluding single seizures, febrile seizures and patients in remission. The lifetime prevalence of a single seizure is 2 to 5% (Sander, 2007). In the UK, annually, 30,000 people develop epilepsy, with about 450,000 currently estimated to be affected individuals. Epilepsy can have substantial physical, psychological and social impact on patients and carries serious risks of injury, impairment of brain function and death.

An epileptic seizure is a transient event caused by an occasional, sudden and excessive discharge of cerebral neurons (Jackson, 1873). Epilepsy is present when seizures are recurrent and not caused by transient metabolic or toxic disorders. A recurrent tendency to have seizures arises secondary to a variety of underlying brain disorders. A causative pathology can be identified in a proportion of cases, but in some patients no cause is found and only a descriptive diagnosis is possible (Dodson, 2004).

Over the years, the wide range of motor, sensory, autonomic, cognitive and psychic phenomena that are produced during epileptic seizures have been described and classified.

1.1.2 Seizure classification

There are many reasons why the classification of seizures and epilepsy is important, both for the individual patient and for the advancement of knowledge of epilepsy. It allows communication within and between the clinical and research settings. It is also important for the diagnosis, prognosis and choice of treatment for any given patient. Accurately identifying the type of seizures is the first step towards a correct diagnosis in a patient with epileptic seizures.

Classically, two major seizure types have been recognised: those arising from focal cortical disturbances – partial or focal seizures, and those characterised by synchronous discharge of both hemispheres - generalised seizures. Differentiation between focal and generalised seizures requires both clinical and electroencephalography (EEG) findings. This formed the basis for the revised International Classification of Epileptic Seizures (ICES), introduced by the International League Against Epilepsy (ILAE) in 1981 (Panayiotopoulos, 2007). This classification divides seizures into partial and generalised, with partial seizures subsequently divided further into 'simple' and 'complex', depending on whether consciousness is retained or lost.

In most surveys, partial seizures appear to be the most common seizure type, with complex partial and secondarily generalised seizures comprising around 60% of prevalent cases, primary generalised tonic-clonic seizures about 30%, and generalised absence and myoclonus less than 5% (Sander, 2007). These however may be biased,

being largely based on populations of patients with relatively severe epilepsy, including large numbers with focal epilepsy. For less severe cases it is often more difficult to determine clinically and electroencephalographically whether it is of primary generalised or focal type.

1.1.3 Syndromic diagnosis of epilepsy

The description of the seizure types is insufficient to provide accurate guidance on treatment, severity of disease and prognosis. An advance in modern epileptology has been the recognition of epileptic syndromes, which are defined by the combination of seizure types, other clinical symptoms, physical signs on examination, imaging findings and laboratory findings. Each epilepsy syndrome has diverse underlying causes and prognoses, and requires different short-term and long-term management.

The fact that epilepsy is not a single disease entity has already been recognised several decades ago. For example, the World Health Organization (WHO) Dictionary of Epilepsy (Gastaut, 1973) proposes the following definition of epilepsy:

'chronic brain disorder of various aetiologies characterised by recurrent seizures due to excessive discharge of cerebral neurones (epileptic seizures), associated with a variety of clinical and laboratory manifestations. Single or occasional epileptic seizures (such as febrile convulsions and the seizures of puerperal eclampsia) as well as those occurring during an acute illness should not be classified as epilepsy.'

The Commission on Classification and Terminology of the ILAE describes epilepsy as requiring *'.... two or more seizures.'*

There still is diagnostic inaccuracy of the term ‘epilepsy’, which needs to be completed with the definition of seizure types, epilepsy syndromic diagnosis and underlying aetiology.

The identification of an epilepsy syndrome requires specific clinical information, including age of onset, seizure manifestations, precipitating factors, associated central nervous system (CNS) symptoms and signs, severity, and course. Findings from other investigations such as EEG and brain imaging are also needed.

The 1989 ILAE Classification of the epilepsies and epileptic syndromes (1989) attempted to provide such a syndromic classification and recognises the heterogeneity of epilepsy. It specified over 40 distinct types of syndromes, classified both according to seizure type and aetiology. However, this is problematic, due to overlap between syndromes, inadequate definitions of syndromes and the complexity of the classification. A Task Force for the classification and terminology concluded that the classification would need to be reviewed periodically based upon emerging new information.

This has subsequently been reviewed, given problems identified through use and progress in the understanding of the basis of the epilepsies. The ILAE Task Force also proposed that the terms partial and localisation-related be replaced with ‘focal’ (Engel, 2001).

1.1.4 Aetiology

In the 1989 ILAE classification, both focal and generalised epilepsies and syndromes are divided according to aetiology into idiopathic, symptomatic and cryptogenic varieties. Idiopathic epilepsies are not associated with structural brain lesions, neurological abnormalities other than seizures, or cognitive impairment. Conversely, in

symptomatic epilepsy, seizures are the consequence of a focal brain abnormality. Cryptogenic epilepsies are those in which a symptomatic aetiology is suspected but the aetiology is not known. The advances in neuroimaging over the past decade have allowed identification of an increasing number of underlying aetiologies and thus decreased the proportion of epilepsies and epilepsy syndromes considered to be cryptogenic. The 2001 Task Force proposed that the term cryptogenic be replaced by 'probable symptomatic epilepsy syndrome' to refer to syndromes believed to be symptomatic, but in which no aetiology has been identified (Engel, 2001). Epilepsy may develop for a number of reasons with brain trauma, CNS infections, cerebrovascular disease and brain tumours all increasing the incidence of epilepsy. The aetiology varies considerably according to age. Onset of epilepsy during adult life is more commonly associated with an underlying neurological disorder than is the case with epilepsies developing in childhood. The aetiologies underlying focal epilepsy also vary according to geography, for example endemic infections such as neurocysticercosis are the commonest cause of epilepsy in parts of South America but are much less common in Europe.

Any condition causing cortical disruption may lead to seizures. The aetiology may be multifactorial, with patients with an inherited predisposition more prone to the development of acquired conditions. A prospective cohort population-based study of patients with newly-diagnosed epilepsy in the United Kingdom reported that the aetiology was cerebrovascular disease in 15%, cerebral tumour in 6%, alcohol-related in 6% and post-traumatic in 3% of patients (Sander et al., 1990). Notably, seizures were classified as cryptogenic in 62% of cases.

Although the majority of epilepsies lack an overt genetic cause, underlying genetic contributions to aetiology have been estimated to be present in about 40% of patients

with epilepsy (Robinson et al., 2009), and are particularly important in the idiopathic generalised epilepsies (IGE). There are over 200 Mendelian diseases which include epilepsy as part of the phenotype although these account for less than 1% of all epilepsies (Robinson et al., 2009). Many of these, such as tuberous sclerosis, are associated with structural lesions although several families exhibiting idiopathic epilepsy transmitted in a Mendelian manner have recently been found to have mutations in single genes. They are all dominantly inherited and all but one code for ion channels, underlying the importance of these signalling proteins in determining the excitability of neuronal circuits (Kullmann, 2002).The theory of a genetically determined increased excitability of neuronal circuits provides an attractive explanation why otherwise normal individuals should develop unprovoked seizures without an identifiable locus of onset.

Although this pattern of Mendelian inheritance is rare, first degree relatives of patients with IGE have a roughly two- to threefold elevated risk of being affected (Ottman et al., 1996). Where these patterns of complex inheritance exist, the interaction of susceptibility genes and environmental factors is likely to be important. At present, a number of large families with many affected members are currently under investigation and it is likely that further genes will be identified, some of which will be responsible for monogenic epilepsy and others that turn out to be epilepsy susceptibility genes.

1.2 Description of Epilepsy Syndromes

1.2.1 Juvenile myoclonic epilepsy

1.2.1.1 Introduction

Juvenile myoclonic epilepsy (JME) is the most frequent generalised epilepsy syndrome in adolescents, with an estimated incidence of 1 per 100000, accounting for 5-10% of all epilepsies (Janz, 1985) (Jallon and Latour, 2005). Its predominant clinical feature is myoclonic jerks of the proximal upper extremities, mainly occurring in the morning hours. Most patients have occasional generalised tonic-clonic seizures and about one third has additional absences (Genton et al., 2013).

Patients typically seek medical attention for the first time after their first generalised tonic-clonic seizure, often triggered by sleep deprivation, stress or alcohol consumption. In most cases this first generalised seizure was preceded by several myoclonic jerks, which were not recognized as seizures. Most patients report myoclonic jerks only when this is specifically, sometimes repeatedly, asked. Often myoclonic jerks are not considered as relevant or mistaken for clumsiness, but already preceded generalised seizures by months or years.

The correct diagnosis of JME is often initially missed, with a mean delay of 8 years from first symptoms to correct diagnosis (Panayiotopoulos et al., 1991).

Age of onset is typically between 12 and 18 years, although late onset up to the fourth decade of life has been described (Delgado-Escueta and Enrile-Bacsal, 1984). There is a

subgroup of JME patients, evolving from previous childhood absence epilepsy (18% in (Martínez-Juárez et al., 2006), which may lead to confusion regarding the age of onset.

1.2.1.2 Current diagnostic criteria

In 2011, an international workshop of clinical experts in JME reached a consensus on diagnostic criteria for JME (Kasteleijn-Nolst Trenité et al., 2013b). Class I diagnostic criteria are:

- Myoclonic jerks without loss of consciousness repeatedly occurring on awakening, i.e., within 2 h after awakening;
- EEG (routine, sleep, or sleep deprivation EEG) that shows normal background activity and ictal generalised high amplitude polyspikes (or polyspike and wave) with concomitant myoclonic jerks;
- Normal intelligence;
- Age at onset of between 10 and 25 years.

The diagnostic criteria have been broadened in the past few years, which is also reflected by the more generous class II criteria from this consensus, where, for example, spikes must have been recorded at least once in EEG, and the age of onset may be as early as 6 years of age.

There is also an increased awareness that focal features in seizure semiology or EEG may be present in JME, but also that incidental lesions in brain MRI do not preclude the diagnosis of JME and do not influence the generally good prognosis (Gelisse et al., 2000).

1.2.1.3 Personality traits in JME

In his initial description of the syndrome JME, called "impulsive petit mal" at that time, Janz also included a detailed description of characteristic personality traits in patients with JME (Janz and Christian, 1957). Janz described: *"... their mental behaviour is very often characterized by unsteadiness, lack of discipline, hedonism and indifference towards their disease... They promise more than they can deliver... Their behaviour often has effects on their therapy. They will declare that they adhere to all prescriptions, but in fact they forget to attend control visits and to take their medication regularly... Their mood changes rapidly and frequently... They are easy to encourage and to discourage; they are gullible and unreliable..."*.

This description of personality traits in JME still holds true over 50 years later. Many patients impress with their impulsivity, unreliability keeping appointments and repetitive problems with compliance to both medication and lifestyle recommendations. In our study, patients with JME required significantly more contacts and phone calls to arrange, confirm and organise their attendance for investigations than patients with frontal lobe epilepsy.

1.2.1.4 Comorbidities in JME

Headache is one of the most frequent comorbidities in JME, reported by more than 60% of the patients. Compared to the general population, the relative risk is 4.4 for migraine and 3.4 for tension-type headache in JME patients (Schankin et al., 2011).

Psychiatric comorbidities are also common in JME, affecting about one third of JME patients (de Araujo Filho and Yacubian, 2013) (Schneider-von Podewils et al., 2014).

The most frequently described psychiatric disorders were depression, anxiety (Filho et al., 2008) and personality disorder (Trinka et al., 2006).

1.2.1.5 Treatment and Prognosis

The majority of patients respond well to medication. The antiepileptic drugs of choice include, in descending order, sodium valproate, lamotrigine, levetiracetam, topiramate and zonisamide (Crespel et al., 2013).

In two of three patients, all seizures are controlled by medication, and about 80% are free of generalised tonic-clonic seizures under medication, while occasional myoclonic jerks persist. Some patients show pseudo-resistance due to problems with treatment, compliance or lifestyle (Baykan et al., 2013), but only one in six is truly refractory to medication (Gelisse et al., 2001). The presence of all three different seizure types has repeatedly been associated with an unfavourable response to medication (Baykan et al., 2008) (Camfield and Camfield, 2009) (Gelisse et al., 2001).

JME is considered to be a lifelong disease and termination of antiepileptic medication is usually discouraged. The risk of seizure recurrence is high if medication is discontinued. However, there is increasing recent evidence that a small subgroup of JME patients (around 10%) remains seizure free after cessation of anticonvulsive medication, particularly at older age (Martínez-Juárez et al., 2006).

Although seizures are often well controlled, a 25-year follow-up study showed that 74% of patients had at least one unfavourable social outcome, such as divorce or unplanned pregnancy. In spite of educational success, 31% were later unemployed. Social isolation was reported by 30% and 61% had taken mood or behaviour-altering medication during follow-up (Camfield and Camfield, 2009).

1.2.1.6 Neurophysiology in JME

The EEG in patients with JME typically shows normal background activity, with generalised, often irregular, spike or polyspike-wave complexes with frontocentral maximum (Delgado-Escueta and Enrile-Bacsal, 1984). The generalised polyspikes often show an interhemispheric time interval of about 10 ms, indicating unilateral onset and transcallosal propagation (Serafini et al., 2013). These epileptiform discharges occur more frequently in the morning than in the afternoon (Labate et al., 2007). However, focal epileptiform discharges are not uncommon and occur in about one third of patients with JME (Aliberti et al., 1994). Focal spikes can cause uncertainty about the diagnosis and lead to misclassification as focal epilepsy, particularly when focal semiological features, such as asymmetric myoclonic jerks are also reported.

A crucial role of the motor cortex in the generation of myoclonic jerks is supported by a study that used jerk-locked back-averaging of EEG and found a focal cortical generation of myoclonic jerks in JME. Frontocentral polyspikes (but not single spikes) preceded the myoclonic jerks by 10 ms, indicating a cortical generation (Panzica et al., 2001) (Serafini et al., 2013).

Photosensitivity, an abnormal response to photic stimulation, can be shown in EEG recordings in about 30% of JME patients (Kasteleijn-Nolst Trenité et al., 2013a), ranging from 5% to 90% depending on study population, age, medication and details of the photic stimulation protocol (Appleton et al., 2000).

1.2.1.7 Provocative factors in JME

Patients with JME are highly susceptible to certain trigger factors. Some seizure triggers in JME, such as sleep deprivation, stress, alcohol consumption or photostimulation were already described by Janz (Janz, 1985). A prospective study showed that seizures are triggered by external factors in 93% of JME patients (Panayiotopoulos et al., 1994). Other triggers that are not commonly mentioned in other epilepsy syndromes play an additional role in precipitating seizures in JME. Inoue described a group of patients in whom seizures were induced by praxis, which can be defined as the "ideation or execution of complicated movements, including sequential spatial processing, such as playing games, construction, calculation, complicated finger manipulation, drawing and writing" (Inoue et al., 1994) (Yacubian and Wolf, 2014). Other studies have confirmed these findings and reported additional cognitive activities, like reading or decision making to trigger seizures in patients with JME (da Silva Sousa et al., 2005a, 2005b)

These findings are in line with electrophysiological studies that showed a provocative effect of cognitive tasks on EEG discharges. Matsuoka et al found a provocative effect of neuropsychological activation on EEG discharges in 38 out of 480 epilepsy patients: 36 of these patients had generalised epilepsies, with JME being the largest group with 22 patients (Matsuoka et al., 2005).. Guaranha et al reported a similar provocative effect in 38% of their JME patients (Guaranha et al., 2009) and both studies reported that the combination of a cognitive task with a motor response is a stronger provocative factor for EEG discharges in JME than tasks involving pure thinking and no motor response.

1.2.1.8 Cortical excitability in JME

The predominance of myoclonic jerks in JME has led to the motor circuitry hyperexcitability hypothesis, where impaired cortical inhibition of the motor cortex is a key mechanism of ictogenesis. This has been addressed by several transcranial magnetic stimulation (TMS) studies in the past. Using paired-pulse paradigms these studies have documented an impaired cortical inhibition in the motor cortex in JME (Manganotti et al., 2004) (Akgun et al., 2009).

This hyperexcitability was shown to be worse after sleep deprivation (Badawy et al., 2006) (Manganotti et al., 2006) and worse in the morning than in the afternoon in patients with JME (Badawy et al., 2009b), matching their circadian predominance of seizures and spikes occurring mostly in the morning.

Some studies suggested this hyperexcitability is specific to JME (Caramia et al., 1996), but later studies also reported similar effects in other IGE syndromes and even in focal epilepsies (Badawy et al., 2013). Investigating paired-pulse paradigms with different interstimulus intervals (ISI) allows further differentiation of early and late cortical inhibition and provided evidence that impaired inhibition in JME patients is mainly mediated via an impaired early GABA-A receptor mediated inhibition (ISI 1 to 4 ms) (Manganotti et al., 2000). Other syndromes, such as progressive myoclonic epilepsy, show a predominant impairment of the late, GABA-B receptor mediated cortical inhibition at ISI of 50 to 400 ms (Badawy et al., 2010).

Most interestingly, recent TMS studies could show that cortical hyperexcitability does not only exist in epilepsy patients, but also in unaffected siblings of JME patients (Akgun et al., 2009) and in siblings of patients with focal epilepsy (Badawy et al., 2013). This is in line with previous studies on EEG, which reported an increased occurrence of epileptiform discharges in siblings of epilepsy patients (Doose et al., 1977).

These findings in unaffected siblings highlight the complex interaction between hereditary predisposition and developmental and environmental factors, adding up in the multifactorial epileptogenesis in JME and other epilepsy syndromes.

1.2.1.9 Genetic findings in JME

The pathophysiology of JME is multifactorial and includes both Mendelian and complex genetic inheritance factors, even though the currently known genetic alterations can only be shown in a minority of patients (Delgado-Escueta et al., 2013). There are familial forms of JME suggesting autosomal dominant inheritance, and other cases where the known mutations show small effects, most likely contributing to susceptibility along with other unknown genetic and environmental factors.

Currently more than 20 different genetic alterations are associated with JME, affecting, amongst others, proteins of several ion channels, GABA receptors and protofilaments relevant for cell migration(de Nijs et al., 2012) (Delgado-Escueta, 2007). We recently described a new mutation of gephyrin, a postsynaptic scaffolding protein relevant for clustering of GABA receptors in a patient with JME and his unaffected father (Dejanovic et al., 2014) and could show the resulting effect of impaired cortical inhibition with paired-pulse TMS.

The field of genetics in JME is advancing rapidly, and the availability of new analysis methods, including next-generation whole-genome and whole-exome sequencing, will certainly shed more light on different mechanisms in JME in the coming years.

The wide spectrum of genetic alterations associated with JME illustrates the multiple genetic contributions to different aspects of epileptogenesis in JME.

1.2.1.10 Neuroimaging in JME

By definition of the syndrome, conventional clinical neuroimaging is generally normal in patients with JME. However, advanced image analysis techniques have revealed a number of subtle focal alterations in patients with JME, which are discussed in detail in chapter 5.4 (page 190).

Studies using voxel-based morphometry (VBM) have reported subtle structural changes in the frontomesial (Woermann et al., 1999a) and frontobasal (Betting et al., 2006) cortex. Whereas some studies report an increase in frontomesial cortical grey matter (Kim et al., 2007; Woermann et al., 1999a), others reported a reduced frontal grey matter volume (Tae et al., 2006), or found no difference between JME and healthy controls (Roebling et al., 2009).

Another volumetric MRI study in new onset JME reported reduced thalamic volume which correlated with performance in several executive functions (Pulsipher et al., 2009). The same study reported increased frontal CSF volumes in children with JME, but frontal grey and white matter where not reduced.

Diffusion tensor imaging in JME showed reduced FA, indicating reduced white matter integrity in the anterior limb of the internal capsule, which contains the anterior thalamic radiation to the frontal lobes. This reduction was correlated with frequency of generalised tonic-clonic seizures in patients with JME (Deppe et al., 2008).

Magnetic resonance spectroscopy revealed two main findings in JME: the N-acetyl-aspartate (NAA) concentration was reduced in the primary motor cortex, the mesial pre-

frontal cortex and thalamus, indicating neuronal damage. Furthermore, the ratio of excitatory glutamate-glutamine was reduced in the same cortical areas, but increased in insula and the (left) striatum (Lin et al., 2009a). Thalamic NAA reductions had been previously described before in JME (Mory et al., 2003)..

So far, only a few studies have addressed functional imaging in JME. Swartz et al. reported an inability of JME patients to activate the frontal cortex in a positron emission tomography (PET) study with 18-fluorodeoxyglucose during a visual working memory task (Swartz et al., 1996). Roebling et al used a verbal and spatial working memory fMRI experiment and reported no difference between JME and healthy controls (Roebling et al., 2009).

In summary, there is increasing evidence from neuroimaging for a particular involvement of the frontal lobe and thalamo-cortical connections in the pathophysiology of JME (Koepp 2005), but there is no consistent picture about the different structural and functional alterations and their mutual relationship in JME.

1.2.1.11 Neuropsychology in JME

Several studies reported neuropsychological deficits in patients with JME. The initial description of the syndrome already described impaired planning and learning (Janz, 1985). More specific neuropsychological studies in patients with JME showed impairment in mental flexibility, concept formation and abstract reasoning (Devinsky et al., 1997), reduced verbal fluency (Piazzini et al., 2008), impaired attention and

inhibition control (Pascalicchio et al., 2007) and impaired verbal and visual memory (Sonmez et al., 2004).

Some of these functional deficits were suggested to partly correlate with interictal spike activity (Rodin and Ancheta, 1987) and they could also be a secondary effect of seizures or medication. But an impairment of prospective memory (Wandschneider et al., 2010) and a reduced verbal fluency and executive dysfunction (Iqbal et al., 2009) could also be demonstrated in unaffected siblings of JME, suggesting that at least part of the cognitive effects in JME may have a genetic component.

Unsurprisingly, neuropsychological deficits were found to be more pronounced in patients with refractory JME and persisting seizures than in patients with well-controlled seizures (Thomas et al., 2014).

In our JME cohort, we could show impaired learning, resulting in increased risk-taking behaviour in refractory JME patients, but not in those who were seizure free (Wandschneider et al., 2013).

1.2.2 Frontal Lobe Epilepsy

1.2.2.1 Introduction:

Frontal lobe epilepsy (FLE) is defined as focal epilepsy, arising anywhere in the frontal lobe. In the group of focal epilepsies, frontal lobe epilepsy is the second most common type after temporal lobe epilepsy. However, in many national referral centres FLE represents the largest patient group, especially in video-EEG monitoring units for presurgical assessment. This increased incidence of FLE in referral centres reflects the diagnostic and therapeutic difficulty of these cases, compared to more clear-cut epilepsies which are often managed successfully by local hospital and smaller centres.

1.2.2.2 Aetiology of FLE

The reported aetiologies underlying a frontal lobe epilepsy varies between different series. As for all focal epilepsies, almost every type of lesion in the frontal lobe may potentially result in frontal lobe epilepsy. The most common pathologies include vascular malformations, tumours, and malformations of cortical development, posttraumatic defects, stroke and infectious diseases. These aetiologies are largely age-dependent, with a higher fraction of congenital malformations in children, posttraumatic epilepsies in young adults and strokes in older patients. Most of the above mentioned pathologies can reliably be detected by neuroimaging, even though congenital malformations like focal cortical dysplasia can be subtle and are often not diagnosed in the first routine scans. Specialized MRI protocols, focused on the clinically suspected area with a higher resolution can improve the yield (Von Oertzen et al., 2002).

However, approximately one third of patients with frontal lobe epilepsy do not show any abnormality on structural imaging, including contemporary MRI with a dedicated epilepsy protocol at 3T. These cases are particularly challenging, because in the absence of a structural lesion, epilepsy surgery lacks a clear target. Unfortunately, the absence of a visible lesion does not reduce the severity of epilepsy. Many patients with cryptogenic frontal lobe epilepsy suffer from frequent, violent and disabling seizures. Additional neuroimaging techniques like interictal PET and ictal SPECT can be helpful to identify focal abnormalities in about half of these 'non-lesional' patients. Histopathology of specimen from patients non-lesional frontal lobe epilepsy most frequently show subtle forms of malformations of cortical development (Wang et al., 2013), too subtle to be seen in conventional MRI.

1.2.2.3 Seizure Semiology in FLE

The seizure semiology of FLE shows a huge diversity. However some features are more frequent and some are specific for frontal lobe epilepsy.

One common specific effect for all seizure types in FLE is a nocturnal predominance. Many patients with FLE report that most, or even all of their seizures occur at night, waking them from sleep.

As discussed in section 1.4.1.4 (page 59) on the localization concept in focal epilepsies, the seizure semiology is determined by the normal function of the cortex that is activated during the seizure.

Consequently one typical feature of frontal lobe epilepsy is motor activity. Epileptic activation of the primary motor cortex usually results in a clonic movement on the contralateral side of the body. This has a high localizing value and was already

described by Hughlings Jackson in 1873 (Jackson, 1873). The 'Jacksonian march' named after him describes the continuous seizure propagation within the precentral gyrus, resulting in a correlated evolution of clonic motor response, e.g. starting in the face, then reaching the shoulder, arm and finally the leg of the contralateral body side.

Adjacent to the primary motor cortex is the supplementary motor area. Its activation usually results in bilateral tonic motor response. This mostly affects the arms with a tonic extension and elevation, but can also affect the legs and trunk. About half of these seizures are asymmetric and the contralateral arm is affected earlier or more intense or always extended, but the other half of SMA-seizures lack lateralising signs. Assessment of postictal pronator drift can be helpful and identify subtle lateralizing dysfunction. Tonic seizures originating from the SMA are typically short, with a sudden onset, lasting just a few, hardly ever more than 10 seconds and end as abruptly as they began. Consciousness is usually preserved, even when the seizure arises in the dominant hemisphere, indicating that only a small volume of cortex is affected.

The third type of motor seizures, typical of FLE, is classified as 'hypermotor' seizures according to the semiological seizure classification by Lüders (Lüders et al., 1999). This term describes extensive, gross movement of all extremities and the trunk, often in a trashing, violent fashion. They are characterized by a sudden onset, often accompanied by some vocalization and patients frequently hurt themselves during these attacks.

Another ictal phenomenon of high lateralizing value is the version of eyes and head to the contralateral side, which is elicited by epileptic activation of the frontal eye field, typically located on the posterior aspect of the middle frontal gyrus. This can occur during secondary spread of any focal seizure before it generalizes, but it is more frequent and occurs much earlier during the seizure evolution in patients with frontal lobe epilepsy (O'Dwyer et al., 2007).

However, not all ictal signs in FLE are so easy to identify and localize. Seizures can also manifest with a wide variety of behavioural changes like ictal laughing, suddenly getting up and wandering around, as well as states of confusion and inadequate behaviour. The latter is clinically relevant, because such episodes of confusion and altered behaviour can occur as non-convulsive status epilepticus, that requires immediate treatment but is frequently missed if no EEG can be recorded during such an episode.

In general, seizures in FLE present with a wide range of semiology, some of them can appear very bizarre and are frequently misdiagnosed as non-epileptic attacks, delaying a correct diagnosis and adequate treatment.

1.2.2.4 Personality traits in FLE

Some of the higher functions of the frontal lobes involve regulation of behaviour and social interaction and some personality traits of patients with FLE illustrate dysfunction of this domain (Helmstaedter, 2001). Antisocial behaviour has been described in patients with FLE and was shown to be reversible, once seizures were controlled by epilepsy surgery (Trebuchon et al., 2013). Less severe effects of FLE on behaviour may represent as impaired inhibition, lack of emotional detachment, or just an “awkward” appearance in daily life interactions

1.2.2.5 Neuropsychology in FLE

Neuropsychological evaluation of patients with FLE has shown a heterogeneous picture. Motor skills, for example, were shown to be impaired in patients with left-sided FLE and in those with right FLE and an age of onset after 7 years of age. Earlier right-sided

FLE onset did not cause impairment, indicating the functional disturbance occurred early enough, to allow for successful reorganisation and compensation (Upton and Thompson, 1997). And motor function is probably one of the simpler functions of the frontal lobes, so it might not come as a surprise, that neuropsychological finding regarding executive functions were very variable and inconclusive (Risse, 2006).

Probably the only consistent pattern is, that an early disease onset (Riva et al., 2005) and left-sided FLE (McDonald et al., 2005) leads to more severe impairment of executive functions.

1.2.2.6 Neurophysiology in FLE

EEG in FLE often shows focal interictal discharges with a frontal maximum. However, EEG in cases with a mesial seizure onset can prove difficult. They can show bilateral synchronized discharges that may be difficult to separate from generalised discharges and paradoxical lateralization can occur (Tukel and Jasper 1952) (Catarino et al., 2012). In summary, only half of the patients with FLE have all or most of their interictal spikes in the frontal lobe, whereas about 25% show most spikes outside the frontal lobe (mostly over the temporal lobe), and about 15% of the patients do not show any interictal discharges at all (Rémi et al., 2011). The localisation of ictal EEG showed a similar distribution, with only about 60% of FLE patients showing exclusive or predominant frontal seizure patterns.

The absence of interictal spikes or seizure pattern in scalp EEG indicates a very small affected cortical area, where discharges do not recruit a big enough volume of cortex to be detected in scalp EEG. The frequent occurrence of extra-frontal discharges illustrates

the multiple possible propagation pathways, which must be taken into account to avoid wrongly localising EEG interpretation.

1.2.2.7 Treatment of FLE

Also in FLE, the majority of patients responds well to medication, although the seizure free rate is lower than in JME and patients are more likely to still suffer from occasional focal seizures. In approximately one third of patients with FLE, seizures are refractory to medication with frequent recurrent seizures and epilepsy surgery can be a treatment option for these patients (Kwan and Brodie 2000).

1.3 Epilepsy Surgery

1.3.1 Principle

The key principle of epilepsy surgery was nicely summarised in the catch phrase "no brain is better than bad brain" by canadian neurosurgeon Wilder G. Penfield (1891-1976).

Healthy brain tissue does not cause epileptic seizures. So if it does, it is not healthy – any more. It is "bad brain" according to Penfield, causing nothing but trouble and not serving any useful brain function any more. It can therefore be resected safely, leaving the patient better off, than with this "bad brain" in place. This is of course a simplification, but the key message certainly still holds true today.

1.3.2 Cortical reorganization

The good thing about focal epilepsy – in terms of neuronal plasticity – is that it is a chronic, typically slowly progressive disease. It is not a sudden, abrupt insult to the brain like a stroke. Instead it typically starts with single, subclinical electric discharges, later followed by focal seizures in increasing frequency and – often many years later – the first secondary generalized seizure. This slow progression allows for extensive reorganisation of function, paralleling the increasing functional deficit that develops in the vicinity of the seizure onset zone. Of course this ability to reorganize strongly depends on several factors, such as the age of onset, the location and spatial extent of the seizure onset zone, the individual functional reserve capacity and others. But in many cases this reorganization is so complete, that not only the seizure onset zone, but also the surrounding cortical areas do not carry out their initial function any more. And

this is a crucial prerequisite for epilepsy surgery: with no remaining functional cortex close by, the epileptogenic zone can be resected safely.

Of course some functions are more easily reorganized than others. As a rule, all primary cortical functions, particularly the primary motor function, are relative "hard-wired" in their initial location and hardly reorganize to a significant extend. Language is already carried out by a network of frontal and temporal cortical areas, some of which exist bilaterally. This seems to help reorganization by redistribution of functions within a pre-existing functional network, for example by increasing recruitment of homolog contralateral cortical areas. Higher cognitive functions such as executive functions, involve even larger bilateral cortical networks and are seemingly even more flexible to reorganise.

Of course such reorganisation does not always restore or maintain the premorbid functional level. Factors such as widespread pathologies, frequent seizure with secondary generalization, frequent interictal discharges or coexisting structural brain damage can severely limit the capacity and efficiency of reorganization, resulting in cognitive decline, often progressing over the course of the disease.

1.3.3 Presurgical evaluation

Presurgical evaluation it usually recommended for patients with pharmacoresistant focal epilepsy, to assess if resective surgery is a treatment option. In some syndromes epilepsy surgery is clearly superior to medical treatment (Wiebe et al., 2001).

A presurgical assessment almost invariably takes place in form of a prolonged video-EEG monitoring admission, where scalp-EEG is recorded continuously for several days,

while anticonvulsive medication is ceased to provoke seizures. Typically, several seizures are recorded with video and EEG in about a week and allow a thorough evaluation of seizure semiology and both, ictal and interictal EEG. Many centres have the possibility to also acquire ictal SPECT, where the regional brain perfusion during a seizure is measured. Repeat and complementary neuroimaging, such as MRI or PET and neuropsychological assessment are performed at the same time, allowing for a most comprehensive evaluation of the patient. Typically the evaluation is completed by an interdisciplinary team meeting where each individual case is discussed extensively between neurologists, neurophysiologists, neuroradiologists, neurosurgeons, neuropsychologists and nuclear medicine specialists and consensus about the recommended next steps is achieved.

The aims of presurgical investigation are twofold:

1. Identification of the seizure onset zone.

   This includes the confirmation that there is only a single seizure onset zone, and the exact localisation and delineation thereof.

2. Identification of eloquent cortex.

   In case a patient turns out to be a surgical candidate, this is necessary to estimate the risk of functional decline following surgery.

1.3.3.1 Identification of the seizure onset zone

The main principle for identification of the seizure onset zone is, to use as many independent diagnostic modalities as possible and check these for consistency.

If all modalities point to the same single location, epilepsy surgery typically has good chances to render the patient seizure free. The more methods show diffuse or conflicting

results, the more likely there is a diffuse, multifocal pathology, typically not suitable for resective epilepsy surgery.

The individual contribution from different diagnostic modalities and their interpretation is described in more detail below, in chapter 1.4.1 (page 57)

1.3.3.2 Identification of eloquent cortex

Several methods are combined to estimate the proximity of eloquent cortex.

The simplest method is to thoroughly test the patient during his seizures, continuously assessing consciousness and cognitive functions such as memory and language. If a patient always remains fully responsive during his focal seizures and does not show any ictal or postictal cognitive impairment, it is safe to assume, that no eloquent cortex is in close proximity to the seizure onset zone. If, on the other hand, a patient shows severe dysfunction, such as aphasia during or after short focal seizures, a close spatial relationship between the seizure onset zone and eloquent cortex is likely.

fMRI can help to lateralize language dominance, but the gold standard to test for eloquent areas is electrical cortical stimulation. Short electrical stimuli, in the order of a few mA, are applied to cortical areas, while the patient has to perform certain tasks. An impaired naming ability caused by the electrical stimulation would indicate a language relevant area was stimulated. This stimulation can be done intraoperatively during a resection if an awake craniotomy is possible. Alternatively cortical stimulation can be performed extraoperatively via intracranial electrodes if invasive monitoring is performed.

1.3.4 Invasive presurgical evaluation

In some cases, the possibility of epilepsy surgery cannot be fully answered after the first presurgical evaluation with scalp-EEG, particularly for patients with non-lesional, extratemporal focal epilepsy. When the initial evaluation could narrow the possible seizure onset zone to areas, amenable with intracranial electrodes, invasive monitoring can be performed, where subdural or depth electrodes are implanted to further refine results from the first evaluation (Pondal-Sordo et al., 2007). One typical scenario is the implantation of bilateral frontal electrodes, is case of clear frontal lobe epilepsy but with missing lateralisation. Also the invasive investigation of two lobes in one hemisphere is common, if the first evaluation could clearly lateralize seizure onset to one hemisphere but left doubt about a temporal or frontal onset. A suspected seizure onset zone close to eloquent cortex also necessitates invasive evaluation to allow for electrical cortex stimulation to map eloquent cortex.

If candidates are well selected, the majority of patients can be offerd resective surgery after invasive evaluation. There is, however, a subgroup of patients, where invasive evaluation confirms multifocal seizure onset , precluding resective surgery.

That said, there are rare desperate patients with frequent, diabling seizures, where a resection might be offered not as curative approach, but rather as a palliative measure to redice the seizure frequency and intensity.

1.3.5 Surgical Outcome

Generally, epilepsy surgery is effective (Bien et al., 2013). Depending on the syndrome, aetiology and individual presurgical investigation results, 50% to 70% of patients are rendered seizure free by resective surgery (Jette and Wiebe, 2013). In some specific

cases, for example a newly diagnosed temporal lobe epilepsy with consistent findings, the success rate can reach up to 90%. Success is generally lower in extratemporal lobe epilepsy, in non-lesional epilepsy (So and Lee, 2014), and in longer standing chronic epilepsy with frequent generalized seizures (Simasathien et al., 2013).

Longer term follow up studies showed, that there can be seizure relapse after many years, resulting in lower success rate in case of longer follow up (de Tisi et al., 2011). However, for a young adult epilepsy patient, a seizure free interval of some years can be very beneficial and crucial for his biographical development, even if seizures return later.

1.3.6 Surgical Complications

Epilepsy surgery is a safe procedure and the risk for major complications is less than one percent (Hader et al., 2013). However, this risk varies depending on the individual findings, and the patient has to be counselled, taking into account his individual chances for seizure freedom and risk from surgery to allow him an informed choice.

1.4 Diagnostic methods in Epilepsy

1.4.1 Conceptual Considerations

In patients with medically intractable focal epilepsies, in whom epilepsy surgery is being considered, extensive imaging studies may be performed to identify the epileptogenic zone and to determine its boundaries. Each diagnostic modality represents different aspects of the epileptogenic pathophysiology, and the individual results are either confirmatory or complementary.

Some conceptual considerations are important for the interpretation of the different diagnostic techniques (EEG, MRI, PET, SPECT, video-EEG monitoring).

1.4.1.1 Epileptogenic lesion

Structural lesions causing epilepsies are called epileptogenic lesions. The best method to visualize them is high-resolution MRI (Kuzniecky and Knowlton, 2002). Typically the lesion itself, e.g., a tumour, is not the generator of the epileptic activity, but instead the effect it has on adjacent neurons.

It is important to keep in mind that a lesion identified by imaging studies does not necessarily reflect the aetiology of a given epilepsy syndrome. For instance, a patient with juvenile myoclonic epilepsy, a common idiopathic generalised epilepsy syndrome, may have a temporal cavernoma, but this does not represent an epileptogenic lesion, unless it is proven that in addition to the generalised seizures, other seizures arise from the temporal cavernoma. Therefore, results of imaging studies always have to be interpreted in the light of the epilepsy syndrome that a given patient has.

1.4.1.2 Irritative zone

The irritative zone is defined as the area generating interictal epileptiform discharges which are recorded on EEG. This region is usually more extensive than the epileptogenic lesion. Considerable experience with surface EEG has established that patients with mesial temporal lobe epilepsy, for example, also exhibit temporal epileptiform discharges. Localization of the irritative zone may be improved by using source analysis tools to evaluate EEG and MEG data (Stefan et al., 2003) or spike-triggered fMRI to localize a circumscribed BOLD response as a result of the spike activity (Jäger et al., 2002).

1.4.1.3 Seizure onset zone

The seizure onset zone is the cortical area from which the patient's habitual seizures originate. Since the epileptic discharge will spread outside this zone in clinical seizures, it is usually difficult to identify it precisely. Even EEG recordings with invasive electrodes may have difficulties to define the seizure onset zone and delineate it from early propagation to adjacent regions. Ictal SPECT shows a regional hyperperfusion in the region of epileptic seizure activity, and thus is able to provide localizing information. However, rapid seizure spread may influence the results, particularly in extratemporal epilepsies (Noachtar et al., 1998). Therefore, ictal perfusion SPECT will most likely show a combination of the seizure onset zone and propagation of epileptic activity to other regions, depending on the time of tracer injection after seizure onset. The seizure onset zone is almost always included in the irritative zone.

1.4.1.4 Symptomatogenic zone

Epileptic activity will only lead to clinical signs and symptoms if symptomatogenic cortex is involved in the epileptic activity. Extensive invasive EEG evaluations have shown that there are cortical regions in which epileptic activation is not associated with any clinical symptomatology. In such cases only the spread of epileptic activity to symptomatogenic areas will lead to ictal clinical symptoms. For example, a seizure starting in the frontopolar region will lead to contralateral version of the eyes and head when the epileptic activity has spread to the frontal eye field. The initial clinical symptomatology has high localizing value, because it is usually close to the seizure onset zone.

1.4.1.5 Functional deficit zone

The functional deficit zone defines the areas of cortical dysfunction in the interictal state. The underlying cause of the dysfunction can be the effect of an epileptogenic lesion itself or of secondary reactions like oedema. Also a high frequency of seizures or interictal discharges is held responsible for causing functional deficits(Engel, 2002). These deficits can usually be identified by neurological or neuropsychological testing. In some patients the functional deficit zone may show a close topographic relationship to the seizure onset zone or the irritative zone, such as memory deficits in patients with temporal lobe epilepsy. However, due to remote effects of epileptic brain activity the functional deficit zone is typically more extensive than the seizure onset zone (Arnold et al., 1996). This is consistent with the extended areas revealed in neuroimaging which show reduced glucose metabolism in FDG-PET scans and reduced interictal perfusion in SPECT.

1.4.1.6 Epileptogenic zone

The epileptogenic zone is defined as the cortical area, whose complete removal is necessary and sufficient to achieve seizure freedom. However, the epileptogenic zone is basically a theoretical concept that is not directly accessible to diagnostic procedures. Of course, the seizure onset zone is an essential part of the epileptogenic zone, but there is evidence that additional areas have to be resected to ensure seizure freedom. For instance, parts of the irritative zone seem capable of assuming the pacemaker function and of generating seizures after removal of the initial seizure onset zone. To what extent parts of the irritative zone should be resected for good post-surgical outcome is still an open question.

1.4.2 Structural MRI

Structural MRI is the most important imaging modality in epilepsy and frequently identifies structural pathology in the epileptic brain (Wieshmann, 2003) (Koepp and Woermann, 2005). The percentage of patients with lesions identified by MRI is continuously increasing because of improvements in image acquisition and data processing in recent years (Von Oertzen et al., 2002). Thus, whenever a neuroimaging study is reported as 'normal' and the patient's epilepsy syndrome is classified as 'cryptogenic', it is important to consider which MR protocol and techniques were used (Woermann and Vollmar, 2009). It is likely that state-of-the-art neuroimaging using techniques appropriate for a given clinical question may reveal new findings that would be missed by standard MR protocols. One study compared the sensitivity of "standard MRI" examinations rated by general radiologists and neuroradiological experts in

epilepsy with the results of expert reading of epilepsy specific MRI scans. The most striking difference was found for the detection of mesial temporal sclerosis: non-experts reading standard MRI detected mesial temporal sclerosis in only 7% of the 123 patients with refractory focal epilepsies. Re-evaluation of standard MRI by experts improved the yield to 18% and experts reading specific MRI scans revealed mesial temporal sclerosis in 45%. The discrepancy was similar in extratemporal lesions. In total, epilepsy specific MRI read by experts detected lesions in 85% of the patients with prior negative standard MRI (Von Oertzen et al., 2002).

For epilepsy diagnosis, a structural MRI usually includes transverse T1, T2 and FLAIR (fluid attenuated inversion recovery) images with a slice thickness of not more than 5 mm. FLAIR images also known as 'dark fluid' images are T2 images with suppressed signal of the cerebrospinal fluid.

In temporal lobe epilepsy, additional coronal 3 mm T1, T2 and FLAIR images perpendicular to the long axis of the hippocampus are helpful. Planning of these slices is improved with an extended scout-scan providing several sagittal planes, in which the hippocampus can be identified. The use of T1-weighted inversion recovery sequences provides a better contrast between gray and white matter and improves the analysis of the hippocampal formations internal architecture. High-resolution T1 images with slice thickness of 1 mm are only needed for volumetric studies and can be omitted for visual analysis. FLAIR images have a higher sensitivity for sclerosis than T2-weighted images (Jack et al., 1996).

In extratemporal lobe epilepsy, the acquisition of a high-resolution T1-weighted gradient echo sequence with an in-plane resolution and slice thickness of 1 mm is recommended. This allows reconstruction of arbitrary planes in the dataset without

significant loss of image quality and aids the detection of subtle focal cortical dysplasia. Additional Inversion Recovery (IR) sequences with 3 mm slice thickness can further improve the detection of cortical dysplasia or heterotopia, due to the improved gray and white matter contrast. Increasing the resolution of FLAIR images enhances the detection of tumours and posttraumatic scars (Wieshmann et al., 1998).

1.4.3 Functional MRI (fMRI)

Functional MRI (fMRI) allows non-invasive indirect measurement of neuronal activity and imaging of activated cortical areas (Logothetis, 2008). Measurements are based on the fact that neuronal activity is associated with an increased local brain metabolism. This metabolic activity causes a local haemodynamic effect with changes in regional cerebral blood flow (rCBF) and blood volume (rCBV) and changes of the magnetic properties of blood, which can be imaged by fMRI.

1.4.3.1 Principles of fMRI

Most fMRI techniques are based on repetitive measurements where signal changes are caused by the susceptibility difference between oxygenated and deoxygenated blood - the blood oxygenation level-dependent (BOLD) effect.

The energy consumption during neuronal activity is fuelled by the conversion of adenosine triphosphate (ATP) into adenosine diphosphate (ADP). Free ADP molecules have a capillary vasodilatory effect and cause an increase of rCBV and rCBF of up to 30%. The resulting increase in oxygen supply allows the back transformation of ADT into ATD under oxygen consumption. However, this process of increased deoxygenation yields only about 5%, i.e. the main regional effect is dominated by

increasing cerebral blood flow with an increased supply of oxygenated blood. Even though the *absolute* amount of deoxyhemoglobin increases in the capillaries, the oxygen extraction is overcompensated by the much larger increase in rCBF and rCBV, resulting in an effective reduction of the deoxyhemoglobin *concentration* in the blood.

Whilst fully oxygenated oxyhemoglobin has diamagnetic properties, deoxyhemoglobin is paramagnetic, introducing additional magnetic field gradients which result in local differences of the magnetic field. These differences in the local magnetic field result in a shortened effective spin–spin relaxation time T2*. As described above, neuronal activation results in a gross *reduction* of the deoxyhemoglobin concentration, thereby creating a more homogeneous local magnetic field with a prolongation of the T2* time. Using MR sequences with high sensitivity to such T2* variations like FLASH or EPI, a signal increase can be detected in activated brain regions. The signal increase is typically about 2%, the typical time scale for changes in rCBV and rCBF is in the order of seconds.

Given the relatively small signal change, it is necessary to sample data over a long period of time, to gain enough statistical power to localize signal changes reliably. Therefore in a typical fMRI experiment, the brain region of interest is scanned repeatedly with a TR of a few seconds, collecting several hundred data volumes over time.

1.4.3.2 Preprocessing

1.4.3.2.1 Realignment

Head motion during an fMRI experiment will result in slightly different positions of every volume in the acquired time series. Movements of a few mm during an fMRI

experiment are frequent. The first preprocessing step involves realigning the complete imaging time series to the same space to correct for subject movement during scanning (Figure 1.1). This is necessary to ensure each voxel in the time series represents the same anatomical region throughout the experiment, before any conclusions about this voxels signal change are made. This step, however, does not correct for possible changes in signal intensity caused by motion, a problem which will be addressed later.

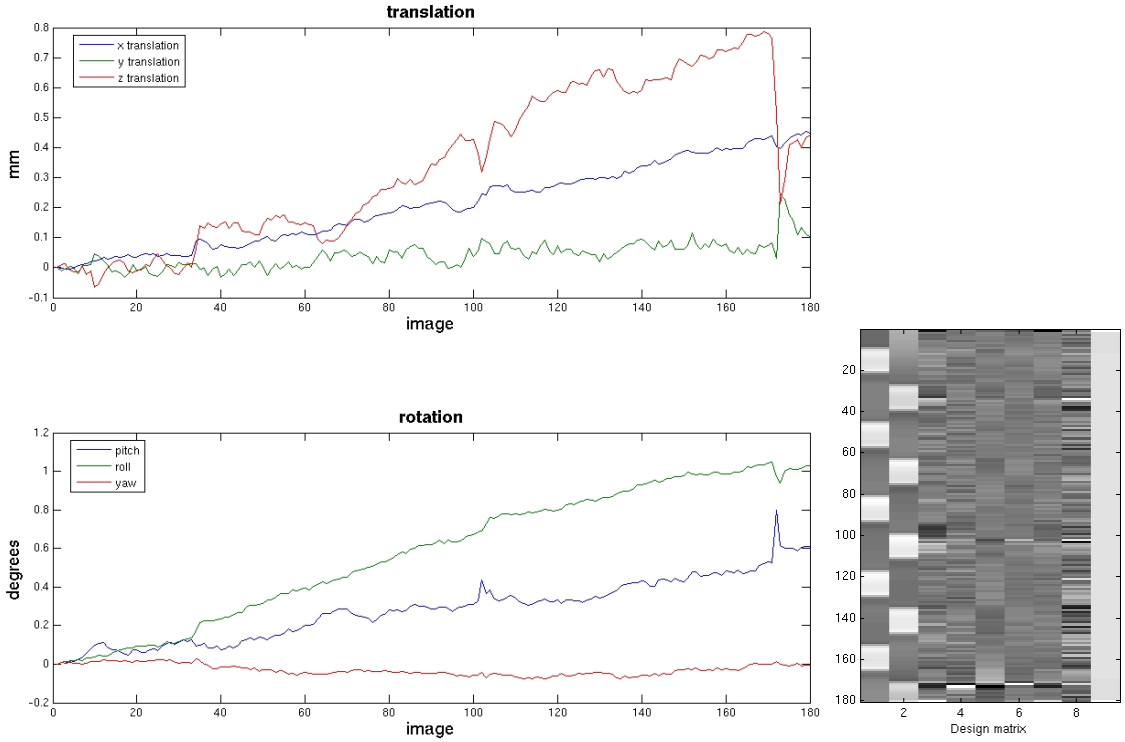

Figure 1.1Realignment of fMRI volumes

The realignment parameters determined by SPM software are plotted against the scan number. Here 180 image volumes were realigned to the first one. The plots show rotation and translation along three orthogonal axes. There is a clear correlation between translation and rotation. The range of corrected movement – about 1 mm translation and 1 degree rotation is typical for an fMRI experiment of several minutes duration.

The SPM design matrix reflects the two task conditions in the first two columns, followed by the realignment parameters from image preprocessing as regressors modelling subject motion

1.4.3.2.2 Normalisation

Once the images are correctly realigned, statistical analysis can be carried out for that individual subject. However, in multisubject studies it is common, to transform each individuals data into a standard anatomical space (Ashburner et al., 2000). This is known as spatial normalization and allows group analyses to be performed and allows reporting of results within standardized coordinate systems. A mean image can be created from the realigned time series, providing better signal to noise ratio than a single volume. This mean image is then normalised to a template image in common space using a combination of linear and non-linear transformations.

The resulting transformation parameters are then applied to the whole time series of images.

1.4.3.2.3 Smoothing

As most fMRI acquisitions contain a significant amount of noise, the data benefits from spatial smoothing before statistical analysis (Friston et al., 2000). Smoothing is achieved by averaging voxels with surrounding voxels in an image. The blurring effect of smoothing reduces the signal from noisy voxels and helps to achieve more consistent regional image intensities with a higher SNR. Typically a Gaussian kernel of known width is applied to each voxel. The width of the Gaussian is described as the width of the kernel, at half of the maximum of its height - the Full Width at Half Maximum (FWHM). As a rule of thumb, a FWHM of twice the voxel size results in appropriate smoothness to carry out statistical analysis. For group analysis across subjects, stronger smoothing with larger FWHM may be necessary to account for differences in individual

subject's anatomy. Smoothing is also necessary to meet the assumptions of Gaussian field theory.

1.4.3.3 Statistical analysis

Complex statistical models are applied to the image data, to identify voxels or clusters of voxels, whose signal intensity changes in accordance with the experimental design.

1.4.3.3.1 The general linear model

The basic assumption behind the general linear model is, that the measured signal Y for a given voxel can be described as a linear combination of several explanatory variables x and an residual error term ε:

$$Y = x_1\beta_1 + \ldots + x_l\beta_l + \ldots + x_n\beta_n + \varepsilon$$

Each explanatory variable contributes differently to the total signal, which is expressed by the unknown scaling factor β for each variable (Friston, 2005).

A completely specified fMRI model consists of a design matrix with one row per observation (i.e. each scan) and one column per model parameter and the residual error column. The individual scaling factor for each variable β is determined by a least square algorithm, iteratively minimizing the residual error.

SPM uses a univariate statistical analysis in which each voxel is tested for experimentally-induced effects independently and simultaneously, using a general linear model. Corrections for multiple comparisons are carried out later.

Firstly it does an analysis of variance separately at each voxel. It then makes t-statistics from the results of this analysis and works out a Z score equivalent for the t-statistic, before making an image of the t-statistics, i.e. a statistical parametric map. Finally, an inference is drawn from this SPM, reliably locating voxels where an effect is present, while guarding against false positives, with the significance value taking the multiple comparisons into account.

SPM uses much of the same underlying mathematics as other statistics packages and commonly used statistical tests such as linear regression, t-tests and analysis of variance are all special cases of the general linear model used by SPM.

The design matrix X is displayed graphically by SPM and consists of a number of columns, each one corresponding to some effect that has been built in to the experiment (Figure 1.1). The relative contribution of each of these columns to the experimental variance (i.e. the parameter estimate for each column) is assessed by using least squares of the residuals. We can test the null hypothesis that there is no relationship between our experimental model and the voxel data by calculating t-statistics for specific linear combinations or 'contrasts' of parameter estimates, by dividing the contrast of parameter estimates by the standard error of that contrast. The standard error can be worked out using the remaining error matrix ε above and is the variance of the residuals about the least squares fit. After calculating the t-statistic, SPM converts the t-statistics to Z scores. The Z scores are the numbers from the unit normal distribution that would give the same p value as the t-statistic.

Before the statistical analysis, fMRI time series are temporally filtered to remove any low-frequency noise due, for example to scanner drift. The regressors are convolved with the haemodynamic response function (HRF) of the BOLD effect in order to

account for the delayed nature of the response. Because the data are typically correlated from one scan to the next the scans cannot be treated as independent observations. The general linear model accounts for these autocorrelations by imposing a temporal smoothing function on the time-series.

1.4.3.3.2 Movement parameters

In the section on fMRI data preprocessing the problem of subject movement during the experiment was discussed. The pure spatial misalignment of volumes is corrected by the Realignment procedure, but subject movement has further impact on the fMRI data.

Firstly, the magnetic field of an MRI scanner contains regional inhomogeneities which result in variation of the image signal intensity. For example the signal can be brighter at the top of the head compared to more inferior portions. The T2* weighted acquisitions for fMRI are particularly susceptible to such effects and they can contribute to up to 10% intensity change within a typical field of view. If a subject moves his head into one of these 'high brightness zones' during an fMRI experiment, the acquired voxels will have a higher value. This is not corrected during the Realignment procedure. It is therefore usually recommended, to include the Realignment parameters from the preprocessing as explanatory variables in the design matrix. Figure 1.1 shows the plot of the Realignment process across the time series of an fMRI experiment and the corresponding design matrix, including the Realignment parameters as covariates. These additional variables now 'explain' for a sudden change in signal intensity at a given time which would otherwise not match the specified statistical model. The plot of the signal in an activated voxel from the same experiment indeed shows a sudden signal increase at the end of the second activation block. In this example there were 'spikes' of movement approximately at the time of scan number 103 and 172.

An additional reason for including the movement parameters as variables is the simple assumption that whatever caused the movement probably also had an impact on the subject's performance at that time. If the subject nodded of and woke up again, felt an itch or had to cough – it all is likely to affect its performance of a cognitive task.

The movement parameters can show a continuous slow rotational movement, reflecting the subject's relaxation of cervical muscles and subsequent anterior rotation of the head during the experiment. This illustrates how movement parameters can indirectly reflect a subjects 'state of mind' and justifies their inclusion in the design matrix.

This removes variance from the time series which would either be attributable to error (hence decreasing sensitivity) or to evoked effects, in the case of stimulus-correlated motion.

1.4.3.3.3 Functional connectivity analysis

Low frequency fluctuations in fMRI signal intensity are highly correlated between functionally connected areas. This was initially described by Biswal et al (Biswal et al., 1995) and has subsequently been applied to numerous studies on functional connectivity in both resting state and task-related fMRI. The principal method for functional connectivity is to extract the time series from one region of interest (ROI) and use this time series as regressor for an fMRI analysis across the whole volume. This allows the identification of areas, whose signal fluctuation is correlated with the signal in the ROI.

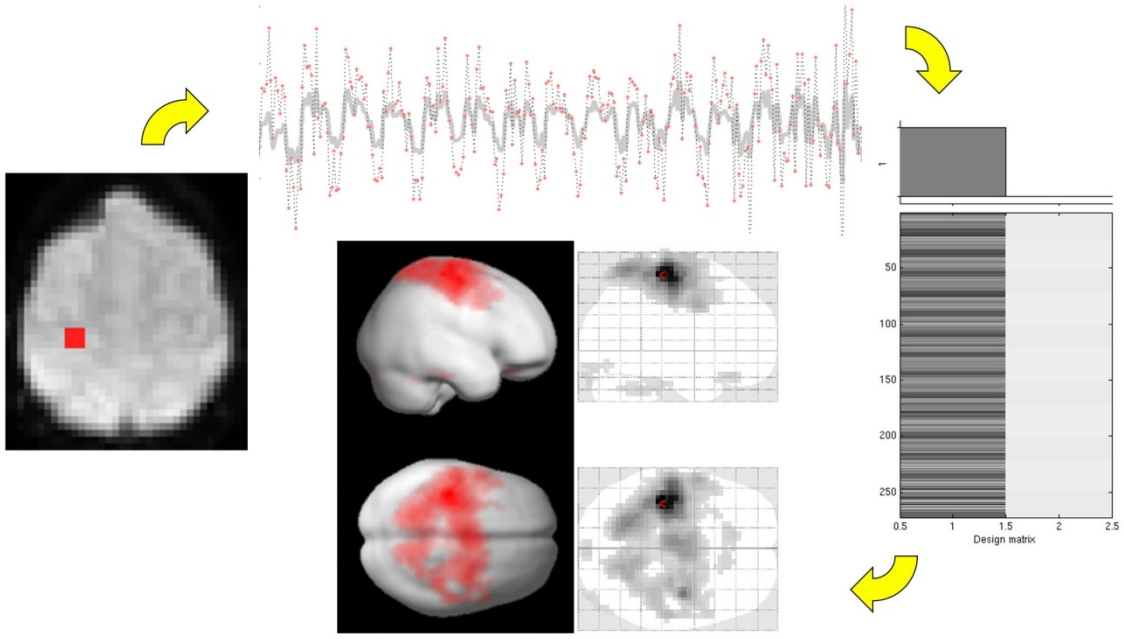

Figure 1.2 Functional connectivity analysis.

For functional connectivity analyses, the time series of an fMRI dataset is extracted from a region of interest (here: red voxel in the motor cortex) and used as variable of interest in a new fMRI analysis of the same dataset. This reveals voxels within the dataset with a similar signal change over time, indicating functional connectivity to the initial region of interest.

1.4.3.3.4 Independent component analysis

Independent component analysis (ICA) is an alternative, model free way to analyse fMRI data. Instead of prior specification of a design matrix with given individual times of task and rest and different conditions, the data is analysed without any prior knowledge about the paradigm or timing (Beckmann and Smith, 2004). The algorithm identifies clusters of voxels in the dataset, which share a similar behaviour in terms of their signal time series. This also takes into account the spatial relationship between voxels, preferring to cluster neighbouring voxels.

ICA can be applied to paradigm free, resting state fMRI or to task based fMRI time series. It can be performed on single subject data, or on groups of subjects. In case of group analyses, components common to all subjects are identified.

This approach is able to reliably identify major functional systems of the brain without any prior information, as shown by the following example:

Figure 1.3 shows an example from group-ICA analysis of the Dot-back paradigm, where a bilateral fronto-parietal component is identified, representing the working memory network. Red-yellow voxels indicate an increased BOLD signal corresponding to the time course plotted underneath, blue voxels indicate a decreased BOLD signal at the same time. The average time course across subjects perfectly resembles the paradigm design with distinct blocks of activation of variable intensity. Fourier analysis identifies a peak frequency of signal change at 0.22 Hz – equivalent to the 45 second cycle of one task and rest block.

Figure 1.4 shows the component representing the visual system with a more constant response amplitude.

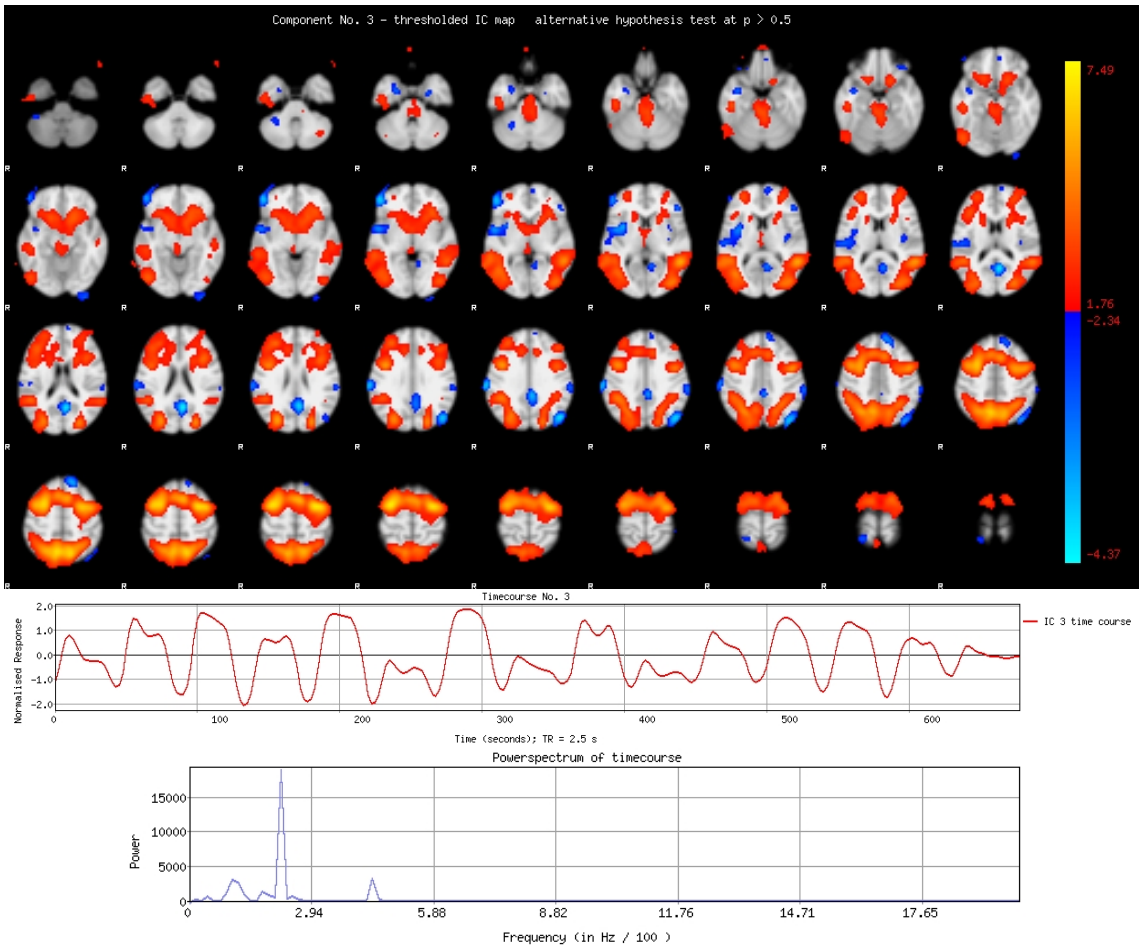

Figure 1.3 Independent component analysis, working memory network

ICA automatically identifies this bilateral fronto-parietal working memory component, common to all subjects in the group analysis. The plotted time course resembles the paradigm design. The frequency of signal fluctuation peaks at 0.22 Hz

Other components might represent signal noise or artefacts, but these can usually be easily distinguished based on their spatial distribution and frequency spectrum not matching the paradigm timing (Figure 1.5).

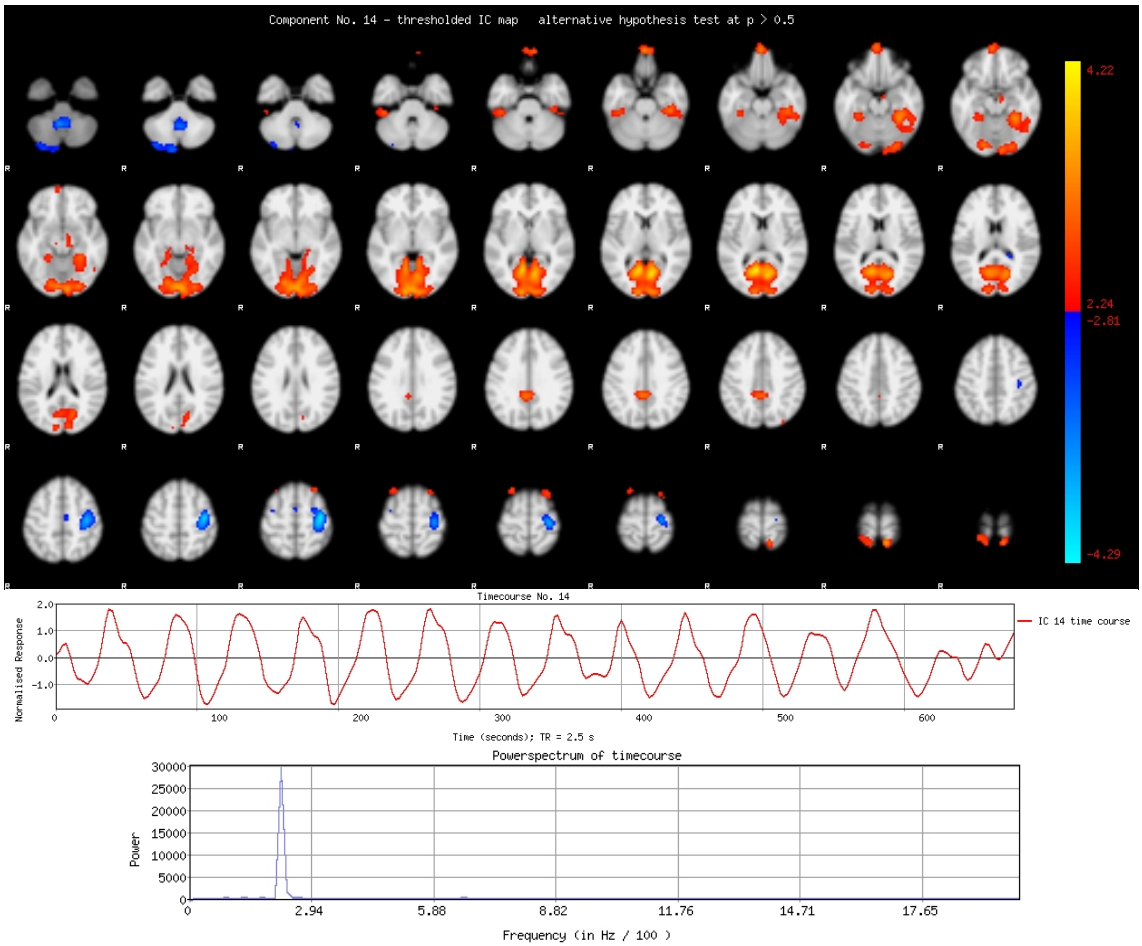

Figure 1.4 Independent component analysis, visual system

The visual system of bilateral occipital cortex is also identified as common in all subjects. It also shows a strictly task-driven time course with a relatively constant response amplitude across different conditions

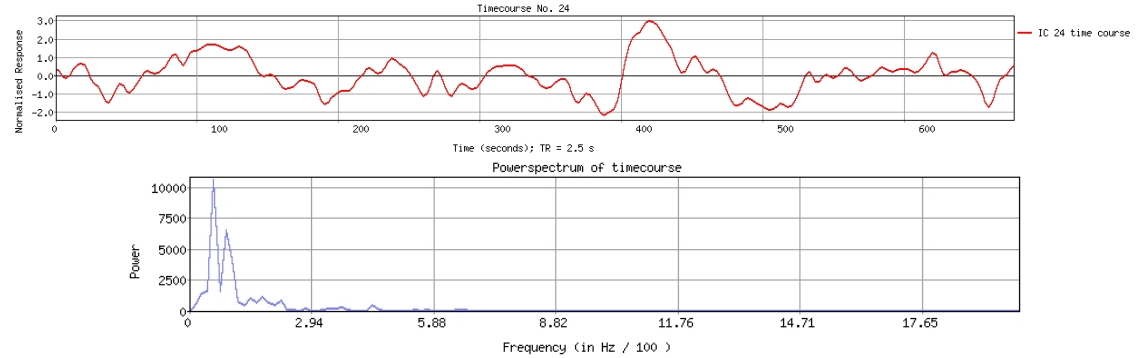

Figure 1.5 Independent component analysis, low frequency noise

1.4.4 Diffusion MR Imaging

1.4.4.1 Diffusion

Diffusion occurs as a result of the constant random movement of water molecules, energized by our body temperature. This random movement of molecules is called "Brownian motion" named after the Botanist Robert Brown who first described it in 1828. Even though Brown first wrongly assumed the random movement of pollen particles in water he observed under the microscope reflected an active biological process, he quickly found the same molecular movement also when inorganic material was immersed in water, clarifying that movement of water molecules is the driving force.

Einstein later specified diffusion, introducing the concept of a "displacement distribution", which quantifies the fraction of particles that will travel a certain distance within a particular timeframe. In free diffusion the average squared displacement r is proportional to the observation time t and to a specific diffusion coefficient D, as specified in Einstein's equation from 1905:

$$r^2 = 6\,D\,t$$

This diffusion coefficient for free diffusion in water at a temperature of 37°C is 3×10^{-3} $mm^2\,s^{-1}$, translating to an average displacement of 30 μm in 50 ms (Jones, 2014).

In biological tissue, however, diffusion is not free, but is hindered by certain tissue characteristics.

1.4.4.2 Diffusion-weighted imaging

Using specific MRI acquisition schemes, it is possible to assess quantitatively the water diffusion in biological tissue, using this to make inferences about the structural properties of the tissue.

Diffusion-weighted MRI cannot measure the diffusion coefficient directly, it can only make inferences from observations and determine the "apparent diffusion coefficient" (ADC), indicating that the "real" diffusion coefficients for the different compartments within an MRI voxel cannot be distinguished.

The basic principle of diffusion-weighted MRI sequences is the application of an additional, bipolar gradient pulse between excitation and read out. This can be applied in the form of a two gradient of opposite polarity, or by two identical gradients, with a 180° pulse in between. The first additional gradient will add a location specific positive phase to each spin. Later, the second, inverse gradient will add a similar negative phase to the spin, resulting in no net change of magnetisation if the spin has not moved, and the positive and negative gradient pulses 'hit' it with the same, location specific intensity. If, however, the spin has moved between the two inverse gradient pulses, the positive and negative phase will not have the same intensity, resulting in increased phase incoherence and signal loss for that spin. Hence, spins in regions with high diffusivity will have more signal loss, than spins in regions with restricted diffusivity. Typically this is translated directly to pixel intensity in diffusion-weighted images, where low-pixel intensity indicates high diffusivity and bright pixels indicate restricted diffusion.

In clinical neuroimaging, the most important application of diffusion-weighted imaging is the differentiation between interstitial and intracellular oedema, both of which showing up as high signal intensity areas in conventional T2-weighted images. In case of an interstitial oedema diffusivity is increased because more water molecules can travel freely between cells in this region. Contrary, in case of an intracellular oedema, diffusivity is reduced, because water is trapped inside cells and can diffuse less freely than normal. This “diffusion restriction“ is the hallmark of hypoxic cell damage in the brain and can be seen minutes after an ischemic event. Ischemia leads to a break-down of the neurons active sodium and potassium transport, resulting in intracellular accumulation of sodium and subsequent osmotic inflow of interstitial water into the swelling cell. Diffusion-weighted imaging has therefore become a most valuable clinical tool in the early diagnosis of stroke.

In epilepsy, there are few applications for diffusion-weighted imaging, even though there have been case reports, where patients with cryptogenic focal epilepsy showed focal diffusion restrictions following prolonged seizures.

1.4.4.3 Diffusion Tensor Imaging

If a sufficient number of diffusion-weighted pulse sequences is combined, measuring the diffusivity along different directions, it is possible to measure not only the degree of diffusivity, but also to determine its preferred direction, the diffusion tensor (Basser et al., 1994). Diffusion tensor imaging (DTI) allows for a more detailed analysis of structural tissue properties, beyond diffusion-weighted imaging.

It is possible to determine the diffusion tensor from diffusion-weighted acquisitions with a minimum of six directions. However, measuring more directions increases both, the signal to noise ratio and the angular resolution (Jones, 2004). When the number of diffusion-weighted directions is increased, it is usually recommended, to aim at an even distribution of angles across space, and also to cover all main directions first and then add further volumes covering angels in between (Cook et al., 2007). It is usually recommended to rather acquire additional different diffusion-weighted directions than to acquire multiple acquisitions of the same directions for in scanner averaging (Ni et al., 2006)

In regions where water molecules are not obstructed by cellular structures (for example in the CSF space), the diffusion is free and "isotropic", which means that, on average, water molecules travel the same distance in all directions. However, in brain tissue this movement is usually restricted by cell membranes and cellular organs, which can result in a spatial constrain of water diffusivity.

In the cerebral cortex, diffusion is restricted compared to CSF, but usually without a preferred spatial orientation, resulting in a reduced, but still relatively isotropic diffusion.

The most restrictive structures for water diffusion in the brain are axonal bundles in the white matter. Here, water can travel easily along the axonal lumen, but much less perpendicular to it, where cell membrane and myelin sheaths obstruct diffusivity. This results in a highly "anisotropic" diffusion, where diffusion along one particular direction is larger than in other directions. Hence, in the white matter of the brain, the preferred direction of water diffusivity indicates the principal direction of axonal bundles.

1.4.4.4 The diffusion tensor, Eigenvector and Eigenvalues

When diffusion is measured in different directions, a single scalar such as the ADC is no longer sufficient to describe diffusion. The next complex possibility to describe diffusion where the average displacement is different for different directions is the diffusion tensor. It is a 3 x 3 matrix, describing diffusivity in three-dimensional space.

$$D = \begin{bmatrix} Dxx\ Dxy\ Dxz \\ Dyx\ Dyy\ Dyz \\ Dzx\ Dzy\ Dzz \end{bmatrix}$$

The diagonal elements of this matrix correspond to the diffusivity along the three orthogonal axes x y and z and the off-diagonal elements describe the correlation between them. Only when the tensor is aligned parallel to one of the coordinate systems axis, the off-diagonal elements become zero, i.e. there is no covariance between them, and the tensor is "diagonalised". In this case the diagonal matrix elements correspond to the tensors eigenvalues λ_1 λ_2 and λ_3, the diffusivity along the three orthogonal axis defined by the corresponding eigenvectors ε_1 ε_2 and ε_3.

A more graphic representation of the diffusion tensor is an ellipsoid in space. In case of isotropic diffusion, the tensor is represented by a symmetric ellipsoid, a sphere. The more directed the diffusion, the more elongated the corresponding ellipsoid. The surface of the ellipsoid represents the distance to which a molecule will diffuse with equal probability from the origin (Jones, 2014). The relative size of the ellipsoid represents the mean diffusivity.

1.4.4.5 Fractional anisotropy, trace and mean diffusivity

Fractional anisotropy (FA) describes the degree of directionality of water diffusion and can be calculated from the three eigenvalues:

$$FA = \sqrt{\frac{3}{2}} \frac{\sqrt{(\lambda_1 - \langle\lambda\rangle)^2 + (\lambda_2 - \langle\lambda\rangle)^2 + (\lambda_3 - \langle\lambda\rangle)^2}}{\sqrt{\lambda_1^2 + \lambda_2^2 + \lambda_3^2}}$$

FA values ranges from 0 in case of completely undirected, random diffusion to a maximum of 1 in case of an extremely strong directionality, where diffusion is restricted exclusively to one single direction with no perpendicular diffusivity (Basser and Pierpaoli, 1996).

The trace *T* is the sum of the three diagonal elements of the diffusion tensor

$$T = (Dxx + Dxy + Dxz) \quad ,$$

which is equal to the sum of the tensors' three eigenvalues λ_1 λ_2 and λ_3.

Dividing the Trace by three gives the directionally averaged mean diffusivity (MD)

The MD represents a measure for the total diffusivity in a voxel, regardless of the directionality.

Both scalar parameters, FA and MD describe different tissue characteristic and are usually written out for every image voxel to corresponding FA and MD maps, representing these values for the whole brain.

Both maps can be determined relatively quickly, and are usually generated by the MR scanner software for immediate availability.

It is therefore not surprising, that early research using DTI essentially meant quantitative analyses of FA and MD maps.

In many neurological diseases, including epilepsy, reductions of FA and increases of MD have been described. FA reductions are usually interpreted as reduced white matter integrity, reflecting damage to myelin or a loss of axonal bundles, underlying the reduced FA. Increased MD, often found in the same regions, is usually interpreted to reflect oedema, indicating neuronal damage, such as from inflammation or ischemia.

In fact there are only few neurological diseases, where no FA reductions have been described in the past decade, probably indicating some unspecificity of this method. Also, there are a number of alternative explanations for reduced FA, including regular tissue properties such as crossing fibres, partial volume effect or any technical affects such as increased movement artefacts during the DTI data acquisition.

1.4.4.6 Technical challenges in DTI

Given the nature of diffusion-weighted imaging, sensitive to molecular movement, these acquisitions are particularly sensitive to movement artefacts. These cannot only stem from subject head movement, but also from physiological pulsations of brain tissue. To overcome the latter, cardiac gating has been proposed, where a peripheral pulse sensor triggers DTI acquisition. This allows acquisition of images always at the same point in time of the cardiac cycle, reducing the impact of physiological noise. Because this requires waiting for the right time to acquire an image slice, scan time is prolonged by approximately 30% (Chung et al., 2010). The discussion if one should rather use cardiac-gating or instead use the same scanning time to acquire more diffusion-weighted directions is still ongoing.

The relatively long acquisition time makes DTI acquisitions susceptible to subject head movement, most frequently a rotation around the x-axis caused by relaxation of neck muscles

The rapid switching of strong diffusion gradients leads to frequent changes in the bore field, which in turn induce currents in all conductors in the scanner – including the head coil. These so called eddy currents lead to image distortions during the acquisitions, essentially resulting in a slightly different shape of every single image volume.

1.4.4.7 DTI preprocessing

For the correct estimation of the diffusion tensor, the voxels from all diffusion-weighted images must be spatially aligned correctly.

This necessitates the correction of both, subject head movement during the DTI data acquisition and eddy current-induced volume distortions. This is done by image Realignment before any further processing is performed. All volumes of the DTI acquisition are realigned to the first image volume, typically using a 12-degree of freedom linear transformation which allows translation, rotation, scaling and shearing along all three orthogonal axes.

In the resulting, realigned 4D volume, all diffusion-weighted volumes are properly aligned, allowing further processing and a reliably estimation of the diffusion tensor and scalar measures such as FA and MD for every voxel.

One major limitation in scanner processing is that such Realignment is not performed. The resulting FA and MD maps will therefore always be contaminated with noise from misalignment on a voxel scale.

1.4.4.8 Clinical application of DTI in epilepsy

In epilepsy one of the first applications of quantitative DTI, based on FA maps has described reduced FA in the ipsilateral temporal lobe in temporal lobe epilepsy. Further studies then showed more widespread alterations, including extratemporal and contralateral brain regions.

1.4.4.9 Diffusion tensor tracking

Once the degree and directionality of water diffusion has been determined for every voxel in the brain, the next step of analyses can be taken:

Diffusion tensor tracking, fibre tracking, tractography and other similar terms describe the process of consecutively connecting the principal diffusion vectors of adjacent voxels to a continuous diffusion pathway.

It has been shown that such a model of connected diffusion vectors across neighbouring voxels indeed resembles the course of axonal bundles so closely, that today the term "fibre tracking" is established for this procedure. Of course it is crucial to be aware that these techniques are of course not actually tracking fibres, but only provide a virtual approximation thereof, based on water diffusion and many assumptions and preprocessing steps, each of which may be flawed. Interpretation of the resulting data requires caution and awareness of technical limitations and possible pitfalls (Jones et al., 2013).

These limitations in mind, when used reasonably, DTI tractography is a fascinating technique and has provided numerous new insights in neuroimaging in the past years.

Tracking algorithms can be divided in two broad categories, deterministic and probabilistic tracking.

Deterministic tracking is the simplest possible approach, where the principal diffusion vector is determined for every voxel in the brain and tracking follows this pathway of principal directions, until some termination criteria is reached.

Probabilistic tracking on the other hand tries to take into account uncertainties about the principal diffusion vector. Most importantly, it tries to deal with brain regions, where multiple fibre populations with different spatial orientations are present in one voxel. This is actually true for the majority of brain voxels. Instead of determining one diffusion tensor per voxel, probabilistic algorithms determine multiple possible tensors, weighted by their likelihood for each voxel. The resulting measures such as "orientation distribution probability" are then used for the tracking process, where typically several hundred or thousand iterations are performed for every seed voxel and the resulting tract is not a binary line, but rather a probability distribution, showing, how many of he repeated trials took which pathway. Naturally the computing demand for probabilistic preprocessing and tracking is several magnitudes higher than for deterministic tracking.

Regardless of the specific algorithm used, there are some basic "ingredients" for tracking, used by most programs:

A seed region defines the starting point of the tracking procedure. This can be a single voxel, but usually involves an anatomically defined region of several cm^3. For some applications the tracking can also be performed for the whole brain, the largest possible seed region.

For some applications it is helpful to also define a target region, i.e. an area that must be reached by the tracking procedure. All tracts emerging from the seed that do not reach the target will be discarded.

The tracking of some complex shaped connections may benefit from an additional waypoint mask, a region through which tract must pass before they reach their target.

And finally, in some applications, exclusion masks are used, regions that must not be reached by the resulting tracts. A mask in the midline is commonly used to constrain tracking to one hemisphere only. Many programs allow selecting if a tract reaching an exclusion mask should be truncated at the mask or should be discarded altogether.

Apart from these spatial constraints, a few other termination criteria are defined for most tracking algorithms: The minimum FA value per voxel intends to limit tracking to brain regions with sufficient certainty about the diffusion orientation. When a too low FA voxel is reached, i.e. in the cerebral cortex, the tracking is terminated. Also most algorithms define a maximum angle allowed between adjacent voxels. This intends to avoid too steep turns of a tract which would be anatomically implausible.

1.4.4.10 Clinical application of tractography in epilepsy

In epilepsy, one of the first applications of DTI was the tracking and visualisation of the optic radiation (Powell et al., 2004). The optic radiation spans from the lateral geniculate body to the primary visual cortex of the occipital lobe. Due to the developmental growth of the temporal lobe it once circumvent, parts of the optic radiation are now extending into the temporal lobe, where it is susceptible to damage from resective surgery. Patient with temporal lobe epilepsy, who undergo standard anteromesial temporal lobe resection have risk to suffer a visual field deficit due to

damage to the optic radiation. This risk is higher in surgery on the left side, where the optic radiation reaches further anterior than on the right (Winston et al., 2011). While most patients learn quickly to compensate an upper quadrant anopia, some cases have more extensive damage, in the worst case a hemianopia to the contralateral side. This can then be prohibitive of driving, even if patients are rendered seizure free with surgery. The preoperative visualisation of the maximum anterior extend of the optic radiation can help reduce the risk of deficits.

The visualisation of other functionally relevant tracts in epilepsy surgery is also applied, just like in general neurosurgery. One potential pitfall to keep in mind is the risk of false negative findings from DTI tractography in the vicinity of structural lesions. Many brain pathologies are associated with perilesional oedema. The increased proportion of water will affect measured from DTI, typically increasing diffusivity in this region and typically reducing anisotropy, as diffusivity is undirected. Most DTI tracking algorithms include a minimum value of FA as termination criteria – and this is likely to be met in the region of oedema. This means tracking will terminate, indicating that fibres are not continuing toward and through the lesion. And this can be a misleading artefact. Hence cautious interpretation is needed, when DTI indicates fibre pathways are travelling safely around a structural lesion. Technically it would be very difficult to reliably identify fibres actually passing through a lesion with perilesional oedema.

1.5 Aims of this study

The aim of this project is to use functional and structural neuroimaging methods to investigate cortical activation, structural properties and functional and structural connectivity of brain regions in healthy controls, in patients with juvenile myoclonic epilepsy (JME) and in patients with frontal lobe epilepsy (FLE). Group comparisons will be performed to identify syndrome specific alterations and these will be correlated with measures of neuropsychological performance and clinical parameters of patients.

The underlying objective is to understand better the interaction of neuronal system and the basis of cognitive impairments commonly observed in these two epilepsy syndromes. We also aim to explore whether knowledge about structural and functional connectivity of the frontal lobes assists in consideration of surgical treatment of refractory FLE.

2. Subjects and Methods – common part

2.1 Ethics approval

This study was approved by the relevant local Ethics Committees of the UCL Institute of Neurology and of King's College London

All patients provided written informed consent to participate in this study.

2.2 Subjects

Patients were recruited from the outpatient clinic of the National Hospital for Neurology and Neurosurgery, from the National Society for Epilepsy (now epilepsy society) and from the outpatient clinic of the King's College Hospital. Healthy controls were recruited from hospital staff, students and friends or carers of recruited patients.

2.2.1 JME

Inclusion criteria for JME patients were: a typical clinical history of JME with onset of myoclonic jerks and generalised seizures in adolescence. All JME patients had at least one EEG recoding showing generalised spike-wave or polyspike-wave complexes and all had normal clinical MR imaging.

2.2.2 FLE

Inclusion criteria required an electroclinical diagnosis of FLE, with:

- seizure semiology includes bilateral tonic seizures, early head version or focal clonic seizures;
- interictal and ictal frontal discharges in EEG; and
- MRI of the brain does not show relevant extra-frontal pathology.

Patients with predominant seizure semiology pointing to extra-frontal seizure onset (such as visual auras) were excluded.

Most patients underwent prolonged Video-EEG monitoring for confirmation of the syndromic diagnosis, about half of the patients were potential candidates for epilepsy surgery.

2.2.3 Controls

Healthy controls were matched for age and gender. All had no history of neurological disease and no family history of epilepsy and had a normal neurological examination.

2.3 Schedule and order of examinations

All subjects were contacted before the examination and the study information sheet was sent by mail or email. After subject arrival at the Epilepsy Society MRI Unit, the information sheet was reviewed, open questions were discussed and written informed consent was obtained.

Subjects were informed about the planned order of investigations and familiarized with the MRI scanner and the fMRI paradigms.

MRI scanning started with Localizer and calibration scans, followed by the Dot-back, N-back, verbal fluency and verb generation paradigms. Patients were reminded of the next upcoming paradigm with a brief repetition of the instructions via the MRI scanner intercom or in person. After these four cognitive tasks, structural images were acquired, comprising a T1-weighted 3D volume acquisition, axial T2-weighted images and, for the patients with frontal lobe epilepsy, an axial FLAIR sequence with 3-mm slice thickness. Scan time for this first block of imaging was about one hour and a pause was made afterwards.

All subjects had a short break of 10-30 minutes before MRI scanning resumed.

The second scanning block started with a new localizer and calibration scan, followed by the memory-encoding paradigm, and the DTI acquisition. Scan time for the second block was about 45 minutes.

After another short break, the recall test for items presented during the memory fMRI task was carried out.

This was followed by complementary neuropsychological testing, including a computerized spatial working memory test, the Iowa gambling task and the trail making test.

Before discharge, subjects were encouraged to provide feedback on the investigations carried out and asked for consent to be contacted for further research studies.

The total time on site at the MRI Unit was about 4 hours.

2.4 MRI

MRI was acquired on a GE Excite HDx 3T scanner (General Electric, Wakashua, Milwaukee, WI, USA). Standard imaging gradients were used with a maximum strength of 40 mT/m and slew rate of 150 T/m/s. All images were acquired with an 8-channel phased array head-coil for reception and the body coil for transmission.

2.5 Functional MRI

Images for all functional paradigms were acquired with the same sequence, varying only in total duration.

Gradient-echo planar T2*-weighted images were acquired, providing blood oxygenation level dependent (BOLD) contrast. The acquisition consisted of 50 axial slices in AC-PC orientation with 2.4 mm thickness and 0.1 mm gap, providing full brain coverage. Slices had a 64x64 in plane matrix with 3.75 x 3.75 mm voxel size. Repetition time was 2500 ms and echo time 20ms. Accelerated parallel imaging with a Sense factor of two was used. All fMRI acquisitions were preceded with four excitations to ensure steady magnetisation before the paradigm started and data was recorded.

2.5.1 fMRI paradigms

All paradigms were explained in detail before the MRI scan, using printed instructions with screenshots of the paradigm presentation.

Paradigms were presented by in-house software running on a personal computer, synchronised to the MRI scanner via a TTL trigger signal. The paradigm presentation was back-projected on a semi-transparent screen in front of the MRI scanner, which

could be seen by the subjects via the standard mirror system attached to the head-coil. Appropriate vision was tested for every subject before the fMRI acquisition. MRI-compatible frameless glasses were provided to subjects with impaired vision if needed.

A MRI compatible joystick was provided at the right hand side for responses, positioned individually with Velcro for comfortable use.

2.5.1.1 Dot-Back paradigm

The dot-back task was used to assess spatial working memory. Subjects were presented with yellow dots, appearing randomly in any of the four corners of a diamond box on the screen every 2 seconds. Subjects had to respond to the dots sequentially with a joystick at their right hand in three different ways: In the '0-back' condition, they were instructed to move the joystick to the position of the current dot. In the '1 back' condition they had to move the joystick to the position of the previous dot. In the '2 back' condition they were instructed to move the joystick to the position of the dot two presentations back, requiring high continuous attention throughout the block. Each block lasted 30 seconds, during which 15 dots were presented and was followed by 15 seconds of rest, where dots in all four corners were presented. All three conditions were repeated five times in a pseudo-randomized order, resulting in a total duration time of 11:15 minutes during which 272 image volumes were acquired.

2.5.1.2 N-Back paradigm

The N-Back task was used to assess verbal working memory. Single words were presented sequentially for 3 seconds each in blocks of 30 seconds. In the control condition, subjects were instructed to watch out for the word 'Bird' and respond with

the joystick when they spotted it. In the actual verbal working memory condition "Two back", subjects were instructed to look out for a repeated word, which is the same as two presentations earlier and indicate this with a joystick response. As resting condition, 15 second blocks of crosshair fixation were interleaved.

2.5.1.3 Verbal Fluency paradigm

For this language task, subjects were presented with single letters presented every 3 seconds in blocks of 30 seconds and were instructed to think of any word starting with the presented letter every time the letter is presented. These blocks alternated with 30-second rest block with presentation of an asterisk.

2.5.1.4 Verb Generation paradigm

This second language paradigm included two conditions of 30 second blocks. Ten single words were presented to the subjects and they were instructed to either repeat the very same word in their mind in the "repeat" condition or to think of a verb, related to the presented noun in the "generate" condition (for example to think of "open" or "lock" when "door" is shown).

2.5.1.5 Memory encoding paradigm

During this task, subjects were presented 30 second blocks of ten items each, followed by 15 second resting blocks. Items were either ten words, ten pictures or ten faces and subjects were instructed to memorize them. As distractor task, they were also instructed to indicate with a joystick response if they liked the presented item or not. Faces had

different emotional expressions and could be neutral, happy or fearful, allowing for event related analyses of specific responses.

Recall of memorized items was tested after the MRI scan, approximately 30 minutes after item presentation. All presented items plus additional new items were presented and subjects were instructed to indicate whether they had seen the item before or not.

2.5.2 fMRI analysis

All fMRI analyses were performed with SPM 5 software, Release 0958 (www.fil.ion.ucl.ac.uk/spm/), including preprocessing, first level single subject analyses, group analyses and functional connectivity analyses.

Only for ICA analyses of fMRI data, I used FSL 4.1 software (www.fmrib.ox.ac.uk/fsl/)

2.5.2.1 Preprocessing

The preprocessing described in this section was applied identically to the data from all five cognitive paradigms.

2.5.2.1.1 Realignment

Images were realigned for movement correction using SPM's realign function with a 'Quality' setting of 1. Realigned images were not resliced to avoid unnecessary interpolation which could result in loss of image quality. The Realignment parameters were stored in each image's header file and were taken into account before the next preprocessing step. A mean image was created from the realigned time series and saved.

2.5.2.1.2 Normalisation

As the image contrast and spatial distortions from our acquisition differed considerably from the standard EPI template provided with SPM, a scanner and acquisition specific template was created. For this purpose, a symmetric version of SPM's EPI template image was used as initial target and 60 mean EPI images from 20 FLE patients, 20 JME patients and 20 healthy controls were normalised to this template using affine registration and non-linear warping with 32 iterations. Normalised images were re-sampled to isotropic 3x3x3 mm^3 voxels, resulting in a voxel volume similar to the initial acquisition. In the next step the average image from these 60 normalised images was created and served as new template for all normalization steps, including the repeat normalization of these 60 subjects.

2.5.2.1.3 Smoothing

Normalised images were smoothed with an 8x8x8 mm FWHM Gaussian kernel to reduce noise. All further statistical analyses were carried out on these realigned, normalised and smoothed images.

2.5.2.2 First level statistical analysis

First level statistical analysis for every subject was carried out, using a block design based on the known paradigm timing, modelling each different paradigm condition separately. Realignment parameters from image realignment were included as multiple regressors modelling subject motion.

2.5.2.3 First level contrasts

Different T-contrasts were specified for each paradigm, comparing each paradigm condition against the baseline or comparing different conditions against each other.

2.5.2.3.1 Dot-Back paradigm

For the dot-back paradigm, different contrasts were defined, comparing each of the three conditions against the resting period and also comparing conditions with different memory load. For example the '2 back - 0 back' contrast (004 in Figure 2.1) controls for the visual input and for the motor response which were the same in both conditions. The resulting contrast between these conditions reveals specifically the additional cortical responses to the additional spatial working memory load.

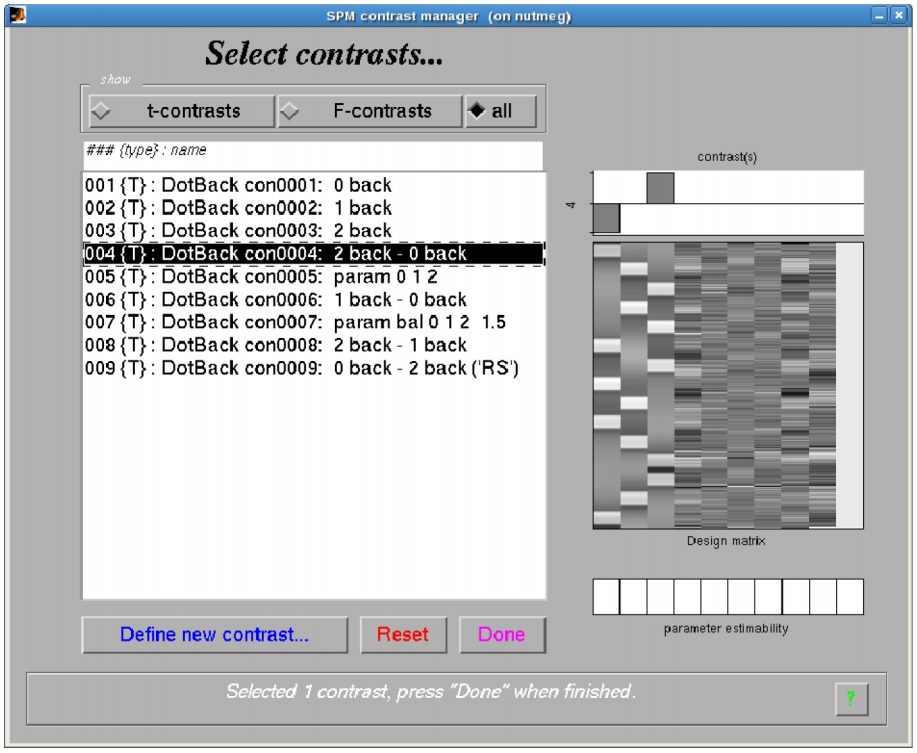

Figure 2.1 SPM contrasts, dot-back paradigm

2.5.2.3.2 N-Back paradigm

For the n-back paradigm, three contrasts were defined (Figure 2.2). Here the “Two back – Is it Bird” contrast reveals the specific additional activation from the verbal working memory load

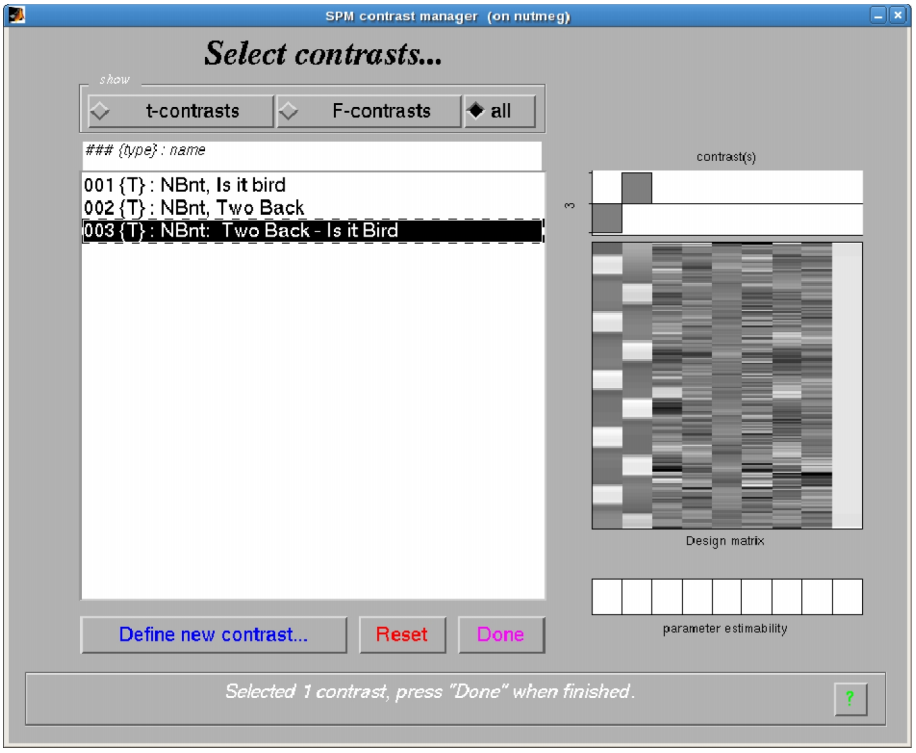

Figure 2.2 SPM contrasts, n-back paradigm

2.5.2.3.3 Verbal Fluency paradigm

The verbal fluency paradigm contained only one condition and only one contrast against the baseline was defined.

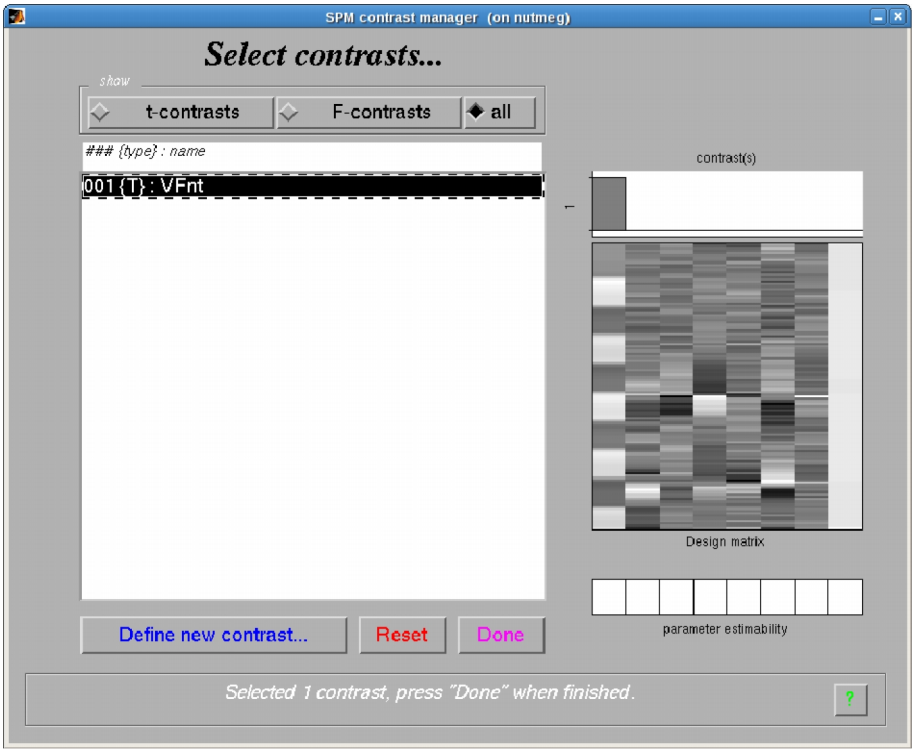

Figure 2.3 SPM contrast, verbal fluency paradigm

2.5.2.3.4 Verb Generation paradigm

For the verb generation paradigm four contrasts were defined, including a “Generate – Repeat” contrast, sensitive to the specific additional activation from the semantic demand of verb generation.

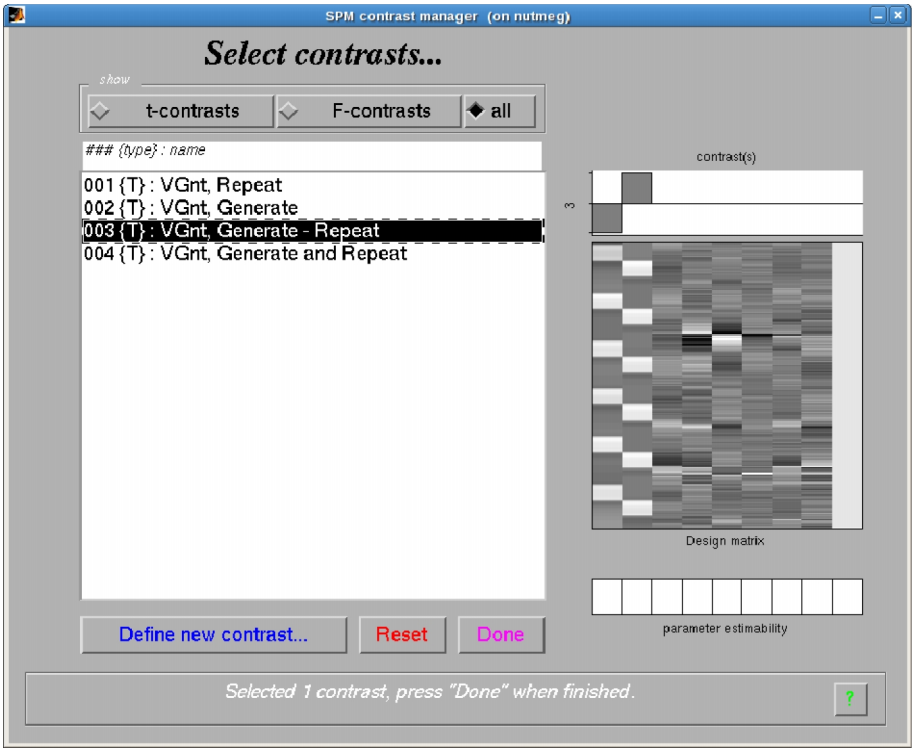

Figure 2.4 SPM contrasts, verb generation paradigm

2.5.2.4 Second level statistical analysis

Group comparisons were carried out as two sample T-tests, comparing the first level contrast files from all subjects within a group. Group comparisons were performed for all first level contrasts for each paradigm to assess specific group differences for all different paradigm conditions. Increases and decreases in response were investigated.

Subjects who did not show any activation in the first level analysis, or whose results were suggestive of artefacts from movement, or whose realignment showed movement of more than 2 mm were excluded from further group analyses.

2.5.2.5 Functional connectivity

Functional connectivity was analysed by extracting the average time series from a 3x3x3 voxel region of interest from individual fMRI data.

In controls and patients with JME, individual subject results showed a high degree of overlap, so the region for time series extraction was initially defined by the peak activation in group activation maps for each paradigm, using the same region for all subjects.

In patients with FLE, however, extensive reorganisation was seen in many subjects, so that a region of interest at a fixed position would not have picked up any signal in some subjects. Therefore a larger "search area" was defined, for example the posterior half of the superior and middle temporal gyrus. Then each subject's individual peak response in this large region was identified in individual contrast images, and the signal time series for functional connectivity was extracted from there.

To ensure group comparability, this “find individual peak” approach was then also applied in healthy controls and JME patients.

The extracted time series was used as a regressor of interest in a new general linear model for each subject, the individual realignment parameters were again included to account for subject motion.

The resulting functional connectivity maps reveal for every subjects voxels in the brain, whose signal time series correlates with the extracted signal time series from the initial seed region

Functional connectivity maps were created for multiple regions per paradigm, for example for the left inferior frontal gyrus and superior temporal gyrus for language paradigms.

Functional connectivity maps from all single subjects were compared in second level analysis using two sample t-tests, similar to the group comparison of conventional fMRI contrasts images.

2.6 Diffusion tensor imaging

2.6.1 DTI acquisition

In this study, two different DTI acquisition schemes were used, one with 32 diffusion weighted directions and one with 52. The 32 direction acquisition was initially used and was used for the test retest assessment of DTI reproducibility on both study sites. Shortly thereafter the acquisition scheme with 52 directions was established and used for all further scanning. Healthy controls who were scanned as part of the test retest study were rescanned with the new 52 direction scheme.

In summary, the 32 direction scheme was only acquired in the subgroup of controls for the DTI test retest study, described in chapter 3.

The 52 direction scheme was acquired in all patients and all controls and used for all other analyses.

The 52 direction DTI acquisition was a single-shot spin-echo planar imaging sequence, cardiac gated with TE=73 ms. Sets of 60 contiguous 2.4-mm thick axial slices were obtained, covering the whole brain, with diffusion-sensitizing gradients applied in each of 52 non-collinear directions [maximum b value of 1200 mm^2 s^{-1}] along with six non-diffusion-weighted (b=0) scans. The field of view was 24 cm, and the acquisition matrix size was 96 x 96, zero filled to 128 x 128 during reconstruction so that the reconstructed voxel size was 1.875 x 1.875 x 2.4 mm^3. The parallel imaging factor (SENSE) was 2 and total DTI acquisition time for 3480 image slices was approximately 25minutes, depending on subject heart rate.

2.6.2 DTI preprocessing

All DTI datasets were converted to 4D analyse file format for further processing.

The B0 images were extracted from the 4D file, averaged and saved as separate image file. The FSL eddy_correct command was used to correct for head motion and eddy-current induced distortions (Behrens et al., 2003).

Individual brain masks were created from the B0 images using FSL brain extraction tool (Smith, 2002) and were used to restrict all further processing to this brain mask.

3. DTI Test-retest analysis

(Vollmar et al., 2010)

3.1 Background

Diffusion Tensor Imaging (DTI) is an advanced Magnetic Resonance Imaging (MRI) technique that allows the assessment of water diffusion in the brain. In highly organized tissue like cerebral white matter, diffusion preferentially follows the longitudinal direction of axonal bundles and myelin sheaths while transverse diffusivity is limited by cell membranes, organelles and other structures. The degree of this directionality is described by the fractional anisotropy (FA) and high FA values represent highly anisotropic diffusion. FA is commonly used as a measure of white matter organization or white matter integrity, being higher in densely packed, parallel white matter bundles such as the corpus callosum (CC). FA measures are increasingly used in clinical studies and have shown alterations in various brain diseases such as multiple sclerosis (Ge et al., 2005) and epilepsy (Focke et al., 2008), as well as in normal aging (Sullivan and Pfefferbaum, 2006).

The intra-site test retest reliability of DTI measures has been addressed mainly at 1.5 Tesla (T) (Bonekamp et al., 2007; Ciccarelli et al., 2003; Heiervang et al., 2006; Pfefferbaum et al., 2003) with just two recent studies at 3T (Bisdas et al., 2008; Jansen et al., 2007) (table 1). There is considerably less data on cross centre reliability of DTI measures; previous studies have shown large variability of FA quantification on different 1.5 T scanners (Cercignani et al., 2003) (Pfefferbaum et al., 2003) with an

expected higher inter-site than intra-site variability (Pfefferbaum et al., 2003).Typical current “best-practice” 3T DTI protocols differ considerably from older 1.5T versions, with the inclusion of modern array head coils resulting in higher signal to noise ratios, and the increasing use of parallel imaging methods. There is little or no information on the inter-site reproducibility of measurements made using these recent MR technological developments. Reproducibility studies require image co-registration, for which there are several possible methods, such as affine, non-linear and template based approaches. The quality of these co-registration procedures is likely to affect measurement reproducibility. As repeat measurements of the same subject need to be co-registered, it appears the most straightforward approach to co-register repeat scans in each subject’s native space, avoiding any additional image transformation. However in daily life, it is common practice to use non-linear normalizations to a common template space before further analysis and we have therefore directly compared both approaches.

Clinical studies often target very specific patient populations which are difficult to recruit by one imaging centre alone. Large scale pharmacological investigations are usually multi-centre studies that increase statistical power by pooling patients, but differences in MRI scanner manufacturers, models and set-ups even for the same type of scanner restrict the comparison of imaging parameters across sites. A necessary first step is the acquisition of test-retest data in controls for the assessment of reliability. Test-retest studies allow for an estimation of reproducibility, i.e. within-subject differences.

The purpose of the current study is fourfold:

1. To assess the reproducibility of DTI measures using a contemporary 3T high field scanner system and a protocol typical of that which may be used in multi-centre studies using a variety of scanners

2. To determine whether using this protocol on two nominally identical GE Signa HDx scanners at different sites (National Society for Epilepsy MRI Unit and Institute of Psychiatry, King's College London) results in acceptably low levels of cross-site variability.
3. To assess the impact of different steps of the image processing pipeline on measurement reproducibility: We compared different methods for image co-registration, for ROI definition and the effect of tractography compared to ROI analysis of FA maps.
4. To assess the measurement reproducibility within the scan volume, creating reproducibility maps to identify regions of unfavourably high FA variability.

3.2 Subjects and Methods

3.2.1 Subjects:

Nine healthy subjects (2 female, age range 28-52 years) underwent four MRI scans each, two at each imaging site. The order of scans across sites was randomized, the interval between individual scans ranged from 1 to 95 days, and all scans were acquired within a 12 month period. The study was approved by the Research Ethics Committee of the UCL Institute of Neurology and UCL Hospitals, written informed consent was obtained from each participant.

3.2.2 MR image acquisition:

A 3T MRI scanner was used at each site, with imaging gradients with a maximum strength of 40 mT/m and slew rate 150 mT/m/sec (GE Signa HDx, General Electric, Milwaukee, WI, U.S.A.). The body coil was used for RF transmission, and an 8 channel head coil for signal reception, allowing a parallel imaging (ASSET) speed up factor of two. Each volume was acquired using a multi-slice peripherally-gated doubly refocused spin echo EPI sequence, optimized for precise measurement of the diffusion tensor in parenchyma, from 60 contiguous near-axial slice locations with 128x128 isotropic (2.4 x 2.4 x 2.4 mm) voxels. The echo time was 104.5 ms while to minimize physiological noise, cardiac gated triggering with a peripheral pulse sensor was applied (Wheeler-Kingshott et al., 2002) and the effective repetition time varied between subjects in the range between 12 and 20 RR intervals.

Based on the recommendations of Jones et al (Jones et al., 2002), the maximum diffusion weighting was 1300 s mm-2, and at each slice location, 4 images were acquired with no diffusion gradients applied, together with 32 diffusion-weighted images in which gradient directions were uniformly distributed in space. The total acquisition time for this sequence was approximately 10 minutes, depending on the heart rate.

3.2.3 Image processing:

Image distortions induced by eddy currents and subject movement during the acquisition were corrected using a mutual information based affine Realignment of all volumes to the first non-diffusion-weighted volume (FSL 4, http://www.fmrib.ox.ac.uk/fsl/) (Behrens et al., 2003). The brain tissue was

automatically segmented from skull and background using FSL's deformable brain model based Brain Extraction Tool (Smith, 2002). Brain extraction was performed on a non-diffusion-weighted volume with a fractional intensity threshold of 0.3 and then applied to the whole realigned DTI acquisition.

Diffusion tensors were reconstructed from the 32 diffusion-weighted volumes using Camino software (http://www.cs.ucl.ac.uk/research/medic/camino/, Version 2, rev 530), (Cook et al., 2006). The resulting diffusion tensors were diagonalised, yielding the three principal eigenvalues $\lambda 1$, $\lambda 2$, $\lambda 3$, from which FA maps were calculated (Pierpaoli et al., 1996).

To assess reproducibility, images created in each of the four sessions needed to be co-registered to each other. We used three different methods for co-registration and compared their impact on measurement reproducibility.

1. A rigid body co-registration with 6 degrees of freedom (3 translations, 3 rotations, no scaling) was performed using SPM software (SPM5, http://www.fil.ion.ucl.ac.uk/spm/). This was done using a two pass procedure: To achieve a gross alignment of images, the first FA map of each subject was initially co-registered to a FA template in MNI space by a rigid body transformation, preserving each subject's individual anatomy. Then all four FA images were co-registered to this template aligned image, the average FA was calculated and the rigid body co-registration was repeated, using the average FA as target image. Co-registered images were re-sampled to 1mm isotropic voxels using 2nd degree spline interpolation. This procedure will be referred to as 'affine' co-registration.
2. The same procedure was then repeated, including non-linear warping (32 non-linear iterations) for normalization to each subject's mean FA image. For the non-linear normalization the subject's smoothed average FA image was used as a weighting

mask, assigning more importance to regions with high FA for the normalization procedure.

3. We used FSL's tract based spatial statistics (TBSS) tools to normalize each single FA image to the provided FMRIB58_FA template image in MNI space. TBSS default settings were used for this non-linear transformation.

The masks created by TBSS for each scan were combined to create an average mask image for each subject, which was eroded by two voxels to exclude non-brain voxels for all further processing and analysis. For voxel-wise comparison, the realigned FA images were smoothed with a 4mm FWHM kernel.

3.2.4 Regions of interest

We chose three commonly used regions of interest (ROI), representatively reflecting different characteristics of white matter, and defined these ROIs manually on each subject's individual mean FA image in native space as well as on a FA template image in MNI space using MRIcro software (http://www.sph.sc.edu/comd/rorden/mricro.html) (Rorden and Brett, 2000) (Rorden and Brett, 2000)and the following anatomic guidelines:

1. A region representing an area of white matter with mainly parallel, densely packed fibres was defined in the splenium of the corpus callosum (SCC). A ROI of 0.8 cm^3 was drawn in adjacent coronal slices, and the shape of the ROI was checked in sagittal slices (see Figure 3.1 a). To minimize partial volume effects at the edge of anatomic structures, ROI were restricted to the centre of the CC and two mm distance was kept to its anatomic boundaries.

2. A large, 3.5 cm^3, region representing white matter with fibres of different and crossing orientations, was drawn in the left frontal white matter (LFWM), lateral to the commissural fibres from the CC and including the superior part of the corona radiata (Figure 3.1 b).

3. For the left uncinate fascicle (LUF), a smaller tract with lower average FA, a small 0.3 cm^3 ROI was drawn in sagittal FA slices, selecting the first voxels with high FA values, ascending anteriorly from the inferior longitudinal bundle when scrolling from lateral to mesial. The anterior part of the core of the LUF was best defined in coronal slices where it can easily be depicted as a bright fibre bundle at the inferior frontal lobe (Figure 3.1 c).

All ROI were smoothed with a 3x3x3 voxel mean filter after drawing. ROI defined in template spaced were also back-normalised to each subject's individual native space and measurements were performed in both, template and native space.

For comparison with other studies that used all brain voxels or histogram based statistics to assess DTI reproducibility, we also determined statistics for a whole-brain ROI, using each subject's thresholded b0 image to mask out CSF.

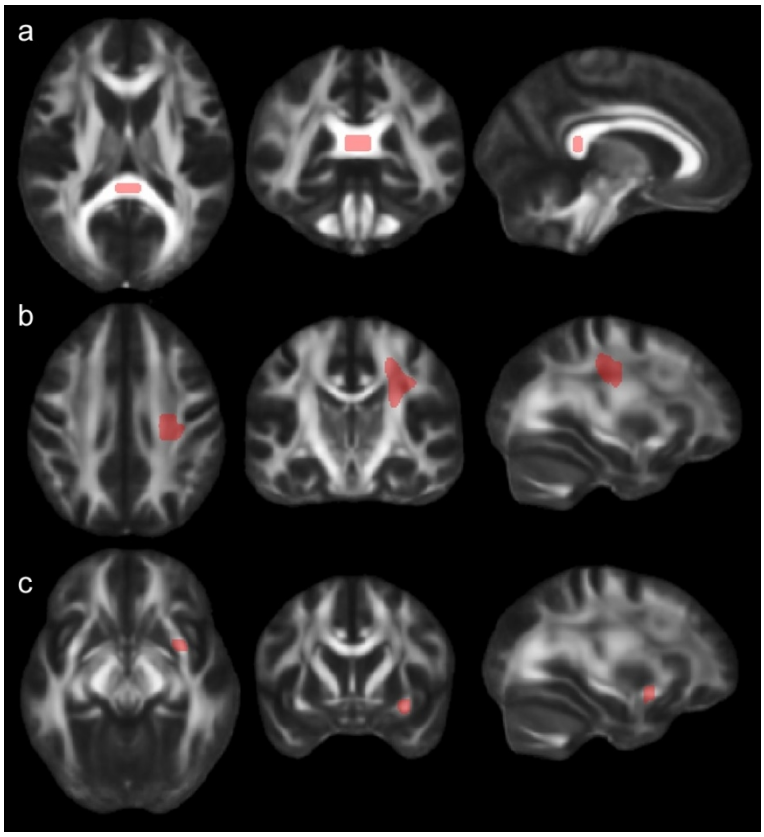

Figure 3.1 ROI placement in template space.

a) splenium of corpus callosum (SCC), b) left frontal white matter (LFWM), c) left uncinate fascicle (LUF).

3.2.5 Tractography

Probabilistic tractography was performed with FSL's probtrack algorithm, using the default settings with 5000 iterations per seed voxel. The above mentioned ROI were defined in template space, back-normalised to each subject's four individual scans and used as seed regions with the following constraints:

1. For the SCC ROI no further restrictions were made, the resulting tract mainly showed the commissural connections between homologous areas of the two parietal and occipital lobes.

2. For the LFWM ROI a waypoint mask in the brainstem was defined in the lowest axial slice, the resulting tract therefore showed the descending fibres of the corticospinal tract.

3. To track from the LUF ROI, exclusion masks were used in the sagittal midline to avoid crossing fibres and posterior to the vertex of the uncinate fascicle to exclude the inferior longitudinal bundle.

Tracking was performed independently for all four scans from each subject and the average FA within the tract and tract volume were calculated, thresholding the probability maps at 2%.

3.2.6 Reproducibility maps

To assess the spatial distribution of FA reproducibility within the scan volume, reproducibility maps were generated. For each subject, a difference image was created for each scan, calculating the absolute (positive or negative) difference of each single FA voxel from the subject's average FA. An average absolute difference image was created as well as an average relative difference image, dividing the absolute difference by the average FA, thereby showing the percentage change of the initial FA value. All maps were normalised to MNI space to create the group average reproducibility maps.

3.2.7 Statistics

ROI were applied to all four FA maps for each subject and ROI statistics were determined using FSLstats (FSL 4). Mean, standard deviation, minimum and maximum FA were extracted per ROI and analysed with SPSS 14 (SPSS Inc., Chicago, IL, USA)

and Microsoft Excel. For voxel-wise comparison, AFNI (http://afni.nimh.nih.gov/afni) was used to extract individual voxel values from the SCC ROI for further correlation analysis.

The coefficient of variation (CV) is defined as the ratio of the measurements standard deviation σ divided by the mean μ and multiplied by 100. It allows an intuitive estimate of measurement variance expressed as relative percentage, regardless of the absolute measurement value. In previous studies on DTI test-retest reliability, the CV is the most commonly reported statistical measure. However, there are different ways to determine the CV for a given ROI:

1. CV of the mean (CV_{mn}): the mean value from each ROI is determined for each scan and the difference between these mean values is determined
2. CV of the median (CV_{md}): Instead of calculating the mean value from a ROI, the median value is determined and compared across scans. Assuming a symmetric distribution of values within a ROI, this should be close to the CV_{mn}.
3. CV of voxel-wise comparison (CV_{vw}): Within each ROI, corresponding voxels from different scans are compared against each other and the CV_{vw} is determined for voxel-wise differences

CV_{mn} were calculated for each ROI and pairs of scans (intra-site and inter-site) per subject and for the group. CV_{vw} were calculated only for the SCC ROI, derived from both the raw and smoothed FA maps.

A different assessment of a method's reliability is the intra-class correlation coefficient (ICC) which relates the within-subject variation to the between-subject variation:

$$ICC = \frac{\sigma^2_{bs}}{\sigma^2_{bs} + \sigma^2_{ws}}$$

where σ_{bs} = between-subjects standard deviation of the population and σ_{ws} = within-subject standard deviation for repeated measurements. The ICC expresses the fraction of the total variance in the data that is caused by true biological variation between subjects rather than by measurement error within subjects. For test-retest data of healthy controls, acquired under similar conditions, true within-subject differences will be small, and the method yielding the highest ICC will be preferable.

3.3 Results

Visual inspection showed a very high similarity between the generated FA maps. Figure 3.2 shows the same mid-axial slice from the four different scans of subject one. Detailed gyral anatomy was reliably reproduced.

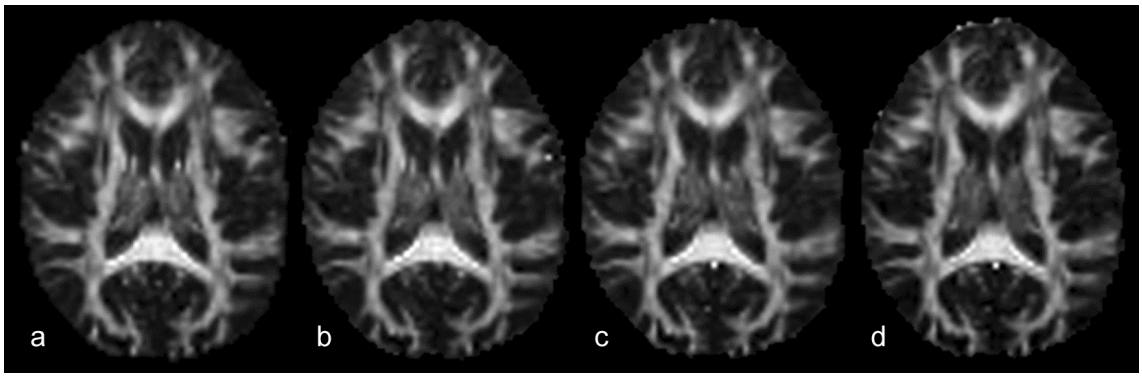

Figure 3.2 Reproducibility.

The same mid axial slice of the first subject's realigned FA maps from all four acquisitions is shown: a) site 1 scan 1, b) site 1 scan 2, c) site 2 scan 1, d) site 2 scan 2. Note the details of gyral anatomy, for example in the occipital pole.

3.3.1 ROI characteristics

The cross subject mean FA, within-subject SD and between-subject SD are summarised in table 2. The average within-subject SD across the four different scans was always lower than the between-subject SD for all FA measures. The between-subject CVmn ranged from 3.1% to 12.1%.

region	ROI size	mean FA	affine		non-linear		template		backnorm.	
	[cm³]		SD_{ws}	SD_{bs}	SD_{ws}	SD_{bs}	SD_{ws}	SD_{bs}	SD_{ws}	SD_{bs}
Whole brain	-	0.28	0.0038	0.0145	0.0033	0.0157	0.0034	0.0073	0.0031	0.0087
SCC	0.8	0.84	0.0148	0.0456	0.0118	0.0550	0.0105	0.0368	0.0117	0.0388
LFWM	3.5	0.48	0.0095	0.0499	0.0074	0.0613	0.0080	0.0227	0.0088	0.0273
LUF	0.3	0.39	0.0169	0.0621	0.0102	0.1035	0.0055	0.0219	0.0094	0.0270

Table 3.1 Size and FA values of the examined regions of interest.

ROI size, Group mean FA. Average within (SD_{ws}) and between (SD_{bs}) subjects SD is shown for all four analysis methods. SCC: splenium of corpus callosum, LFWM: left frontal white matter, LUF: left uncinate fascicle

3.3.2 Coefficient of Variation, CV

CV_{mn} for intra- and inter-site rescans are summarised in Figure 3.3.

Comparing the examined regions, the highest CV was found for the LUF, the smallest of the three regions, and therefore most prone to partial volume effects from imperfect co-registration and interpolation. Unsurprisingly, the whole-brain average FA showed the lowest variation and also the least dependence on the applied co-registration method.

Comparing the different co-registration methods, the affine co-registration resulted, in general, in bigger variation than the non-linear methods, for most measurements. For all three regions, the CV of FA within the tract was higher than the CV of the corresponding back-normalised seed region, on average by 50%.

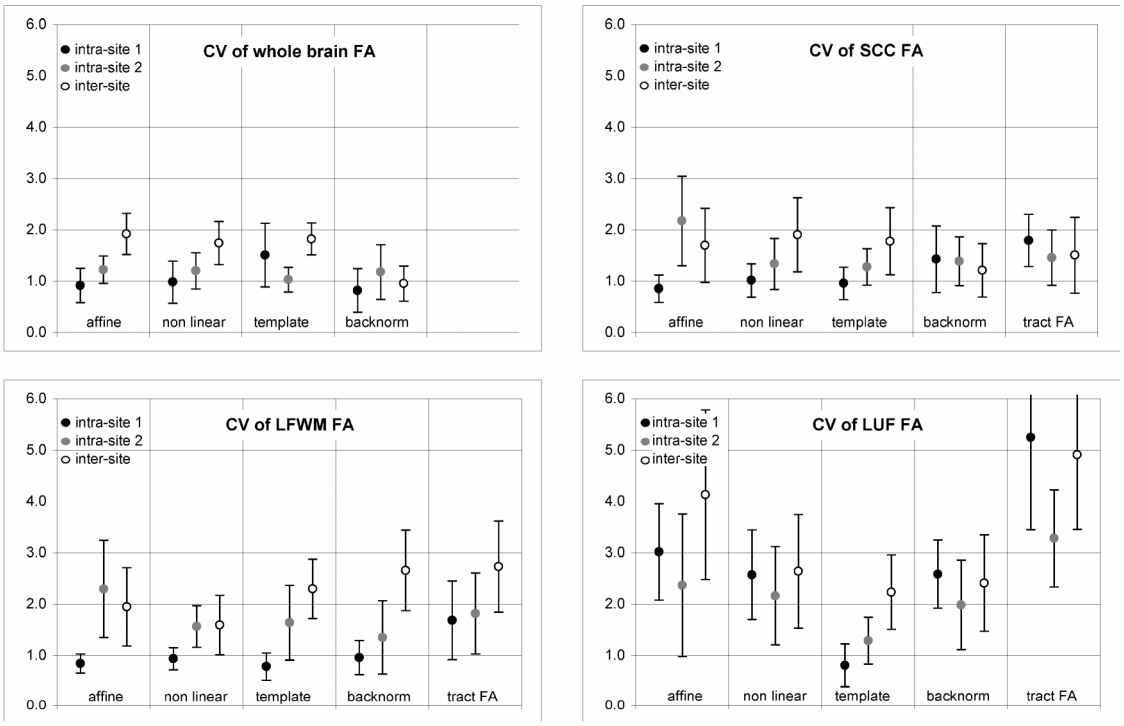

Figure 3.3 Coefficients of variation (CV).

The plots show the results obtained with different image co-registration strategies for the four examined region: The first block in each plot shows results from the rigid body affine co-registration in subject's native space. The second block shows results from non-linear warping to each subject's mean FA image in native space. The third block shows results from images normalised to template space, with all measurements done in template space. The fourth block shows results from ROI defined in template

space and back-normalised to each subject's individual native space. For the three circumscribed regions, a fifth block is included, showing the CV for average FA values within the probabilistic tract seeded from that region.

Figure 3.4 shows the average CV across all regions for a given co-registration method. The three non-linear methods did not differ significantly, but affine co-registration performed worse than any of the three methods including non-linear normalization steps (non-linear in native space, template based and back-normalised from template). The average CV from these three methods were 1.3% for intra-site 1, 1.4% for intra-site 2 and 1.9% for inter-site scan rescan.

There was a non-significant trend toward a higher intra-site CV for site 2 and both intra-site CV were significantly lower than inter-site CV (paired T-test, p=0.0026 and p=0.0015). However, using non-linear co-registration, the average inter-site CV across regions still remained very low at 1.9%.

CV for the tract volume from the three tracts is not shown in the plots; the average was 8.4% intra-site 1, 6.2% intra-site 2 and 7.4% inter-site – more than 2.5 times the variation than for the average FA within tract.

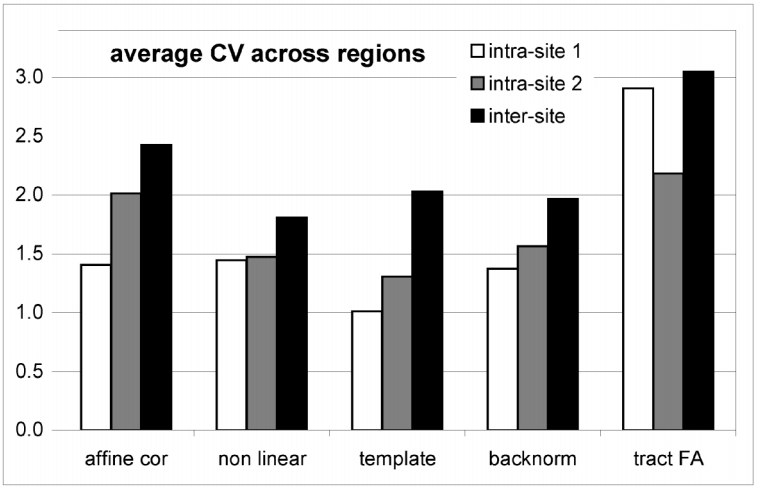

Figure 3.4 Average coefficients of variation.

Average coefficients of variation across regions. Note the additional variation, introduced by probabilistic tracking, compared to the back-normalised seed regions. Affine co-registration performed worse than any of the three methods including non-linear normalization steps (non-linear in native space, template based and back-normalised from template).

3.3.3 Intra-class correlation coefficient, ICC

The ICC relates the within-subjects variation to the between-subject variation. Results are plotted in Figure 5 for all regions and methods. The ICC values were higher for the two normalization methods in native space (affine and non-linear) compared to the two template based methods (template and back-normalised).

Like the CV values, ICC of all tract FA measures showed a much lower reproducibility than the corresponding ROI analyses (Figure 6). The lowest ICC was observed for the LUF tract FA which was only 0.55 for intra-site 1 scan rescan, compared to 0.91 for the corresponding ROI analysis.

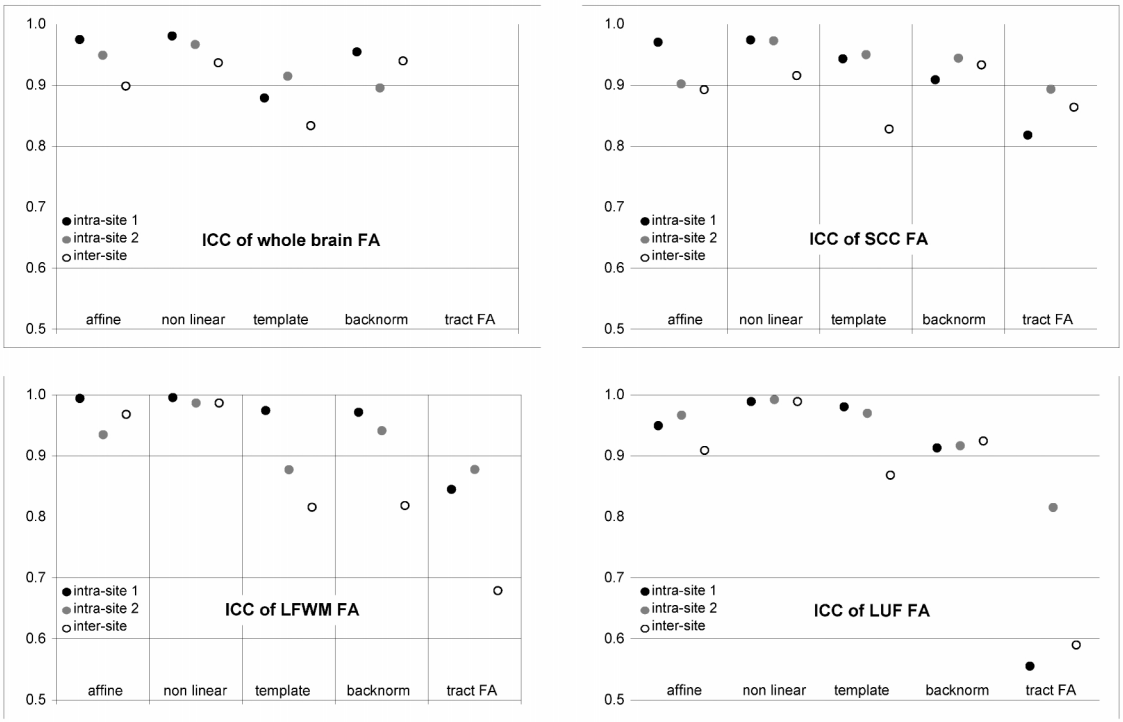

Figure 3.5 Intra-class correlation coefficient (ICC)

Note the lower ICC for template and back-normalised measures, compared to the first two methods in subject's native space. This is mainly caused by a reduced between-subject variation for the template based methods (compare table 2).

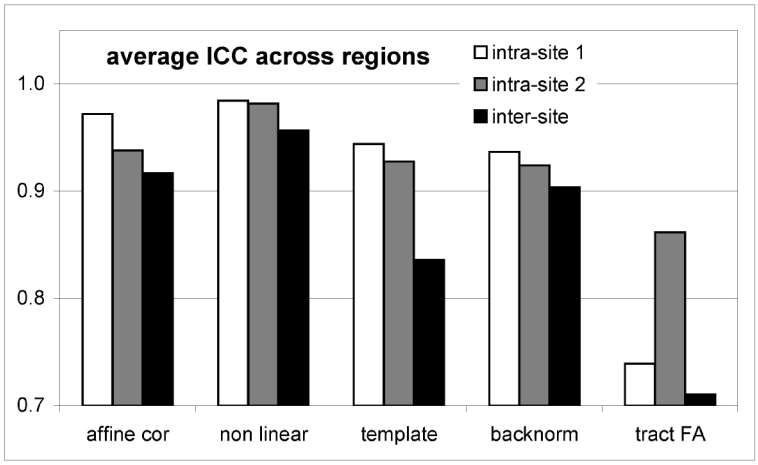

Figure 3.6 Average Intra-class correlation coefficient.

ICC was lower for template based methods (template and back-normalised) than in native space (affine co-registration and non-linear). Tract FA showed much lower ICC than ROI analysis.

3.3.4 Voxel-wise comparison

For the SCC, FA maps from the four scans were compared on a voxel by voxel basis. CVs derived from voxel-wise comparison (CV_{vw}) of raw FA images were 4.2% intra-site-1, 4.4% intra-site-2 and 4.3% inter-site, more than twice as big as those derived from the ROI mean value (CV_{mn}). This illustrates noise in unsmoothed data at a single voxel level and also the averaging effect of a ROI analysis. However smoothing the FA maps with a 4mm FWHM kernel before comparison reduced the CV_{vw} to 1.5%, 1.8% and 2.2% respectively, much closer to the ROI derived CV_{mn}.

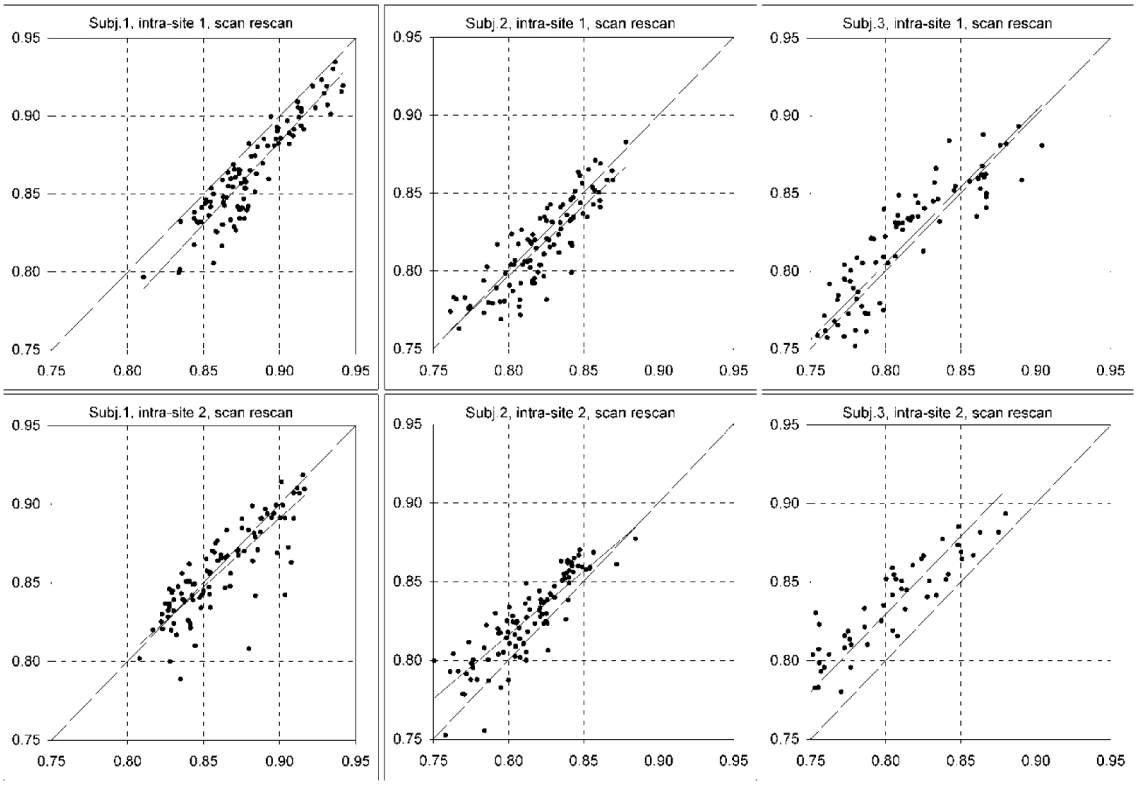

Figure 3.7 Sources of error in FA reproducibility.

This figure shows scatterplots with trend lines comparing the 100 individual voxels from the SCC ROI, derived from the smoothed FA images of the first three subjects. The upper images show intra-site-1 scan rescan correlations, the lower ones intra-site-2 correlations. The plots illustrate two effects contributing to different measurement values in repeated scans: subject 1 shows a shift of mean between the site 1 scans and single voxel outliers in the site 2 scans with an otherwise good correlation. Subjects 2 and 3 show an apparent shift of mean between scans at site 2.

3.3.5 Scanner differences

We found a consistent inter-site bias, FA values on site 2 were 1.0-1.5% lower than on site 1. This difference was slightly higher in areas with higher FA. Correction for this bias with a global scaling factor reduced the average inter-site CV for the non-linear methods from 1.9 to 1.6%. This was no longer significantly different from the intra-site CV of 1.3% and 1.4% (paired T-test, p=0.07 and p=0.18).

3.3.6 Reproducibility maps

Assessing the regional distribution of FA reproducibility throughout the scan volume identified regions with less good reproducibility. (Figure 8) The average absolute changes of FA values per voxel reached about 0.1 in the superior parietal lobe and around the brainstem. (Figure 8a) The map showing the average relative change, expressed as percentage change of the regional FA value, resembles an inverse FA image with low changes in the major white matter tracts, staying well below 5%. (Figure 8b) However, the map also shows that the average changes in cortical and subcortical gray matter were between 10 and 15%, reaching up to 25% in the superior parietal lobe.

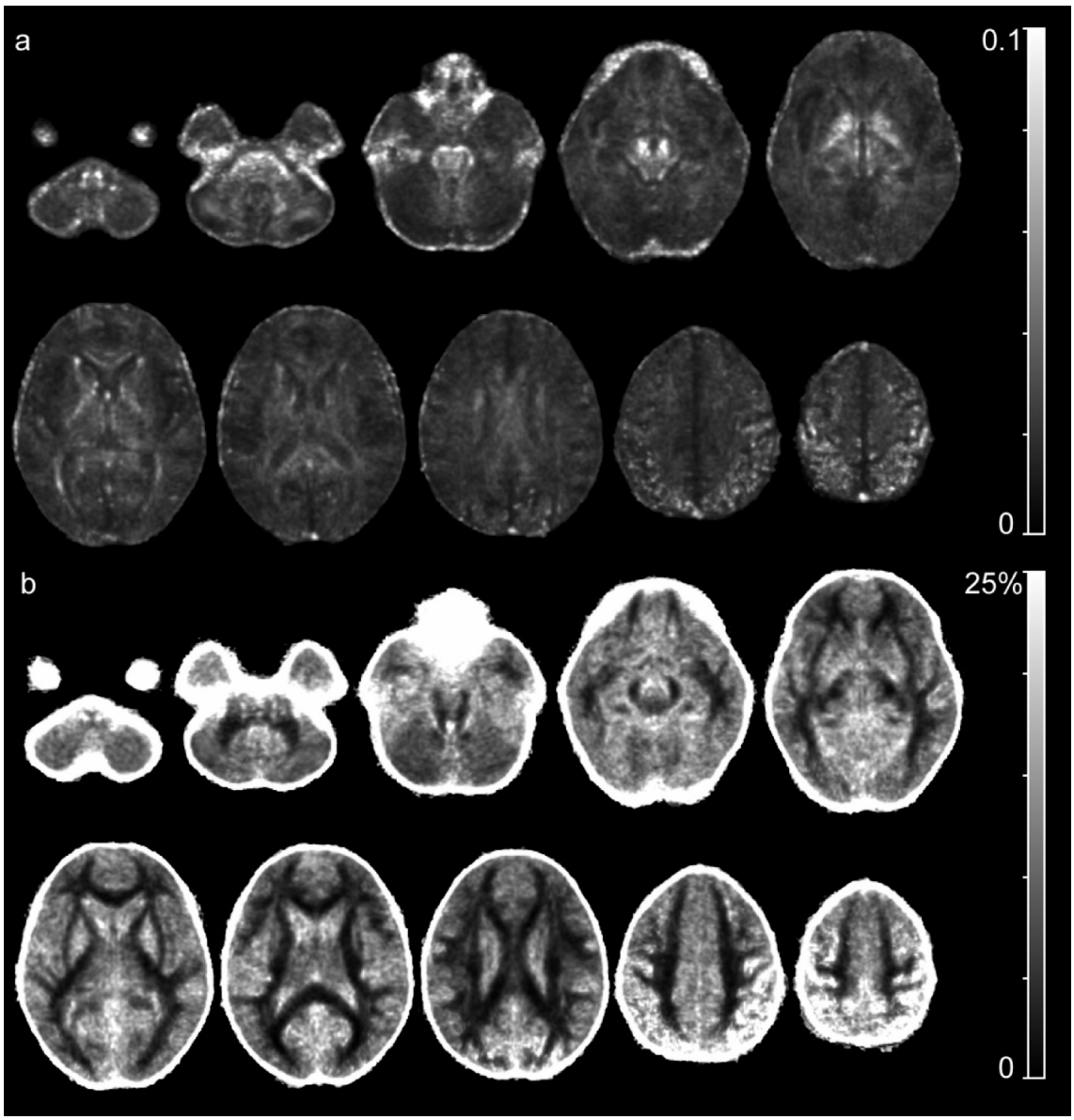

Figure 3.8 Reproducibility maps.

Regional distribution of FA reproducibility throughout the scan volume.

a): Average absolute changes of FA values per voxel were highest close to skull base and around the brainstem.

b): Average relative change, expressed as percentage change of the regional FA value stayed low in major white matter tracts but reached 10-15% in gray matter.

3.4 Discussion

We report for the first time at 3.0Tesla both intra-site and inter-site scan-rescan reproducibility of fractional anisotropy (FA) measures from DTI in nine healthy volunteers using identical scanners and acquisition protocols on two different sites. This is also the first study to assess the contribution of several image processing steps to overall reproducibility. Using appropriate co-registration techniques, intra-site and inter-site reproducibility of FA measures from a typical current best practice DTI protocol showed coefficients of variation (CV) below 2%.

3.4.1 Intra-site comparison - ROI

Our intra-site CV values ranging from 0.8% to 3.0% were considerably lower than previously reported data obtained at either 1.5T or 3T (Table 3.2), underlining the importance of factors other than field strength alone.

There are only two previous studies assessing rescan reliability of FA measures at 3T. Bisdas and colleagues (Bisdas et al., 2008) reported a CV of 2% for the SCC, only slightly larger than our average intra-site CV of 1.5% for manually drawn ROI. Their ROI in the SCC was similarly sized and two acquisitions were averaged with 16 diffusion-weighted volumes each, resulting in a total number of 32 volumes, comparable to our protocol.

The second 3T test-retest study, however, reported considerably larger CV_{md} of 3.0 % and CV_{vw} of 6.5 % for the whole cerebrum FA (Jansen et al., 2007) compared to our average intra-site CV_{mn} of 1.3% measured in template space. This is interesting, as the

'whole cerebrum' is the largest possible ROI and one would expect a low variation, simply because of the averaging effect of the large number of voxels. Indeed in our study the whole-brain measures were most robust. For all four co-registration methods, the intra-site whole-brain CVmn stayed below 1.5 %. The lower CV in our study may be due to the use of cardiac gating, as well as to the higher number of diffusion-weighted directions – 32 compared to the 15 used in Jansen's study – probably resulting in a higher signal to noise ratio (SNR) and better reproducibility in our data.

The majority of DTI reproducibility studies have so far been carried out on 1.5T scanners. Heiervang and colleagues found a whole-brain white matter CV of 0.78%, compared to our 1.3% for the whole brain, including gray and white matter (Heiervang et al., 2006). We did not segment images into gray and white matter, but our reproducibility maps have shown an approximately three times higher variation of FA in regions of gray matter and in gyri in which DTI voxels will include both grey and white matter, than in white matter, explaining the difference between these two whole-brain measures. However, the study by Heiervang study reported a considerably larger regional CV of 4.81% for the CC, compared to our 1.1% in template space. The difference between whole-brain and regional CV most likely reflects the different sized ROI volume: a small ROI is more prone to noise and partial volume effects and more likely to show a greater variation.

For all regions tested, our 3T data showed consistently lower CV than previously reported from studies using 1.5T scanners. Pfefferbaum and colleagues (Pfefferbaum et al., 2003) and Bonekamp's study (Bonekamp et al., 2007) reported intra-site rescan CV for the CC, of 1.9% and 2.6% respectively, using a larger ROI than Heiervang's study. These values are still higher, but closer to our finding of 1.5 % CV for affine co-registration. Increasing ROI size improves reproducibility, as long as contamination from surrounding structures with markedly different voxel values is avoided. This is

especially relevant for the CC, where FA drops dramatically from ~0.8 to essentially 0 in the surrounding CSF. Bonekamp and colleagues (Bonekamp et al., 2007) also assessed a ROI in the 'superior corona radiata', an area quite similar to our LFWM, and reported an CV of 3.8%, more than double our CV of 1.6%.

3.4.2 Intra-site comparison - Tractography

The additional variation introduced by a probabilistic tracking algorithm varies considerably. Two other studies have also assessed reproducibility of probabilistic tractography. Heiervang et al. (Heiervang et al., 2006) investigated the reproducibility of tracking from a seed region in the corpus callosum and their reported CV of 1.94% is very similar to our 1.6% for the average FA within the tract. Comparable to our results, they reported a much higher variation of the tract volume with a CV of 5.03%, also very similar to our average intra-site CV of 4.9%. Reproducibility of callosal fibre tracking was also assessed by Ciccarelli and colleagues (Ciccarelli et al., 2003). They reported a CV of 6.2% for the mean tract FA and 7.8% for the tract volume, both much higher than in our study (1.6% and 4.9% respectively) or in Heiervang's data. This is surprising, because this was the only other study including cardiac gating for the DTI acquisition, and this is expected to improve SNR and thereby aid good reproducibility. The high variation may stem from the specific tractography algorithm used in Ciccarelli's study.

Table 3.2

study	field strength scanner	acquisition dwd, repetitions voxel size x y z duration	N subjects age mean ± SD or [range], years	repeated scans / measures	statistics used	Reported CV whole brain [%]	Reported CV corpus callosum [%]	Reported CV other regions [%]	comment
This study	3.0 T GE Signa + GE Signa	32 dwd 2.4 x 2.4 x 2.4 mm 10 min	9 volunteers 34 ± 8	Intra-site rescan x2 Inter-site rescan x2	Mean FA from ROI	**1.1** ***1.5***	**1.2** ***1.6***	LFWM **1.2** *LFWM **2.2***	ROI SCC: 0.8 cm³ LFWM: left frontal white matter
Bisdas	3.0 T Philips Intera	16 dwd x2 2 x 2 x 3 mm	12 volunteers 38 ± 11	Intra-site rescan x2	Mean FA from ROI		**2**		ROI SCC: 0.2 cm²
Jansen	3.0 T Philips Achieva	15 dwd 2 x 2 x 2 mm 10 minutes	10 volunteers 26 ± 2	Intra-site rescan x2	Median FA Voxel-wise	**3.0** **6.5**			Images normalised to MNI Smoothed 6mm FWHM
Bonekamp	1.5 T GE	15 dwd x2 2.5 x 2.5 x 5 mm 5 minutes	10 volunteers 14.1 ± 2.8	Intra-site rescan x2	Mean FA from ROI		**2.6**	SCR **3.8**	SCR: superior corona radiata ROI: 16 voxels in single slice
Heiervang	1.5 T Siemens Sonata	60 dwd 2 x 2 x 2 mm	8 volunteers [21–34]	Intra-site rescan x3	variable	**0.78** (mean white	**4.81**		Images normalised to MNI, ROI in GCC, size 9 voxels,

					matter FA)			
Ciccarelli	1.5 T GE Signa	60 dwd 2.5 x 2.5 x 2.5 mm 20-30 min (cg)	10 volunteers 37.5 ± 9.7	Intra-site rescan	Mean FA in tract		**6.2**	4 subjects rescanned ROI: 'callosal fibres' after tracking
Cercignani	1.5 T Philips Gyroscan + Siemens Vision	6 dwd x10 or 8 dwd x8 1.95 x 1.95 x 5 mm	12 volunteers 28.9 [23-33]	Intra-site rescan x2 Inter-sequence rescan x3 Inter-site rescan x2	Mean FA from Histogram	not reported 5.45 ***7.71***		4 subjects rescanned intra-site 8 subjects rescanned inter site
Pfefferbaum	1.5 T GE Echospeed + GE Twinspeed	6 dwd x6 not reported	10 volunteers [21-33]	Intra-site rescan x2 Inter-site rescan x2	Mean FA from ROI	**1.36** ***1.93***	**1.90** ***5.20***	Images co-registered to common space ROI: 'outlined in midsagittal FA'

Table 3.2 Previous studies on DTI reproducibility.

Comparison of the results from our study with previous studies on DTI test-retest reliability. The values shown for this study are the average CV from the three non-linear methods. See Figure 3 for other values. dwd = diffusion-weighted directions, CV = coefficient of variation in %, WSV = within-subject variation, cg = cardiac gating, inter-site measures are printed italic.

3.4.3 Inter-site comparison

No study on 3T, and only very few studies on 1.5T instruments have addressed inter-site reliability of DTI measures, with inter-site differences being consistently larger than intra-site measures, as expected. Pfefferbaum (Pfefferbaum et al., 2003) reported higher variability between different scanners than for intra-site rescans, both for all supratentorial brain voxels (inter-site CV 1.93% vs. intra-site 1.36%) and for a single ROI at the CC (5.2% vs. 1.90%) . The inter-site whole-brain CV of 1.93% was similar to our 1.9% for affine co-registration, probably reflecting that a very large sample size partially compensates some regional differences in images from different scanners, even at 1.5T. However, for the region of the CC, their inter-site CV was markedly larger (5.2%) than ours (1.7%).

Cercignani et al. also assessed inter-site and intra-site variability of histogram based DTI measures in eight and four healthy subjects respectively, scanned on two different 1.5 T systems with three different acquisitions (Cercignani et al., 2003). They proposed whole image histogram based measures rather than ROI based measures. Using different scanners, CV of the whole-brain histogram derived mean FA was significantly greater (7.71%) than different acquisition schemes on the same scanner (5.45%). Both CV were relatively high, compared to our results and other studies. Due to the small number of subjects for intra-site rescanning, no direct comparison of intra-site versus inter-site rescanning was made and intra-site rescanning variation was not reported in detail.

3.4.4 Intra-class correlation coefficient, ICC

Comparing the different methods to define and align ROI, there was little difference between the CV obtained with the three methods including non-linear transformations. Because of differences in the between-subjects SD σ_{bs}, the ICC depends more on the processing method. Defining ROI in each subject's native space measures values from a customized region, defined by every subject's individual anatomy. This is optimal to pick up between-subject differences and results in a bigger σ_{bs}. Consequently the within-subject variation σ_{ws} between repeated scans contributes less, resulting in relatively high ICC values. Compared to the affine co-registration, the non-linear normalization of images in native space minimizes the σ_{ws} by a better alignment and therefore achieves the highest ICC scores of all methods. The template based methods on the other hand reduce the σ_{bs} by normalizing the region and its measurement values across subjects, thereby decreasing ICC values. This illustrates how much a statistical measure like the ICC depends on details of the image processing pipeline. For example the inter-site ICC for the LUF ROI was 0.87 for measurements in template space and 0.99 for measurements in individual ROI in native space after non-linear normalisation. Furthermore, this 'equalizing' effect of normalization to template space should to be kept in mind in patient studies, as it may indicate a loss of sensitivity to pathological changes.

Comparing our ICC values to previous studies, we also found a better reproducibility in our study. Jansen reported an ICC for whole-brain median FA at 3T of 0.73 (Jansen et al., 2007), where we measured intra-site ICCs of 0.88 and 0.91. In their 1.5 T study, Bonekamp and colleagues reported an ICC of 0.65 for a ROI in the corpus callosum (Bonekamp et al., 2007) which was 0.97 and 0.90 in our study.

3.4.5 Scanner differences

The use of two nominally identical scanners and identical acquisition protocols minimized inter-site variability. However, in spite of identical hardware, firmware and software, and identical procedures, there were still slight differences between the two scanners and the average inter-site variation was about 40% higher than the intra-site variation in our setting. Even though this is still an improvement over using different scanners with scanner variation being typically twice as high as within one site (Pfefferbaum et al., 2003), these findings also show that nominally identical scanners may operate, and be operated, slightly differently, in varying conditions and should be assessed independently. This was also shown by the consistent inter-site bias, with slightly lower FA values on site 2 (1-1.5% difference). In case of a consistent bias, it may be feasible to apply a global scaling factor to improve cross-site comparability of measurements. In our study this has reduced the average inter-site CV to under 1.7%, which was not significantly different from of the intra-site CV of site 2. In our study there was a trend towards lower variation between scans on site 1 than site 2. A possible explanation is the fact that the scanner is used more intensively on site 2, resulting in higher wear and more frequent servicing and calibrations. Such (re-)calibration may also contribute to the shifts of the mean seen in the offset of the trend lines in figure 7; because the b-value is proportional to the square of the applied gradient strength, even small changes in calibration may lead to relatively large changes in MD (and, if different along different gradient axes, FA). Frequent scanner servicing and calibration by the manufacturer is usually assumed to be beneficial, keeping the scanner performing optimally. However, it may have a disadvantageous effect on data reproducibility for DTI. Nagy et al have demonstrated a method to calibrate gradients for DTI and this may further improve reproducibility (Nagy et al., 2007).

3.4.6 Other factors influencing reproducibility

The degree of reproducibility achievable in any study is likely to be related to a number of factors. Scanner parameters like field strength or gradient performance, as well as acquisition parameters like voxel size, number of diffusion-weighted directions and the use of cardiac gating, are all likely to play a role (Alexander et al., 2006; Ni et al., 2006), as are issues such as the protocol used for subject (re)positioning. The fact that non-linear co-registration improved reproducibility compared to affine co-registration within each subject shows that different non-linear distortions appear when scanning the same healthy subject on the same scanner. Most likely these differences are due to small changes in head positioning, but other biological factors such as fluid in paranasal sinuses may also play a role. The effect of various acquisition parameters on DTI data quality has been addressed in detail in several studies (Ardekani et al., 2006), mostly on 1.5T scanners (Landman et al., 2007; Ni et al., 2006; Papadakis et al., 1999). Many of these studies used quite specific measures of the error or data quality which cannot easily be translated to a measure like the CV typically used to address data reproducibility.

Generalizing our results to other protocols is beyond the scope of the current study, and reproducibility of any proposed protocol will need to be assessed before starting large scale multi-centre studies. Our results do show, however, that with appropriate parameters, acceptable inter- and intra-site reproducibility can be achieved using a contemporary 3T scanner and a 10-minute DTI acquisition protocol.

One factor which has a particular impact on DTI data quality, and should therefore be considered when setting up multi-site studies, is the use (or otherwise) of cardiac gating. DTI sequences are designed to detect molecular diffusion and thus are naturally very sensitive to motion. Pulsation-related movement of the brain is therefore a significant

source of noise in a DTI acquisition, particularly at the level of the brainstem. This can be reduced by limiting the acquisition time to diastole when pulsation effects are minimal, although the resulting gain in data quality is achieved at the expense of a prolonged acquisition time. Several studies have addressed the time efficiency of cardiac gating: Skare et al found a 2.5 - 4 times higher variation in certain regions in ungated DWI images (Skare and Andersson, 2001), while Gui et al reported that cardiac gating roughly halved the 'total variance of the diffusion tensor' (Gui et al., 2008). Recently, Chung et al reported an almost threefold reduction of images with severe artefacts by cardiac gating, while the gating scheme increased scanning time by only 27%. They therefore state that for a given possible scanning time it is more efficient to use cardiac gating than to acquire more excitations (data averages) or more diffusion weighting directions (Chung et al., 2010). Our gating scheme used a minimum delay after peripheral gating and allowed the acquisition of two to four slices per RR cycle, depending on the subject's heart rate.

3.4.7 Reproducibility versus sensitivity

Test-retest studies allow for an estimation of reproducibility, i.e. within-subject differences. Reproducibility, however, represents only one aspect of a measurement. A method can conceivably be very reproducible at the expense of not reflecting parameters of interest at all.

The between-subjects CVmn differs significantly between the four ROI. The much higher between-subjects CVmn for the LFWM and LUF FA results in relatively higher ICC values, as the same amount of 'noise' between repeated scans is less relevant relative to the larger true biological variation between subjects.

These differences illustrate the potential discrepancies between various statistical approaches to assess the test retest reliability and their suitability for a given question. For example the ICC may not be an ideal measure in healthy control populations, as the relatively low between-subjects variation may be unrepresentative for a patient population where different degrees of pathologies will results in higher between-subjects variation. The CV may not be an ideal measure of precision, because of its dependency on the measured mean value. Furthermore, neither the CV nor the ICC takes into account possible shifts of the mean value (i.e. accuracy), which has to be assessed independently. A method's reproducibility needs to be balanced against its sensitivity (Heiervang et al., 2006). Measures with a very good reproducibility - such as whole-brain measurements - may be insensitive to pathological changes in clinical studies. On the other hand, clinically more relevant, hypothesis driven measures, targeted to a specific, smaller region of interest, may show greater sensitivity to pathological changes – and at the same time have a poorer reproducibility, due to a higher sensitivity to subtle variations in data or influences from image processing. It is therefore crucial to know the margin of reproducibility for a given measure, to detect clinically relevant changes beyond the methods noise.

3.5 Conclusion

Using the methods described, with two identical 3T scanners, we obtained a consistently low variation of FA measures between scans for both intra- and inter-site rescanning with average CV between 1% and 2 %. Compared to previous studies on 1.5 T scanners, this represents an improvement of reproducibility by approximately a factor of two.

Improvements in MRI data reproducibility are the result of a number of contributing factors. The gradient performance of a contemporary 3T scanner allows shorter echo times for a particular degree of diffusion sensitization (b-value), and this, along with increased field strength, increases SNR. The use of cardiac gating helps to reduce pulsation-related motion artifacts in the inferior part of the brain, and, the use of cardiac gating is usually recommended in present-day DTI. For an ROI-based study, careful positioning of the ROI can aid reproducibility by reducing partial volume contamination from areas of high variability. Using non-linear normalization between scans is beneficial to account for different distortions between scans. Probabilistic tractography introduced approximately 50% additional variation compared to a ROI analyses. This should be justified by a clear anatomical hypothesis about the involvement of a specific white matter tract, when tracking is used rather than a ROI analysis. Tract volume showed the lowest reproducibility with an average CV of more than 7%. Reproducibility of FA in subcortical gray matter and cortical gyri containing white and gray matter within the scale of DTI voxels was poor, with variations up to 15%, illustrating that DTI is more robust for assessing white matter characteristics.

The observed inter-scanner differences illustrate that nominally identical scanners give slightly different results. However, given the fact that cross-site variation between different scanners is usually more than double the intra-site reproducibility, and that the overall variation in our study was much lower than previously reported, our findings support the feasibility of cross-site pooling of DTI data from identical scanners. An average inter-site CV of less than 2% for FA measures is encouraging, and paves the way for multicentre studies of DTI, allowing the recruitment of larger subject numbers across different sites.

4. Juvenile Myoclonic Epilepsy – functional effects

(Vollmar et al., 2011)

4.1 Background

Juvenile myoclonic epilepsy (JME) is the most frequent idiopathic generalised epilepsy (IGE) syndrome (Janz and Christian, 1957; Janz, 1985). The most characteristic feature of JME is myoclonic jerks of the proximal upper extremities. Patients with JME are particularly susceptible to seizure facilitation through sleep deprivation, alcohol consumption or photic stimulation. Furthermore, there are specific seizure triggers not commonly observed in other epilepsy syndromes, such as cognitive activities like reading, calculation or decision making (da Silva Sousa et al., 2005a, 2005b), and induction of seizures by praxis, i.e. the imagination or execution of complicated movements, including sequential spatial processing, such as drawing, writing, playing games, or instruments (Inoue et al., 1994; Yacubian and Wolf, 2014).

These reports are in line with electrophysiological studies on provocative effects of cognitive tasks on epileptiform discharges, where an increased spike frequency during neuropsychological activation was found in patients with JME (Matsuoka et al., 2005)(Guaranha et al., 2009). Both studies reported that the combination of a cognitive task with a manual motor response was a stronger trigger of EEG discharges than a purely cognitive task.

The predominance of myoclonic jerks in JME has led to the motor circuitry hyperexcitability hypothesis. This has been addressed by studies using transcranial magnetic stimulation with paired-pulse paradigms, which showed increased cortical excitability in the motor cortex of JME patients compared to healthy controls (Manganotti et al., 2004) (Badawy et al., 2006) (Badawy et al., 2009b). The crucial role of motor cortex hyperexcitability in the generation of myoclonic jerks is supported by a study that used jerk-locked back averaging of EEG and found evidence for focal cortical generation of myoclonic jerks in JME, with frontocentral polyspikes preceding the jerks by 10 ms (Panzica et al., 2001). This is the same time difference, also described for the transcallosal propagation of generalised polyspikes after focal onset (Brown et al., 1991) (Serafini et al., 2013).

It is still not clear how myoclonic jerks are facilitated by cognitive effort. Motor circuitry hyperexcitability has not yet been linked to the predominantly frontal changes reported in JME, which consist of (1) generalised spike- and polyspike-wave complexes with frontocentral maximum, (2) neuropsychological deficits in frontal lobe executive and memory functions (Devinsky et al., 1997; Pascalicchio et al., 2007; Piazzini et al., 2008; Wandschneider et al., 2010), and (3) subtle neuroimaging abnormalities in the mesial and dorsolateral pre-frontal lobes (Koepp and Woermann, 2005; O'Muircheartaigh et al., 2011; Vulliemoz et al., 2011; Woermann et al., 1999b)

The aims of the present study were to investigate cognitive activation and functional connectivity patterns of the motor system and pre-frontal cortex, and how these are modulated through cognitive interactions in patients with JME compared to healthy controls.

4.2 Subjects and Methods

4.2.1 Study population

Thirty patients with JME (17 female, mean age 32.8 years, SD 9.9) and 26 age and gender-matched healthy controls (14 female, mean age 31.4 years, SD 8.2) were included in this study. All patients had a typical clinical history of JME with onset of myoclonic jerks and generalised seizures in adolescence, at least one EEG showing generalised spike-wave or polyspike-wave complexes and normal clinical MR imaging. All patients except one were taking antiepileptic medication. Fourteen patients had been seizure free for at least one year. Healthy controls had no history of neurological disease or family history of epilepsy and had normal structural neuroimaging.

4.2.2 Data acquisition

MRI data were acquired on a GE Excite HDx 3T scanner, using a multichannel head coil and parallel imaging with a SENSE factor of two. We used a 50 slice gradient-echo echo-planar imaging (EPI) sequence in AC-PC orientation with 2.4 mm thickness and 0.1 mm gap, providing full brain coverage. Slices had a 64x64 matrix with 3.75x3.75 mm voxel size. TR was 2500 ms and TE 25ms. The first four scans from every functional paradigm were discarded to ensure magnetization equilibrium.

4.2.3 fMRI paradigms

All subjects performed five different cognitive fMRI paradigms, which are described in more detail in chapter 2.5.1 fMRI paradigms (page 90).

4.2.3.1 Dot-Back task

In this spatial working memory paradigm, the subjects were presented with randomly appearing dots and had to respond to the dots sequentially with a joystick at their right hand. They were instructed to move the joystick to the position of the current dot in the "0-back" condition, to the position of the previous dot in "1-back"' and to the position of the dot two presentations back in "2-back"' blocks. These three 30-second active conditions were repeated five times, in pseudo-randomised order and alternated with 15-second rest blocks (Design matrix shown in Figure 4.1).

4.2.3.2 Language tasks

I acquired two different language paradigms:

The Verbal Fluency paradigm consisted of five 30-second blocks where a letter was presented with the instruction to think of words starting with this letter.

The Verb Generation paradigm contained two active conditions in 30-second blocks, interleaved with resting blocks. Subjects were instructed to either mentally repeat the word presented on the screen, or to think of a verb associated with the presented noun.

4.2.3.3 Memory-encoding

During the memory paradigm, subjects were presented ten items each in 30-second blocks and were instructed to memorise them. Additionally they had to indicate whether

they liked an item or not with a joystick response. Blocks comprised either words or pictures or faces in a pseudo-randomised order. Faces had different emotional expressions and could be neutral, happy or fearful. Item recall was assessed after the MRI scan.

4.2.3.4 N-Back task

In this verbal working memory paradigm, words were presented sequentially in 30-second blocks, interleaved with resting blocks. Subjects were instructed to watch out for the word "bird" in the control condition and for a repetition of the word two presentations earlier in the "Two-Back" condition and indicate their occurrence with a joystick response.

4.2.4 fMRI processing and analysis

fMRI analysis was performed using Statistical Parametric Mapping software, (SPM5, Revision 0958, http://www.fil.ion.ucl.ac.uk/spm).

Images were realigned for movement correction, normalised to an acquisition-specific EPI template in MNI space, re-sampled to isotropic 3 x 3 x 3 mm^3 voxels and smoothed with an 8 x 8 x 8 mm^3 kernel.

Single-subject statistical analysis of fMRI data was performed, using a full factorial block design, including movement parameters as regressors. Task conditions were

modelled as 30-second blocks. Convolution with SPM's default canonical haemodynamic response function was applied.

Contrasts were defined, comparing every task conditions against the resting baseline, and comparing different task conditions with each other.

For example in the dot-back task, the "2-back minus 0-back"' contrast controls for the visual input and for the motor response, and selectively reveals the additional cortical responses to the increasing working memory load.

To identify task-negative areas, i.e. areas increasingly deactivated with increasing task difficulty, I defined an additional contrast with values -1, -2 and -3 for the three conditions "0-back", "1-back" and "2-back", modelling linear deactivation compared to the resting periods (Figure 4.1).

Single-subject fMRI results were rendered on sections of individual mean EPI images and group results were rendered on sections or on a 3D surface created from the MNI152_T1 dataset.

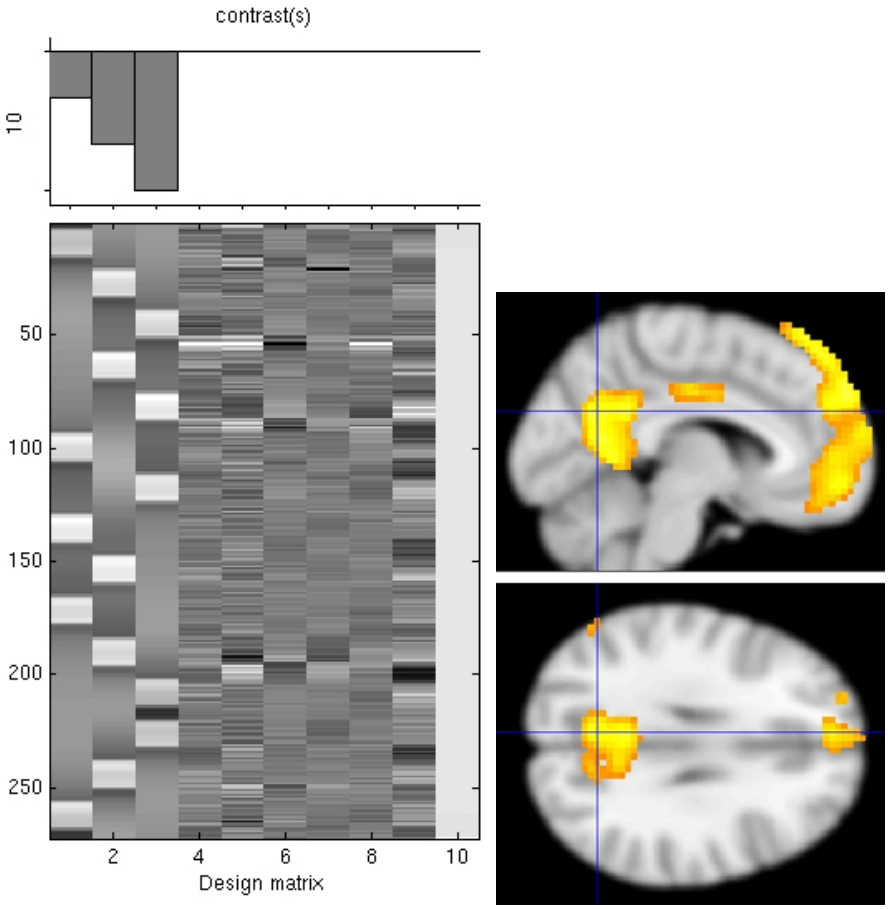

Figure 4.1 Task-negative contrast.

A) SPM contrast and design matrix for the task negative contrast from one subject, modelling increasing deactivation with increasing task difficulty.
B) Typical areas of the default mode network, identified by this contrast in one subject

Group comparisons between JME patients and healthy controls were carried out as two sample t-tests or using a full factorial design. Group statistics were corrected for multiple comparisons across the whole brain, using the false discovery rate method (FDR). As group results vary in statistical strength, the threshold was adjusted between $p<0.05$ and $p<0.0001$ for visual clarity of figures. When no differences between groups are reported, the data have also been tested at a lower, uncorrected, threshold and "no difference" was reported if uncorrected p remained >0.05. An extent threshold with minimum cluster size of 20 voxels (540mm^3) was applied to all analyses.

For correlation analyses, the extracted fMRI response from each subject was correlated against a variable of interest, e.g. the seizure free interval.

4.2.5 Functional connectivity

To assess functional connectivity (FC) between activated areas in the dot-back task, I defined regions of interest (ROI) by activation in the combined group activation maps from JME patients and healthy controls. Two spherical 56 voxel ROI were defined at local maxima of the group activation location from the "0-back" condition: one in the left sensorimotor cortex and one in the left supplementary motor area (SMA). Two additional ROI were defined from the group activation map of the "2-back minus 0-back" contrast, in the left and right dorsolateral pre-frontal cortex (location of ROI shown as crosshair in Figure 4.5). The average time series were extracted from all four ROI for each subject and were used as a regressor for new general linear model fMRI analyses in SPM (also see Figure 1.2, page 70). Correlation of other voxels signal time series with this extracted signal time series from the ROI reveals areas functionally coupled to the ROI.

4.2.6 Independent component analysis

Independent component analysis (ICA) was carried out at a group level using FSL's MELODIC software (http://www.fmrib.ox.ac.uk/fsl/). A 4D file of the realigned, normalised and smoothed images was created for each subject and image data were pre-filtered with a high-pass filter with cut-off at 100 seconds. The algorithm was constrained to identify 32 independent components, common across all subjects in each group and characterized with regard to location, spatial extent and signal time course.

Components were ranked according to their relative contribution to overall signal variance. No manual selection or rejection of components was done.

4.3 Results

The most significant differences between JME and healthy controls were found in the cognitively most demanding Dot-Back task. Hence, this task was analysed in more detail, using different analytical approaches such as functional connectivity or ICA to further investigate these differences.

The findings in other fMRI paradigms were less significant but still confirmatory or contributed additional information. Therefore only basic group comparisons have been carried out for these paradigms

Only subjects with sufficient fMRI activation in the single subject analysis at a threshold of at least $p<0.05$ (uncorrected) with a cluster extend threshold of 20 were included in group analyses. In the JME patient group, this lead to the exclusion of data from 3 patients for the Dot-Back task, 1 for the N-Back task, 2 for the Verbal Fluency task and 2 for the Verb Generation task. In the control group, data from 3, 2, 1 and 2 subjects were excluded accordingly.

4.3.1 Dot-Back task

4.3.1.1 Task performance

Both groups, healthy controls and patients with JME performed equally well during the three conditions ("0-back", "1-back", "2-back") with an average success rate of 88%, 81%, 70% for controls, and 87%, 86% and 68% for JME, respectively (two sample T-test, $p=0.88$). Both groups showed a similar range of success rate from 28% to 100%, with one subject in each group achieving 100% correct responses. Both groups showed

a constant average success rate over the five repetitions of the task, there was no significant improvement or decline of performance during the task in either group.

4.3.1.2 Group effects

In the "0-back" condition all subjects showed left central and bilateral SMA activation, reflecting the right hand motor response, (Figure 4.2 A, motor response shown in blue, FDR, $p<0.0001$). By subtracting "0-back" from "1-back" and "2-back" we controlled for this motor component, the resulting contrast maps showed significant bilateral frontal and parietal activation of the working memory network (Figure 4.2 B and C, cognitive response shown in red, FDR, $p<0.001$).

4.3.1.3 Group differences

Group differences are shown in orange in Figure 4.2 D-F. There was no group difference for the "0-back" task (Figure 4.2 D, $p>0.05$). JME patients showed increased motor cortex and SMA activation in the "1-back minus 0-back" contrast compared to healthy controls (Figure 4.2 E, FDR, $p<0.05$) and this increased with additional task load for the "2-back minus 0-back" contrast (Figure 4.2 F, FDR, $p<0.05$). There were no areas of higher activation in controls compared to JME for any contrast ($p>0.05$).

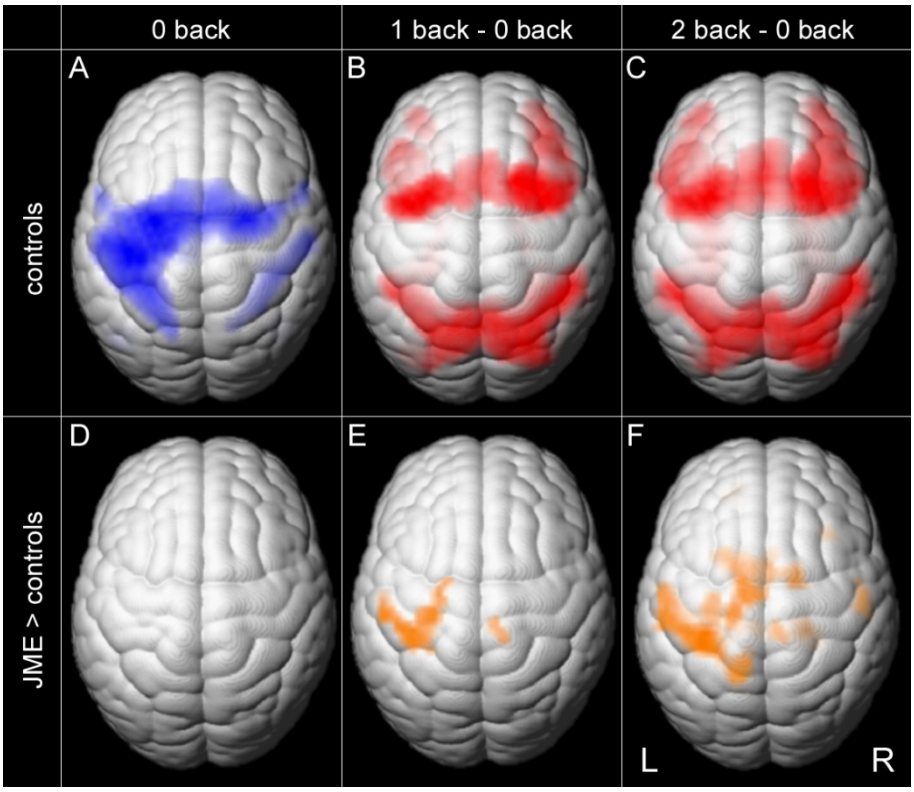

Figure 4.2 fMRI activation from dot-back working memory task.

Group fMRI activation maps of healthy controls (A-C) show cortical activation for the three different task conditions: Motor cortex and SMA activation for "0-back" shown in blue (A, FDR, $p<0.0001$). Bilateral frontal and parietal activation for "1-back minus 0-back" and "2-back minus 0-back" shown in red (B and C, FDR $p<0.001$).

Increased activation in JME patients compared to healthy controls is shown in orange in the lower row: no difference for the "0-back" condition (D, unc., $p>0.05$), but higher activation in motor cortex and SMA was seen in JME with increasing task difficulty in the "1-back minus 0-back" (E, FDR. $p<0.05$) and "2-back minus 0-back" (F, FDR, $p<0.05$) contrasts.

4.3.1.4 Correlation with success rate

In healthy controls, the success rate in the '2 Dot-back' task showed a strong correlation with right parietal cortex activation ($R = 0.91$, image thresholded at $p<0.001$ uncorrected). In JME patients this correlation was not seen. At lower thresholds, a correlation of success rate with left motor cortex activation was seen in JME patients ($R = 0.49$, image thresholded at $p<0.05$ uncorrected) (Figure 4.3).

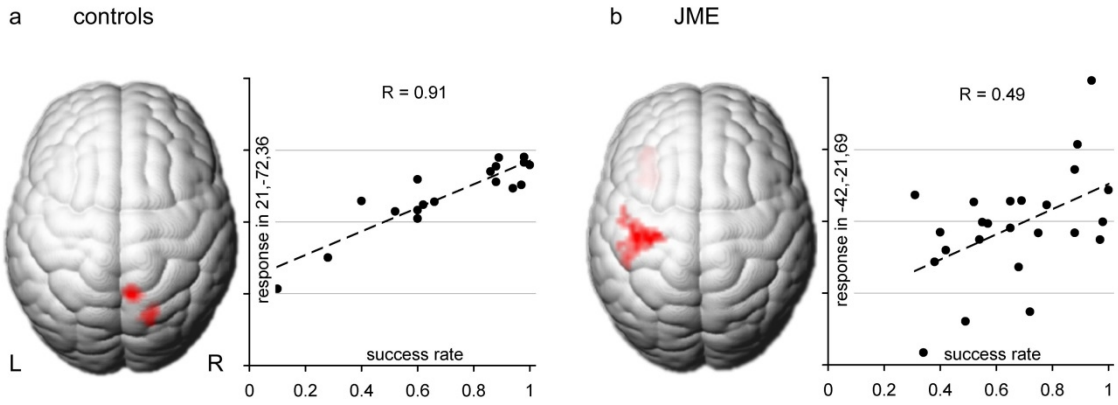

Figure 4.3 Correlation with success rate.

A) In healthy controls, right parietal activation was strongly correlated with success rate during the task. B) This correlation was not seen in JME. Instead, higher success rate was correlated with higher activation of the left motor cortex in JME

4.3.1.5 Correlation with Seizure frequency and medication

In our JME patient cohort, the interval between the date of the last seizure and the fMRI scan ranged from 1 to 4500 days. Left motor cortex activation correlated negatively with duration of the seizure free interval (Figure 4.4 A, voxels overlaid in sectional image thresholded at $p<0.05$ uncorrected, $R=-0.49$). That is, greater motor cortex activation was seen in those JME patients with more recent seizures. No patient reported any myoclonic jerks during the experiments.

Additional post-hoc analyses were carried out to assess the effect of medication on the fMRI response in JME. Twenty-one of the 30 JME patients were treated with sodium valproate (400 to 2400 mg per day, at the time of the study). A negative correlation was found between left motor cortex activation and the daily valproate dose (Figure 4.4 B, $R=-0.52$). Activation of the bilateral frontal and parietal working memory network, on the other hand, correlated positively with the daily dose of valproate in JME patients (Figure 4.4 C, $R=0.63$).

There was no significant correlation between the seizure free interval and the daily valproate dose (R=-0.17)

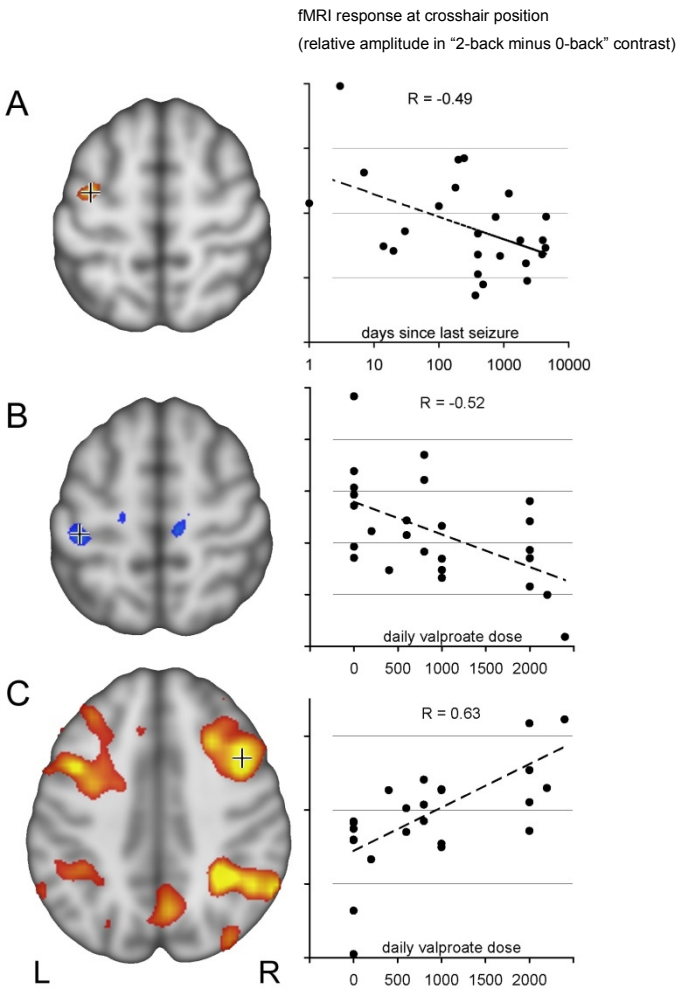

Figure 4.4 Correlations of fMRI activation in patients with JME.

Motor cortex co-activation correlates with seizure activity and treatment with sodium valproate. The crosshair position in the sectional images shows from which voxel the fMRI response was extracted for correlation. fMRI response is the relative amplitude in “2-back minus 0-back” contrast.

(A) Activation in the left central region in “2-back minus 0-back” contrast was stronger in JME patients with more active disease. Overlay is thresholded at $p<0.05$ (uncorrected, R=-0.49).

(B) Post-hoc analysis of drug effects indicates a specific effect of valproate in patients with JME. Left central activation was lower in patients with higher daily valproate dose ($p<0.05$, uncorrected, R=-0.52).

(C) Activity within the typical bilateral frontal and parietal working memory network, on the other hand, correlated positively with valproate dose, indicating a normalizing effect of valproate on the cortical activation pattern in JME ($p<0.05$, uncorrected, R= 0.63).

4.3.1.6 Functional connectivity

The group analysis of functional connectivity (FC) maps in controls showed that the signal from left motor cortex and SMA was highly correlated with the signal from contralateral motor cortex, SMA and bilateral parietal regions (Figure 4.5 A, $p<10^{-8}$, FDR). Group FC maps from the two frontal ROI activated by the "2-back" condition, largely resembled the bilateral frontal and parietal working memory network (Figure 4.5 B, $p<10^{-8}$, FDR).

In patients with JME, FC of the left motor cortex and SMA was increased within the motor system and to bilateral pre-frontal cortex, including areas activated by the working memory task (Figure 4.5 C, $p<0.001$, FDR).

FC analysis of the two dorsolateral pre-frontal regions showed greater functional connectivity to the mesial central region, SMA and mesial pre-frontal areas in JME (Figure 4.5 D, $p<0.005$, FDR).

There were no areas of higher connectivity in controls compared to JME patients in any of the FC maps ($p>0.05$, uncorrected).

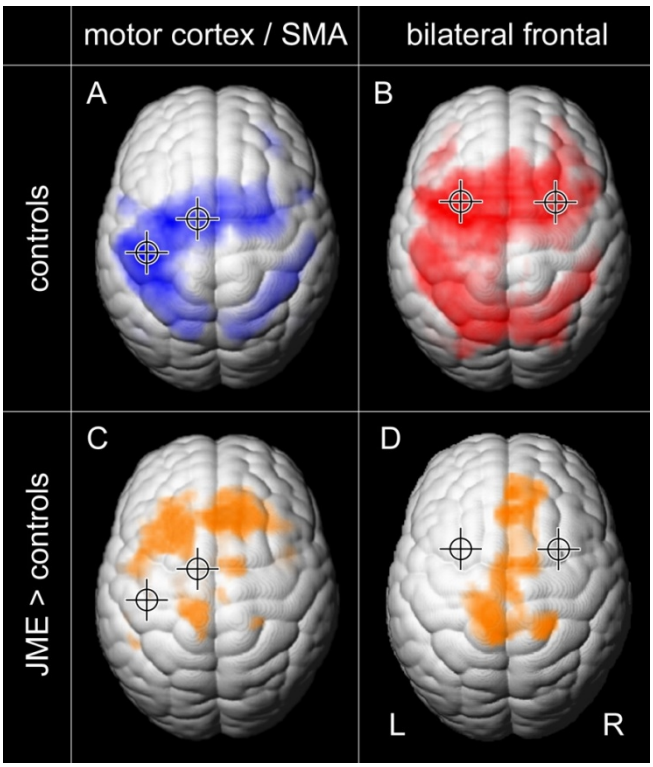

Figure 4.5 Functional connectivity (FC) is increased in JME.

A) Group FC maps of healthy controls show functionally connected cortical areas for the left motor cortex and SMA in blue ($p<10^{-6}$, FDR). Crosshair shows location of the two seed regions.

B) Group FC maps of healthy controls for the bilateral frontal working memory network, seeded from two regions in the dorsolateral pre-frontal cortex, is shown in red ($p<10^{-6}$, FDR).

Group difference maps show increased FC in JME compared to controls in orange:

C) Motor cortex and SMA are increasingly connected to pre-frontal cortex in JME ($p<0.001$, FDR)

D) The bilateral working memory network shows increased FC to the mesial central region, SMA and mesial pre-frontal areas in JME patients ($p<0.005$, FDR).

4.3.1.7 Areas of deactivation during the task

The task-negative contrast showed large clusters of deactivation with increasing task difficulty in the known default mode networks (DMN) in controls, namely the precuneus and anterior mesial pre-frontal cortex (Figure 4.6 A, FDR, $p<0.003$). In JME patients, we observed similar but less extensive deactivations (Figure 4.6 B, $p<0.003$, FDR). Direct group comparison revealed clusters that were less deactivated, i.e.

remained persistently active, in JME in the mesial central and frontal regions (Figure 4.6 C, $p<0.01$, unc., peak voxel survived FDR correction within a 20mm spherical ROI in the SMA, $p_{FDR\text{-}corr}=0.025$).

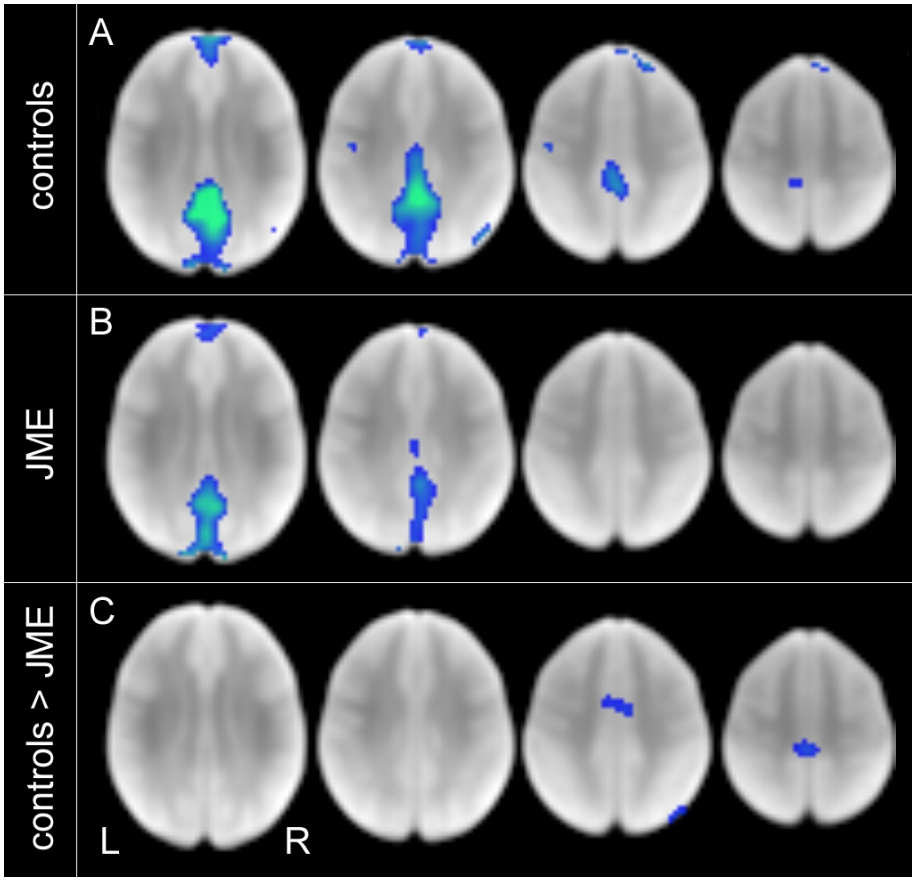

Figure 4.6 Deactivation of the default mode network is reduced in JME.

A) The task-negative contrast shows that both, precuneus and mesial pre-frontal areas are deactivated during the working memory task in healthy controls ($p<0.003$, FDR).

B) Deactivation is also seen in JME, but less pronounced ($p<0.003$, FDR).

C) The most significant group difference: patients with JME deactivate less in mesial central and frontal areas, including the SMA ($p<0.01$, unc.).

4.3.1.8 Independent component analysis

The 32 independent components identified by independent component analysis (ICA) explained 92% of the total fMRI signal variance in controls and 91% in JME. In both groups, the first component (explaining 7.4% and 7.0% of the total signal variance in controls and JME) was located in the left central region, representing the motor response of the task (controls: Figure 4.7 A, JME: Figure 4.7 C). This component's signal changes were time-locked to the task timing (frequency 1/45 sec^{-1}), and the response showed the same amplitude across all three task conditions. The second most relevant component identified in controls and JME patients (explaining 6.6% and 5.3% signal variance) comprised the working memory network, including bilateral frontal and parietal clusters (Figure 4.7 B and D). This component's response showed a strong correlation with the cognitive load of the current task condition, with higher amplitude in more difficult conditions.

Additional components within the left motor area, whose response was also modulated by task difficulty, were found in JME patients (Figure 4.7 E). No such modulated motor components were seen in healthy controls.

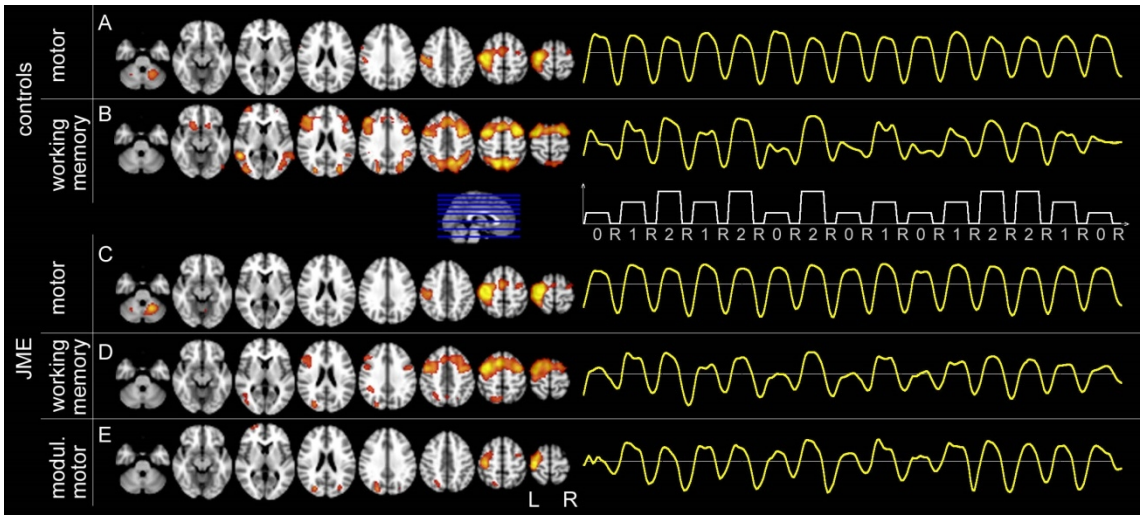

Figure 4.7 Group independent component analysis.

Independent component analysis (ICA) shows additional task-modulated sub-components of the motor system in JME.

This Figure shows the location of major components common to all subjects on the left hand side and the corresponding group average signal time course during the experiment on the right (onset and duration of the three task conditions 0-back (0), 1-back (1), 2-back (2) and rest (R) are indicated by the white plot).

The two most relevant components identified in controls were: motor cortex (A), which shows constant response amplitude throughout all task conditions. The working memory network (B) is modulated by task difficulty, with stronger activation during more demanding task conditions. Similar main components were found in JME: motor cortex (C) and working memory network (D). JME patients showed additional sub-components of the motor system, not seen in controls (E): in this additional component, the motor cortex response was also modulated by task difficulty, similar to the modulation seen for the working memory network component.

4.3.2 Language fMRI

No significant group differences were found for the Verbal Fluency paradigm.

In the Verb Generation paradigm, JME patients showed an increased activation in the left precentral gyrus during the verb generation blocks, but not in the word repetition blocks ($p<0.01$, uncorrected)

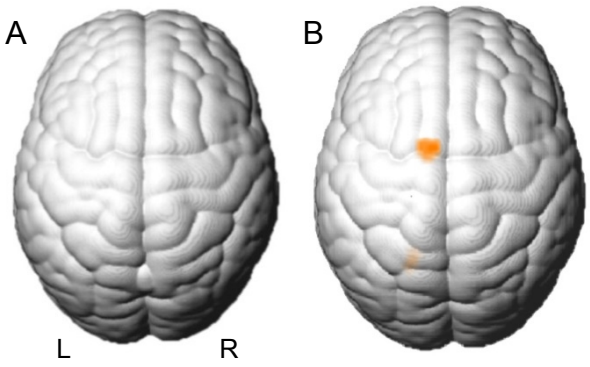

Figure 4.8 Increased activation in JME during Verb Generation.

In the Verb Generation paradigm, there was no group difference during the word repetition block (A), but JME patients showed an increased activation in the left precentral gyrus during the verb generation blocks (B, $p<0.01$ uncorrected)

There were no brain areas of significantly decreased activation in patients with JME as compared to healthy controls in the Verbal Fluency paradigm or in the Verb Generation paradigm.

4.3.3 Memory fMRI

There were no significant differences between JME and controls for the encoding of word or pictures. No differences were found in the block design analysis of encoding faces either. In an event-related analysis of face-encoding, which compared the BOLD

response to viewing neutral faces and to viewing fearful faces, there was increased activation in JME during the viewing and encoding of fearful faces bilaterally in the mesial central and precentral areas bilaterally and in the left amygdala ($p<0.01$ uncorrected).

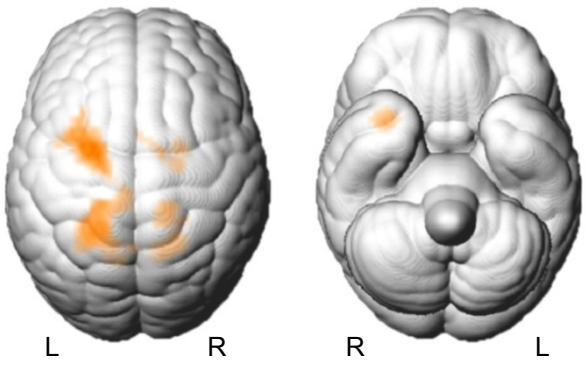

Figure 4.9 Increased activation in JME during encoding of fearful faces.

Encoding of fearful faces resulted in increased activation in JME patients in bilateral mesial central and precentral regions and in the right amygdala ($p<0.01$, uncorrected).

4.3.4 Verbal working memory fMRI

In the N-Back verbal working memory paradigm, there were no group differences for the control condition. For the N-back minus control contrast, JME patients showed lower activation in the bilateral fronto-parietal working memory network ($p<0.05$, uncorrected).

This was the only paradigm where JME patients showed less activation than healthy controls during task performance. At the same time, JME patients showed more

activation than controls in the mesial parietal and frontopolar region, representing the default mode network ($p<0.05$ uncorrected).

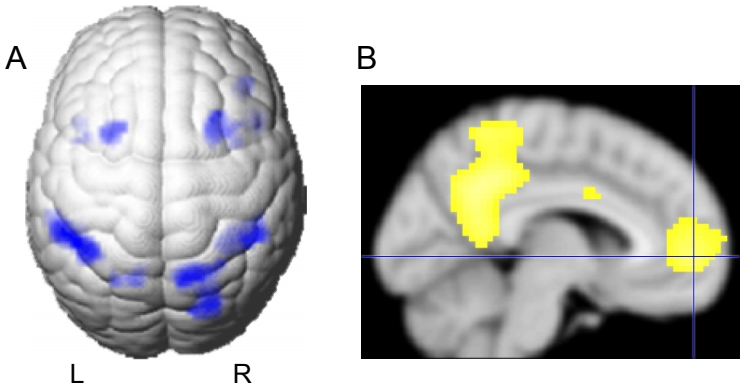

Figure 4.10 Reduced activation with verbal working memory paradigm.

JME patients showed a reduced activation of the bilateral fronto-parietal working memory network during the verbal working memory paradigm, compared to healthy controls (A, $p<0.05$, uncorrected).

Activation of areas from the default mode network was increased in JME (B, $p<0.05$, uncorrected)..

4.4 Discussion

Our study showed increased co-activation of the motor system in patients with JME during a highly demanding cognitive fMRI task. There was an increased functional coupling between pre-frontal and parietal cognitive areas and the motor cortex in patients with JME, compared to healthy controls.

Hyperexcitability within the motor cortex has previously been described in JME, mainly by transcranial magnetic stimulation studies (Badawy et al., 2009a). In our study, we demonstrate increased motor cortex co-activation, triggered by cognitive effort in fMRI. Our findings provide an explanation for the characteristic phenotype of JME, the myoclonic jerks, and its facilitation through cognitive stressors. This is clinically relevant, as such cognitive trigger factors are not always recognized by patients and

physicians (da Silva Sousa et al., 2005b), and may be associated with poor seizure control (Matsuoka et al., 2002).

4.4.1 Seizure facilitation through interaction between cognitive systems and the motor system

Our spatial working memory task is cognitively demanding, requiring continuous attention throughout the task. The motor cortex co-activation seen in JME clearly depended on the task difficulty and only occurred under high cognitive load. This may explain why a previous fMRI study, which used an easier working memory paradigm, failed to find differences between JME patients and controls (Roebling et al., 2009). In their experiment, the two groups achieved a success rate of 93% and 94%, compared to 79% and 68% in our study. This indicates that their task was relatively easy to carry out and suggests that the threshold needed to elicit the hyperactivation in JME was not reached.

Recent neuropsychological-EEG studies have shown, that the combination of a cognitive task with a motor response had the strongest provocative effect on epileptiform discharges or myoclonic jerks (Guaranha et al., 2009; Matsuoka et al., 2005). Our dot-back paradigm design was therefore well-suited to trigger provocative effects.

The fast polyspike component on EEG back-averaging preceding myoclonic jerks (Panzica et al., 2001), and increases of EEG activity by cognitive performance are all in the same frequency band of 16 -27 Hz (Papanicolaou et al., 1986), which is also similar to fast central movement-related rhythms. We hypothesize a trigger mechanism of

cognitive activity with increasing beta rhythms generated in cognitively activated areas, spreading into the motor system, where resonance effects with intrinsic motor cortex frequencies can ultimately result in polyspikes and myoclonic jerks. More demanding tasks recruit larger neuronal networks and therefore are more likely to reach the critical mass for such a spread. The increased provocative effect of combined cognitive and motor tasks could stem from the fact that such tasks elicit activation with similar frequencies in both, the cognitive and the motor networks, which in turn increases the likelihood of interferences between them.

It is important to note that there were no differences in performance between the two groups. While this may reflect a positive selection bias of relatively good performing patients, it is important to note that only in the case of matched performance, it is possible to compare fMRI activation patterns without performance bias.

The differences in fMRI activation correlation with success rate further support this hypothesis. The observed correlation of right parietal activation with increasing success rate in healthy controls is a reasonable finding for a demanding spatial cognitive task. It shows that in the group of healthy controls, subjects with stronger activation of the right parietal lobe achieved better performance in the task. The absence of this correlation between right parietal activation and success rate in JME patients indicates that, in the JME population, there is no such common key region, resulting in good performance. Instead, the individual cognitive networks recruited for successful response to the task differ more between patients with JME than between controls.

While the activation of cognitive cortical areas appears more variable, there is a different common effect in JME: at a lower statistical threshold, there was a correlation

of success rate with left motor cortex activation. JME patients with higher success rate showed higher activation in the motor cortex. This correlation shows that in our group of JME patients, cognitive efforts consistently leads to increased co-activation of the motor cortex, rather than leading to activation of specific cognitive areas.

This interaction between the cognitive system and the motor system, directly relates to the phenomenon of praxis-induction (Yacubian and Wolf, 2014), where the combination of a cognitive task with a motor task triggers seizures in JME patients. The dot-back fMRI paradigm included in our study protocol represents such a combination of a cognitive task and a motor response.

4.4.2 Other seizure-facilitating mechanisms

In JME there are additional provocative factors, such as photic stimulation, that may be based on a similar mechanism, i.e. an increased functional connectivity between visual systems and the motor system. There is evidence for this from a simultaneous EEG-fMRI study using intermittent photic stimulation in the MRI scanner. Moeller et al could elicit photoparoxysmal responses in 6 of 30 Patients, and in all six, there was a BOLD response in the premotor cortex, preceding the generalised discharges by about three seconds (Moeller et al., 2009).

Unfortunately, we have no reliable information about current state of photosensitivity of our patients, as nearly half of them were seizure-free, and investigations involving such provocation mechanisms are not performed unless clinically indicated.

There is also a significant overlap between JME and reading epilepsy (RE), the most prominent example of seizures triggered by cognitive effort. Most interestingly, in a

recent series of simultaneous EEG-fMRI studies in RE, we observed bilateral BOLD increases ictally, time-locked with reading-induced seizures, in the hand area of a patient with RE who was previously diagnosed with JME (patient MH in (Salek-Haddadi et al., 2009)). Spike-triggered fMRI changes induced by cognitive activation were first reported in a 16 year-old female patient with RE showing increased activity, related to individual spikes in the left posterior middle frontal gyrus, that co-localised with the brain regions activated by the working memory component of the reading task, and also bilateral cortical and sub-cortical motor activity in the inferior central sulcus and globus pallidus (Archer et al., 2003). We observed similar ictal fMRI activations within cortical (right mesial frontal gyrus) and subcortical (left putamen) areas during reading-induced seizures (Salek-Haddadi et al., 2009), but no gross abnormalities in cognitive or motor organisation.

These ictal observations in RE not only support our finding of motor cortex hyper-connectivity, but also suggest a functional link for the often noticed association of RE and JME in the same individual, and the recently reported observation of orofacial reflex myocloni triggered by reading and talking in JME (Mayer et al., 2006). Orofacial reflex myocloni also occur in JME where they are always precipitated by talking and in about 40% by reading (Mayer et al., 2006).

4.4.3 Effects of medication

To further investigate the effects of medication, we carried out additional post-hoc analyses. Twenty-one of our 30 JME patients were being treated with valproate, whilst the number of patients treated with other drugs was too small to investigate a specific drug or dose-related effect. The observed negative correlation of left motor cortex co-

activation with increasing daily valproate dose suggests that valproate has a specific effect in reducing this increased activation in JME patients. Furthermore, the positive correlation of valproate dosage with activation in the bilateral frontal and parietal working memory network may indicate a possible normalizing effect of valproate on the cognitive activation pattern. In a different cohort of patients with focal epilepsies, an opposite effect of valproate was found: higher valproate dosages were associated with a widely reduced cortical activation of the working memory network. This matches the clinical observation that valproate is less likely to cause cognitive side-effects in patients with JME than in other epilepsy syndromes. However, our study cannot separate drug effects from subject effects, and these exploratory results require confirmation in subsequent studies, specifically designed to assess drug effects in more detail.

A recent EEG-fMRI study has investigated patients with IGE (half of which were JME), comparing those who were seizure free on valproate against those who were valproate-resistant and continued to have seizures. While in the whole patient group BOLD signal changes preceding epileptiform discharges involved the thalamus, frontal, insular and temporal cortex, the comparison between pharmacoresistant and responsive patients showed a predominant mesial frontal BOLD increase in pharmacoresistant patients (Szaflarski et al., 2013). This could indicate a specific role of the mesial frontal regions in the development of more severe, pharmacoresistant forms of JME.

4.4.4 Correlation with seizure frequency

Motor cortex co-activation was higher in JME patients with more active epilepsy, i.e. with a shorter interval since the last seizure. This indicates a potential role for the degree of hyperconnectivity as biomarker of disease severity.

Neuroimaging findings in patients with epilepsy, regularly lead to the next questions, if these alterations are the cause or rather a consequence of chronic epilepsy. Here it is important to note, that most of our JME patients had well-controlled epilepsy with about half of them free of all seizures for more than one year and some being seizure free for more than 10 years. This strongly argues against our findings being a secondary effect caused by frequent seizures. It is interesting that the observed hyperconnectivity effect can still be seen in such a well-controlled cohort and we hypothesize, that the hyperconnectivity may be even stronger in a drug-naïve cohort of JME patients without the inhibitory, "normalizing" effect of medication.

The most important evidence for our findings being the cause, and not the consequence, was the recent replication of these findings in healthy siblings. In a follow-up project, Wandschneider et al (Wandschneider et al., 2014) recruited healthy siblings of JME patients with no prior history of epilepsy and examined them with the same Dot-back fMRI paradigm and analysis technique. In summary, all key findings described above, were also seen in these healthy siblings: the increased co-activation of the motor cortex, an increased functional connectivity between pre-frontal and motor cortex and modulated motor components in the ICA analysis. This clearly demonstrates that the functional alterations described here are not a secondary effect of chronic epilepsy, seizures or medication – these siblings never had seizures and never took medication. Instead our findings must reflect a pre-existing condition of hyperconnectivity resulting in a predisposition to develop JME. The fact that these hereditary effects were also present in siblings, but less prominent than in JME patients illustrates that such predispositions are not binary, but rather have a continuous spectrum, composed of multiple independent risk factors, with a certain threshold beyond which clinical symptoms occur.

This complements other studies in siblings of JME patients that have shown specific neuropsychological deficits in prospective memory (Wandschneider et al., 2010) or increased cortical excitability in TMS experiments (Badawy et al., 2013), thereby also illustrating the hereditary traits of JEM pathophysiology.

Post-hoc, we also observed greater hyperconnectivity in those patients examined in the morning compared to those examined in the afternoon, in keeping with the known circadian clustering of seizures in JME.

4.4.5 Increased functional connectivity in JME

We observed increased FC between the motor system and higher cognitive systems of the frontal and parietal lobe. No such increase in functional coupling between two independent neuronal systems had been previously described in epilepsy research. Most functional connectivity studies to date have shown disruption of known functional networks in epilepsy, such as the attention (Zhang et al., 2009) or memory networks (Bettus et al., 2009), and reduced connectivity often correlated with an associated cognitive impairment. Here the increased functional connectivity in JME seems to reflect the mechanism underlying cognitively triggered epileptiform discharges and seizures. Compared to the block design fMRI analysis, FC takes into account each subject's individual variation in onset, duration and amplitude of the BOLD response. It is independent from the block design specification and can therefore reveal changes in the absence of differences from traditional fMRI analysis. In our study we assessed FC across the whole duration of the task and there may be differences in FC between rest and cognitive activity. However, the resting periods in our task were short (15 seconds)

and we aimed specifically to investigate effects driven by a cognitive task. Resting state FC was therefore not analysed.

Functional connectivity

The analysis of functional connectivity showed an increased functional coupling between the MC and pre-frontal 'cognitive' cortical areas. This provides further evidence for the hypothesized 'short circuit' between these two systems. It is important to keep in mind that this effect was observed during a high cognitive load and may not be present at times with less demanding processing.

4.4.6 Modulated motor components in Independent Component Analysis

ICA provides a method to identify distinct clusters of functional activation, completely independent of any prior specification of the experimental design or any ROI. Components are identified solely based on correlations of their signal time course, location and commonality throughout the group of subjects. This provides an independent method, complementary to model-based fMRI analysis or region-based FC analysis. In our study, ICA reliably identified components representing the motor system with constant response amplitude, and the working memory system where the response amplitude is modulated by the current task difficulty (Figure 4.7 A-D). Both components were identified in JME patients and in healthy controls, but most importantly, ICA identified additional sub-components of the motor system in JME, whose response amplitude is also modulated by task difficulty (Figure 4.7 E), and these components were not found in healthy controls. This finding was consistent across several iterations of ICA and is consistent with our results from block design and functional connectivity analyses, illustrating the modulatory effect of cognitive effort on the motor system in JME

4.4.7 Impaired deactivation of the default mode network

The task negative contrast was modelled to identify areas, deactivated during task performance. It showed deactivation in areas of the default mode network (DMN) in both groups, but these were less extensive and deactivation was weaker in JME. Patients with JME appeared to be less able to deactivate their DMN during the task, indicating a less efficient reallocation of neuronal resources to task-relevant areas, which may interfere with cognitive processing (Sonuga-Barke and Castellanos, 2007). Franson used the same fMRI paradigm comparing intrinsic activity during rest and the "2-back" task (Fransson, 2006). He showed that spontaneous intrinsic activity in the DMN was not extinguished but rather attenuated and reorganized during a working memory task in healthy controls. Some of our observations in JME could therefore also be interpreted as an imbalance between the task relevant cognitive network and the opposing DMN. An 'overload' of the task positive cognitive network during a highly demanding task, together with impaired deactivation of the DMN, could lead to hyperexcitability and hyperconnectivity across systems, including the motor cortex, and cause myoclonic jerks. Alterations of the DMN modulation are not specific to JME. Similar changes have recently been described in a range of neuropsychiatric disorders (Broyd et al., 2009), including anxiety, attention deficit hyperactivity disorder (Bush, 2010), and schizophrenia (Calhoun et al., 2008; Whitfield-Gabrieli et al., 2009). Voon et al recently described increased functional connectivity between the amygdala and SMA under emotional load in patients with motor conversion disorder (Voon et al., 2010). Impaired DMN deactivation, altered mutual modulation of functional subsystems and increased connectivity between higher order cognitive systems and the motor system may

therefore be common mechanisms in the generation of motor symptoms, triggered by emotional or cognitive stressors.

4.4.8 Effect in Language, Memory and Verbal WM fMRI

The findings in all these paradigms were less prominent than the differences in the most demanding Dot-back task and some of them have not reached statistical significance. They do however, line up with the previous main findings and contribute complementary details about cognitive effects in JME and are therefore included in this discussion.

In the language paradigms, we also saw effects depending on the cognitive load. There were no differences for the relatively easy Verbal Fluency task, or the easy "repeat" condition of the Verb Generation task. Only in the more demanding "verb generation" blocks, was there an increased co-activation of the left SMA, similar to the effect seen in the Dot-back task. Even though the effect was less prominent, it is of particular interest, because this task did not involve any motor response and therefore no "pre-activation" of the SMA as in the Dot-back task.

Furthermore the absence of a motor response can also not explain the asymmetric lateralisation of the increased co-activation of only the left SMA. The right hand motor response of the Dot-Back task provides a clear explanation for this, based on the left-sided motor cortex activation. But here, in the language task, without any motor response, the left-sided SMA co-activation suggests the effect is triggered in the active language dominant hemisphere. This further strengthens the hypothesis of a specific role of the SMA as functional link between the cognitive and the motor system.

During the memory-encoding paradigm, there is less variation of the cognitive load, as the memorization of word, pictures and faces is similarly demanding. The paradigm did, however, include variations of the emotional context for the faces, which were neutral, happy or fearful. Comparing the specific event related response to fearful faces, there was again a group difference, again showing an increased response of JME patients in the mesial central and precentral region. Additionally there was an increased activation of the left amygdala in JME patients.

This demonstrates how in JME different cognitive tasks can lead to similar hyperactivation of the motor system. While this effect depends largely on the cognitive demand of a task, it seems to also be triggered by emotional stress. And an increased emotional response to the fearful faces is documented by the increased amygdala activation in JME. These findings are, however group results of a large cohort, and most likely, individual JME patients do have individual profiles of susceptibility to certain trigger factors.

The verbal working memory task, N-back, is also noteworthy, because it is the only task, where JME patients showed less activation during the cognitive task than healthy controls. A similar impaired activation was described in a PET study, where Swartz et al. reported that JME patients failed to increase their frontal glucose utilization rate during a visual working memory tasks to the same degree as healthy controls (Swartz, Simpkins et al. 1996). However, they also reported a reduced performance score in JME patients, which suggests that their patient population was more severely affected. This was not the case in our present study, where JME patients performed as well as healthy controls.

Also, in our study, the N-Back paradigm was the only task, where no increased co-activation of the motor system was observed in JME patients. The fact that in the same paradigm, JME patients showed more activity in the default mode network indicates that they engaged less in the task, than the controls did.

One possible explanation is that the N-back task was performed directly after the demanding Dot-back paradigm, which was consistently reported to be quite exhausting. Maybe this was even more exhausting for JME patients, leading to a less active participation in the following task. However, this reduced activation in JME patients allows for additional interpretations of our results with regard to task switching:

4.4.9 The default mode networks and task switching

The default mode networks (DMN) represent the areas of the brain, which are more active at rest, and get deactivated as soon as any task is performed that activates other cortical areas.

The specific contrast we used to model this increasing deactivation during the Dot-back paradigm showed that JME patients had a reduced deactivation of the DMN.

This can also be interpreted as an inability to switch between the two states in the same way healthy controls switch between rest and task, alternatingly activating either the task positive cognitive working memory network or the default mode network, while deactivating the other.

This is illustrated schematically in Figure 4.11: During the demanding Dot-back task, the JME patients performed well, achieved the same success rate as controls and activated their cognitive systems to the same level, but his effort results in an over activation, spreading to neighbouring functional systems and an inability to relax during

the resting periods, where all systems remain relatively hyperactivated. During the N-back task on the other hand, JME patients showed a proper default mode network state during rest and did not show any abnormal co-activation, but in turn, have activated their cognitive systems less than controls.

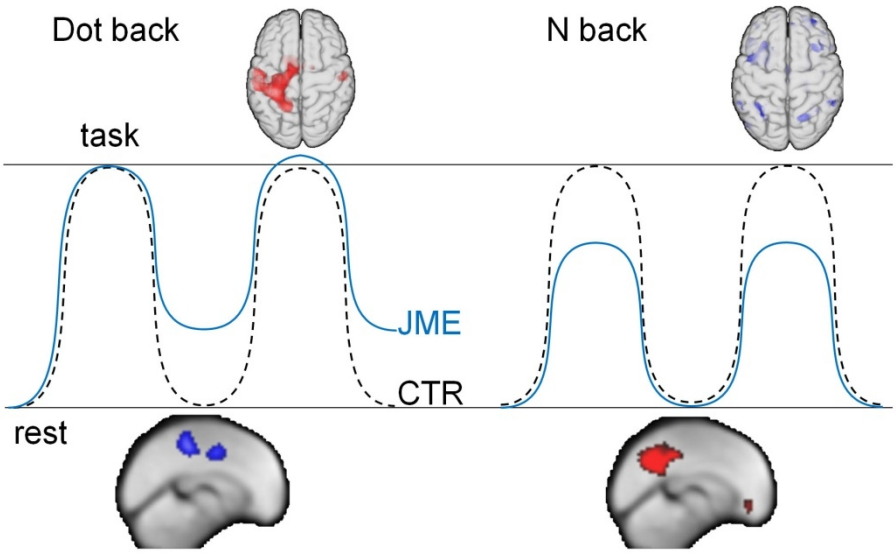

Figure 4.11 Impaired task switching in JME.

Healthy controls (CTR) have a certain range of redistribution of resources when they switch from rest to an active task and back to rest. This range is impaired in JME, resulting either in a relatively incomplete "switching off" during the Dot-back task, or in an incomplete "activation" during the N-back task.

4.4.10 Functional segregation in brain development

Task switching, the efficient transition from rest to activity and an efficient, flexible reallocation of neuronal resources between different functional systems is an important cognitive ability and is typically developed during adolescence (Tau and Peterson, 2010). Synaptic pruning is a key process during the developmental period of adolescence, where the elimination of unnecessary connections allows a re-adjustment of the brains total energetic efficiency (Casey et al., 2000). This maturation process

results in increased functional segregation, where anatomically adjacent, but functionally different brain regions become locally less connected to each other, but increasingly connected to other hubs of their respective functional network (Fair et al., 2007).

The disease onset of JME in adolescence (Craiu, 2013), would support the interpretation that insufficient developmental synaptic pruning and impaired functional segregation, plays a role in the pathophysiology of JME.

In this study I could show, via the increased functional connectivity, that the functional segregation of the motor system from the cognitive system is impaired in JME.

4.4.11 Role of the supplementary motor area

Independent analysis techniques have consistently shown alterations in the SMA in JME. We found a load dependent co-activation of the motor cortex and SMA during different cognitive tasks in JME. This was an effect of increased functional connectivity between the frontal and parietal cognitive networks and the motor system. The areas of greatest difference in task-related deactivation between JME and controls were located in mesial central and frontal regions of the SMA (see Figure 4.12 for spatial relationship between findings).

Our findings complement the wide range of morphometric structural changes previously described in the SMA of JME patients (Bernhardt et al., 2009; O'Muircheartaigh et al., 2011; Woermann et al., 1999b).

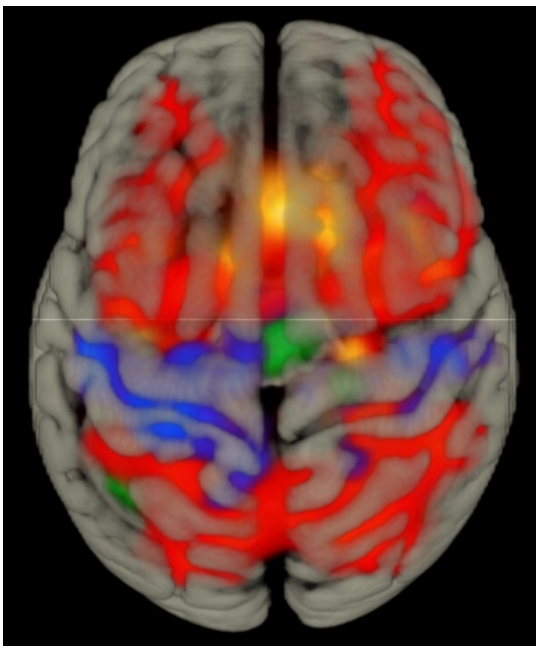

Figure 4.12 Spatial relationship between findings.

This figure summarizes some to the results, to aid the interpretation of their spatial relationship. Activation from the working memory task in controls is shown in red (2-back minus 0-back, as in Figure 4.2 C). Areas of increased activation in JME, compared to controls are shown in blue – mainly in the pre- and post-central gyrus and SMA (as in Figure 4.2 F). The orange clusters show areas of increased functional connectivity to the motor cortex and SMA (as in Figure 4.5 C), mainly in the mesial pre-frontal cortex, overlapping with the task induced activation. The green cluster shows the area of impaired deactivation during the cognitive task in JME (as in Figure 4.6 C). Gyral anatomy is overlaid from the MNI152_T1 template. The horizontal bright line indicates y coordinate 0 in MNI space.

Even though the detailed anatomical and functional parcellation of the SMA is still ongoing (Chouinard and Paus, 2006; Fink et al., 1997), it is clear that the SMA is well connected to both, the primary motor cortex and pre-frontal cognitive networks (Zilles et al., 1995). Impaired task dependent deactivation of certain SMA areas may indicate a specific role of the SMA as relay for the abnormal functional connectivity between the cognitive and the motor system we observed in JME and this could reflect the functional correlate of previously described structural abnormalities in the SMA.

4.5 Conclusion

This data shows an increased co-activation of the motor cortex in patients with JME during demanding cognitive tasks and an increased functional connectivity between their motor cortex and pre-frontal cortical areas. This results in a dynamic modulatory effect of cognitive processes on the motor system that is not seen in healthy controls.

Several studies were able to show increased motor cortex excitability in JME patients, but this is the first study to show an abnormal link between the motor cortex and cognitive cortical areas, providing an explanation for the specific occurrence of cognitively triggered myoclonic jerks in these patients.

The traditional dichotomic classification of epilepsies into focal and generalised epilepsies is increasingly challenged by new insights into their more specific mechanisms. Koepp has already suggested the crucial role of specific thalamo-cortical networks in JME (Koepp, 2005) and Avanzini et al have recently proposed the concept of "system epilepsies" (Avanzini et al., 2012), where clinical characteristics of a syndrome are defined by certain affected neuronal systems. Yacubian and Wolf later referred to our findings from this study, defining JME as an example for a system epilepsy, where the central mechanisms of seizure generation ''hijack'', by hyperexcitation, pre-existing functional anatomic subsystems of the central nervous system (CNS) (Yacubian and Wolf, 2014). This may be based on an impaired developmental separation of these systems during adolescence.

This model of system epilepsy is indeed better suited to explain certain syndrome specific effects of JME and may be more representative than its classification as "generalised epilepsy". Our demonstration of a pre-existing hyperconnectivity between

different neuronal systems has helped to develop a new view at the pathophysiological mechanisms of ictogenesis in JME.

5. Juvenile Myoclonic Epilepsy – structural changes

(Vollmar et al., 2012)

5.1 Background

In the previous chapter, I described increased motor cortex co-activation with increasing cognitive effort, in patients with juvenile myoclonic epilepsy (JME). I also described an increased functional connectivity between the motor cortex and pre-frontal cognitive networks in JME (Vollmar et al., 2011). The finding of impaired task-related deactivation of the supplementary motor area (SMA) suggested a role of the SMA as a relay, which facilitates increased functional coupling between the motor system and the pre-frontal cognitive areas. These results link the motor cortex hyperexcitability hypothesis (Badawy et al., 2007) and the neuropsychology activation studies in JME, which have shown increased spike frequency in the central region during demanding cognitive activities (Matsuoka et al., 2000).

Although conventional structural brain MRI is per definition normal in JME, morphometric analyses of T1-weighted images have identified subtle abnormalities of mesial frontal gray matter (Woermann *et al.*, 1999). Several studies have since reported similar gray matter changes (Seneviratne et al., 2014). There were, however, inconsistencies and both increases and decreases of gray matter have been reported in the mesial frontal region. These changes have been interpreted as either microdysgenesis or regional neuronal loss. Further research into the characterization of the underlying changes responsible for the observed imaging alterations is still needed.

We recently reported reduced fractional anisotropy (FA) of the mesial frontal lobe in JME patients, which correlated with specific neuropsychological deficits

(O'Muircheartaigh et al., 2011). Reduced FA is commonly interpreted as being caused by regional neuronal loss or neuronal damage leading to fewer axonal bundles in the white matter. Another frequent interpretation is that reduced FA may reflect reduced connectivity of adjacent cortical areas. This is, however, not supported by our findings of concomitant significantly *increased* functional connectivity of the SMA in the same group of JME patients (chapter 4, page 134).

In this chapter, we will describe our diffusion tensor imaging (DTI) study in JME. The main aim of this study was to analyse in detail the structural connectivity of the mesial frontal lobes in JME, using DTI, tractography and connectivity-based regional parcellation. We also aimed to clarify the relationship between structural and functional connectivity of the motor system with pre-frontal cognitive networks in JME.

5.2 Subjects and Methods

5.2.1 Subjects

The DTI data was acquired in the same cohort of JME patients and healthy controls described in detail in chapter 4. Thirty JME patients and 26 healthy controls were included in this study.

5.2.2 DTI acquisition

The DTI data was acquired with a single-shot spin-echo planar imaging sequence using cardiac gating with a peripheral pulse sensor to minimise noise. Echo time was 73 ms and the effective repetition time varied, depending on the heart rate. Volumes of 60 contiguous 2.4-mm thick axial slices were acquired, allowing full brain coverage.

Diffusion-weighted volumes were acquired with diffusion-sensitizing gradients in 52 non-collinear directions (maximum b value of 1200mm$^{2\ s-1}$) interleaved with six non-diffusion-weighted (b=0) scans. The gradient directions were calculated and ordered as described elsewhere (Cook et al., 2007). The parallel imaging acceleration factor (SENSE) was 2. The field of view was 24 cm, and the acquisition matrix size was 96x96, zero filled to 128x128 pixels during reconstruction so that the reconstructed voxel size was 1.875 x 1.875 x 2.4mm^3. The DTI acquisition time for a total of 3480 image slices (58 volumes, 60 slices each) was about 25 minutes, depending on subject heart rate. (Yogarajah et al., 2010).

5.2.3 DTI preprocessing

DTI data was processed with FSL 4.1.5 software (www.fmrib.ox.ac.uk/fsl) on a Linux workstation. Preprocessing included spatial Realignment of all 58 image volumes to the first (b=0) volume using a 12-degree of freedom affine transformation which allows correction for head movement during the acquisition and correction for eddy current-induced distortions.

A brain mask was created from the non-diffusion-weighted images, using FSL brain extraction tool and was applied to restrict all further processing to brain voxels only.

For every brain voxel, the principal diffusion tensor was determined and the three eigenvalues (λ_1 λ_2 and λ_3) were calculated, representing the axial diffusivity along axonal bundles (λ_1) and the radial diffusivity perpendicular to the principal axis (λ_2 and λ_3) (Basser and Pierpaoli, 1996). From these vectors, the values for fractional anisotropy (FA) and mean diffusivity (MD) were calculated for every voxel and to create FA and MD maps.

Every subject's FA map was spatially normalised to a FA template in Montréal Neurological Institute (MNI) space at $1mm^3$ resolution using a combination of linear and non-linear transformations in SPM5 software (www.fil.ucl.ac.uk/spm). The determined transformation matrix from individual to MNI space and the inverse transformation (from MNI space to individual space) were saved for later application to other image datasets.

Probabilistic tractography was prepared, calculating the probability distribution of diffusion vectors across the brain volume, using a two-fibre model accounting for crossing fibres within one voxel (Behrens et al., 2007).

5.2.4 DTI tracking and connectivity analyses - overview

Imaging analysis of the mesial frontal region presents challenges, due to the ill-defined anatomic boundaries of the SMA. To overcome this, we have applied DTI-based voxel-wise connectivity profiling and clustering, which allows the delineation of the SMA (part of the motor system), and its separation from the pre-SMA (part of the frontal lobe cognitive network) solely based on their connectivity pattern (Johansen-Berg et al., 2004).

The workflow of the DTI data analysis is summarised in Figure 5.1.

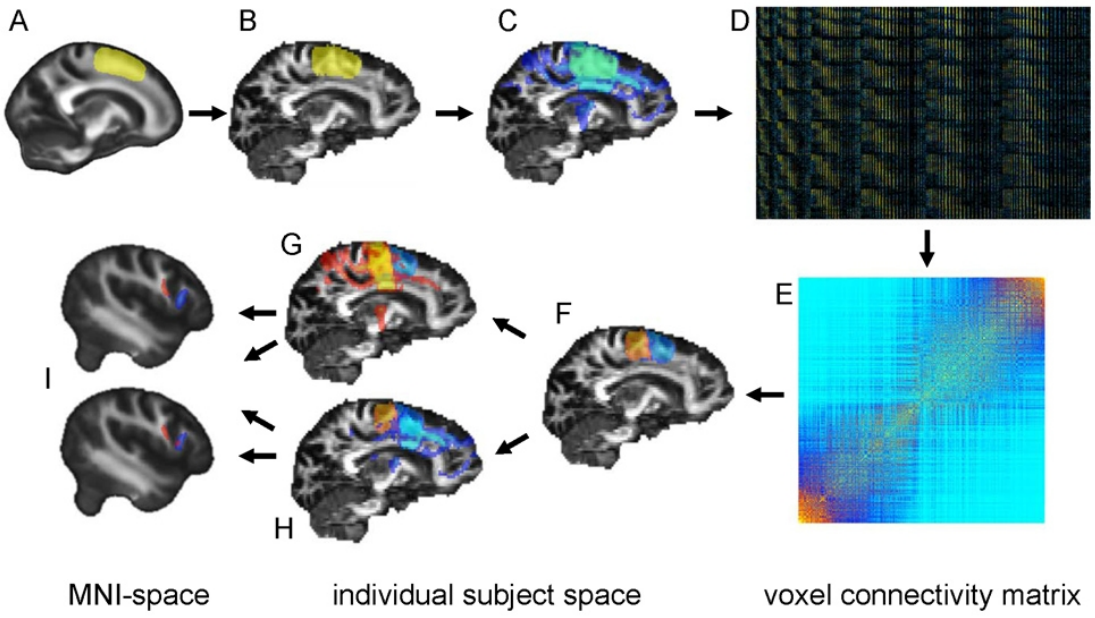

Figure 5.1 Image processing pipeline.

A region of interest (ROI) was defined in the left mesial frontal lobe in MNI space (A), and back-normalised to each subject's individual DTI data space (B). Probabilistic tracking was performed, seeding from every voxel of the ROI (C). A voxel-wise connectivity map was created (D), representing the probability of every seed voxel (y-axis) to be connected to a certain region of the whole brain (x-axis), a representative selection from matrix is shown, (total matrix size: ~1800x9000). This connectivity matrix was re-ordered, using k-means and spectral clustering techniques constrained to identify two clusters. The re-ordered matrix (E) shows two distinct clusters of seed voxels, representing the supplementary motor area (SMA, orange) and pre-SMA regions (blue), separated solely by their DTI connectivity profile. Tracking was repeated from these two clusters (F), with the resulting tracts for the SMA cluster (G) and pre-SMA cluster (H) normalised to MNI space for voxel-wise group comparison (I).

5.2.5 Tracking from initial seed region

A left mesial frontal seed region was manually defined in the white matter of the posterior half of the left superior frontal gyrus in MNI space (Figure 5.1A), including the SMA and pre-SMA with a total volume of 13.479 cm^3. This seed region was back-normalised into each subject's individual DTI data space using the inverse normalization previously determined from normalisation of individual data to MNI space (Figure 5.1B).

Probabilistic tractography was performed in each subjects individual space from every voxel within this seed region using FSL 4.1.5 software and the probtrackx command (www.fmrib.ox.ac.uk/fsl), providing the sum of all connections from this seed region (Figure 5.1C).

Using the default settings of FSL's probtrack algorithm, 5000 streamlines are initiated from every seed voxel, to increase the chance that all possible connections are covered. The most likely connection pathway will show up most frequently. The resulting path maps (or "connectivity maps") show, for every brain voxel, how many streamlines from the seed cluster were passing through it. The maximum possible intensity is therefore determined by the number of samples per voxels (here 5000) and the total number of voxels in the seed region (here about 1450)

5.2.6 Connectivity profile

During the probabilistic tracking, we also determined the individual connectivity profile of every single voxel from the seed region, estimating the likelihood of this voxel being connected to every other region of the brain.

For this purpose, each subject's whole brain was re-sampled to 5x5x5 mm^3 voxels to create a low-resolution whole-brain mask. This reduction of the number of voxels reduced the computational demand of the procedure. The probability of a connection between every voxel in the seed region and every voxel from this low-resolution whole-brain mask was determined and stored in a connectivity matrix (Figure 5.1 D).

5.2.7 Connectivity-based clustering

Following the method of Johansen-Berg (Johansen-Berg et al., 2004), the resulting connectivity matrices were re-ordered with k-means clustering in two distinct clusters (Figure 5.1 E).

First all rows and columns of the connectivity matrices with zero connectivity probability were removed. The remaining seed voxels were then rearranged with the aim to maximize the separation between connected brain regions. All seed voxels with high probability of connection to certain brain areas are assigned to one cluster, and all seed voxels with high connectivity probabilities to other brain areas are assigned to the second cluster. In our application this procedure allows to separate the seed region in two distinct clusters: the SMA and the pre-SMA (Figure 5.1 F), based solely on their DTI connectivity profile.

5.2.8 Tracking from SMA and pre-SMA

The two separate clusters, representing SMA and pre-SMA were saved as region of interest. Tractography was then repeated, seeded separately from the SMA and from the pre-SMA clusters, providing separate connectivity maps for both regions for every subject (Figure 5.1 G, H).

5.2.9 Statistical comparison of tracts

Individual connectivity maps from both seed region, the SMA and pre-SMA, were normalised to MNI space in 1mm resolution, applying the spatial normalisation previously determined from FA maps and smoothed with an 8 mm FWHM kernel.

For voxel-wise group comparison of the normalised connectivity maps, I used a two sample t-test and SPM 5 software (Figure 5.1 I). Statistical analyses were restricted to the left hemisphere where the tracking was initiated.

5.3 Results

5.3.1 Subjects

DTI data was acquired in 29 of the 30 JME patients and 26 healthy controls. In one JME patient, DTI data acquisition failed due to technical problems with the peripheral pulse sensor used for cardiac gating.

5.3.2 Tracking from initial seed region

Probabilistic tracts from the initial seed region were determined for all subjects using FSL probtrackx command with the default settings of 5000 samples and a curvature threshold of 0.2 (approximately 80 degree).

5.3.3 Connectivity profile

A connectivity matrix was created for every subject, with a size of approximately 1500 by 11000. The exact size is determined by each subject's individual number of voxels in the seed region and in the whole-brain mask. An example from one healthy control is shown in Figure 5.2.

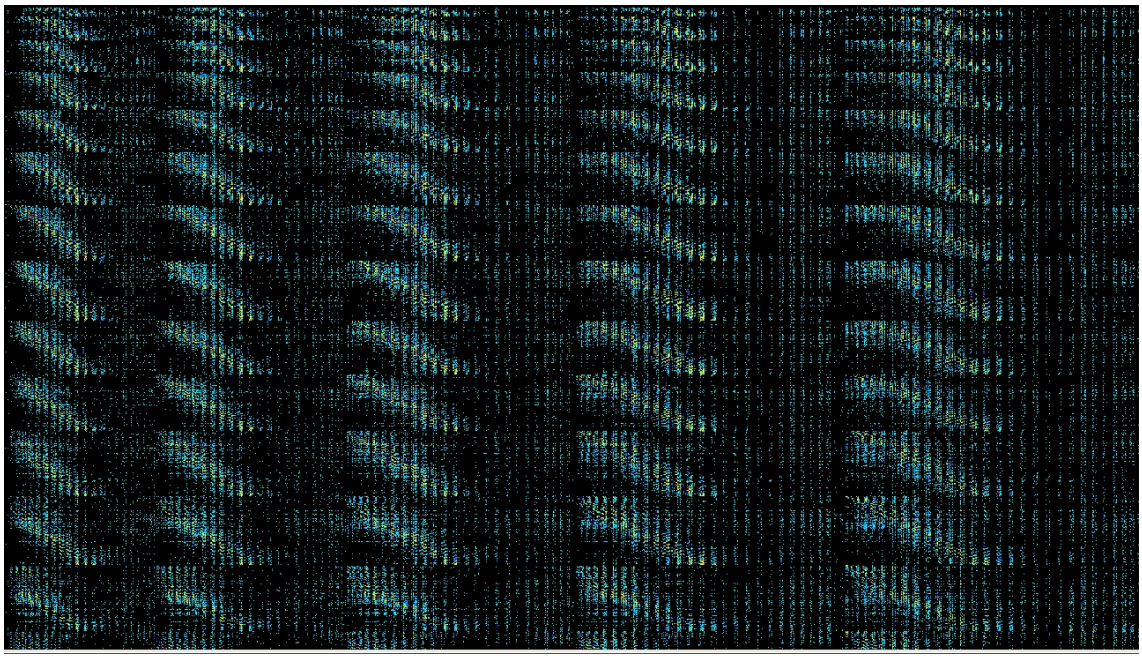

Figure 5.2 Portion of connectivity matrix.

Example of a connectivity matrix determined from DTI data. Voxels of the seed region are ordered along the vertical axis, voxels of the whole-brain mask are ordered along the horizontal axis. For every pair of voxels the probability of a connection between them is colour coded, where black indicates 0 probability and warm colours indicate a high probability. (Only about 20% of the matrix is shown here to allow appreciation of details).

A repetitive pattern can be seen, where certain groups of voxels show similar connectivity profiles. This reflects neighbouring voxels appearing in groups repeatedly in the sequence of voxels ordered along the two axis of the matrix.

5.3.4 Connectivity-based Clustering

Applying k-means clustering, the initial seed region was divided in two clusters, based on their connectivity profile for every subject. The resulting clustered connectivity matrices were saved for every subjects and the resulting region of interest files for the two identified clusters were saved and used to initiate separate probabilistic tracking from either cluster.

There were no differences between JME patients and healthy controls in size or shape of the two determined clusters or in cluster membership probability.

There were no visible systematic differences in the re-ordered connectivity matrices of JME patients and controls, even though a visual interpretation is difficult. There are currently no tools available for a systematic quantitative comparison of connectivity matrices. The matrix size and the order of voxels along both axes vary between individuals.

Two examples of re-ordered connectivity matrices are shown in Figure 5.3 and Figure 5.4.

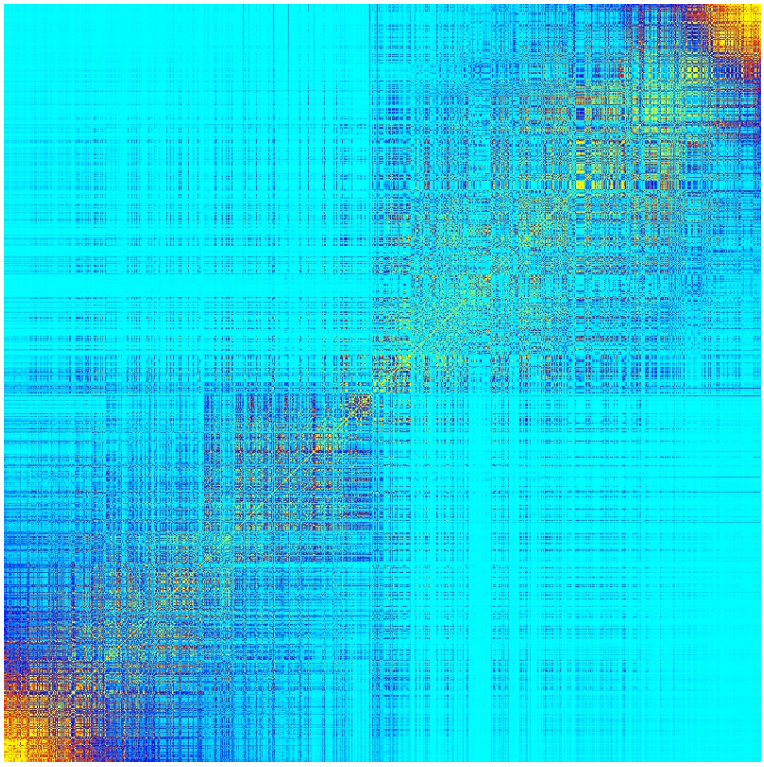

Figure 5.3 Re-ordered connectivity matrix.

The re-ordered connectivity matrix after clustering shows in the lower left and upper right corner the voxels with the most distinct connectivity profiles, connecting very strongly to one brain region, and not at all to other regions. In between there are voxels with a decreasing connectivity preference to one target region. The voxels represented in the middle of the matrix are those with the least distinct connectivity and may have similar probabilities to connect to both identifies target regions. In this example the two clusters are well separated, resulting in a "checkerboard" appearance of the matrix. Most seed voxels show a clear preference towards one group of target voxels (dark blue and orange) and show very low likelihood for connection to other brain areas (light blue)

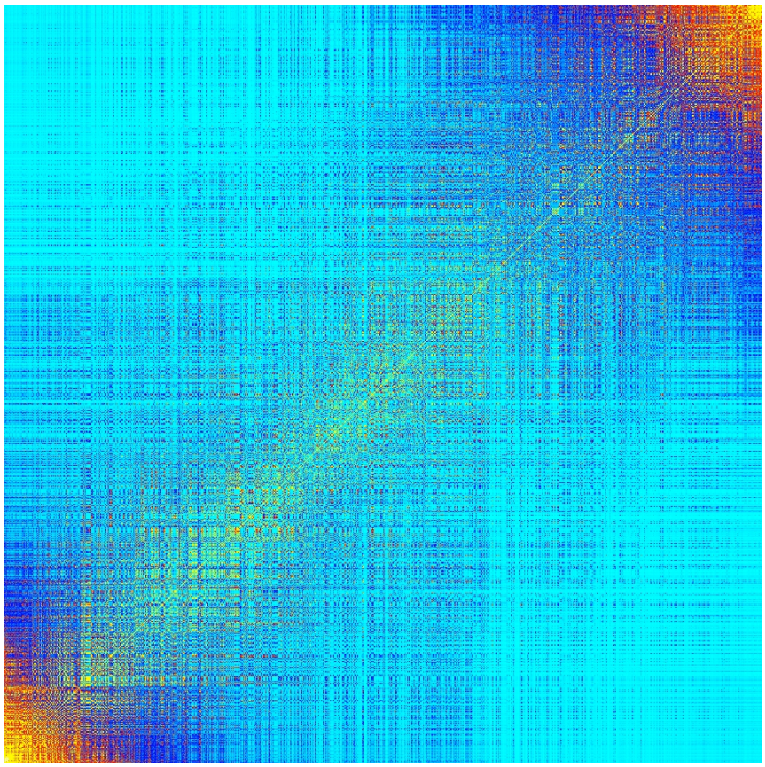

Figure 5.4 Re-ordered connectivity matrix.

This example of a re-ordered connectivity matrix shows a less clear separation of clusters. There are more seed voxels, where the whole line shows dark blue, i.e. where the probability of connections to several target regions is similar. Similarly there are columns with almost continuous dark blue, indicating target regions in the brain with almost similar connectivity to all voxels from the seed region.

5.3.5 Tracking from SMA and pre-SMA

Separate tracking from the SMA and pre-SMA cluster was performed for all subjects. The resulting average connectivity maps from JME patients are shown in Figure 5.5. There was no obvious visual difference between the average connectivity maps from JME patients and healthy controls.

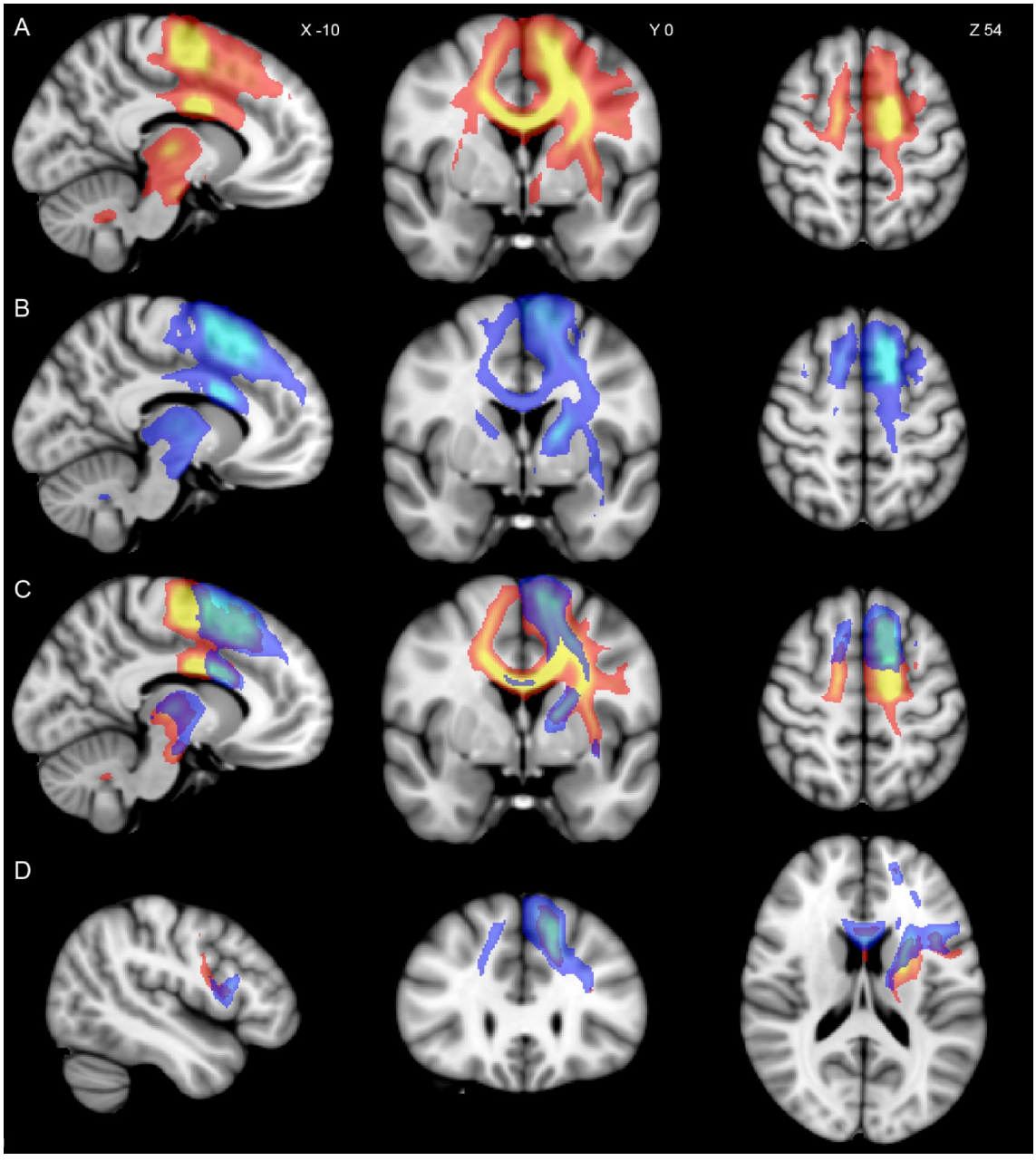

Figure 5.5 Tracking from SMA and pre-SMA.

Average tracking results from the SMA (A) and from the pre-SMA cluster (B) thresholded at 2000 streamlines. Even with an increased threshold of at least 5000 streamlines, there is overlap between the possible connections of both clusters (C). Note the anatomic detail (D): the SMA cluster (red, part of the motor system) connects to the inferior precentral gyrus, whereas the pre-SMA cluster (blue, part of the cognitive system) connects to Broca's area in the inferior frontal gyrus.

Using probabilistic tracking leads to considerable overlap between the resulting tracks. For better illustration of the different spatial distribution of typical connections from the SMA and pre-SMA cluster, I have included an additional figure using deterministic streamline tracking from the SMA and pre-SMA cluster, keeping a distance of 5 mm between them to ensure good separation of resulting tracks (Figure 5.6).

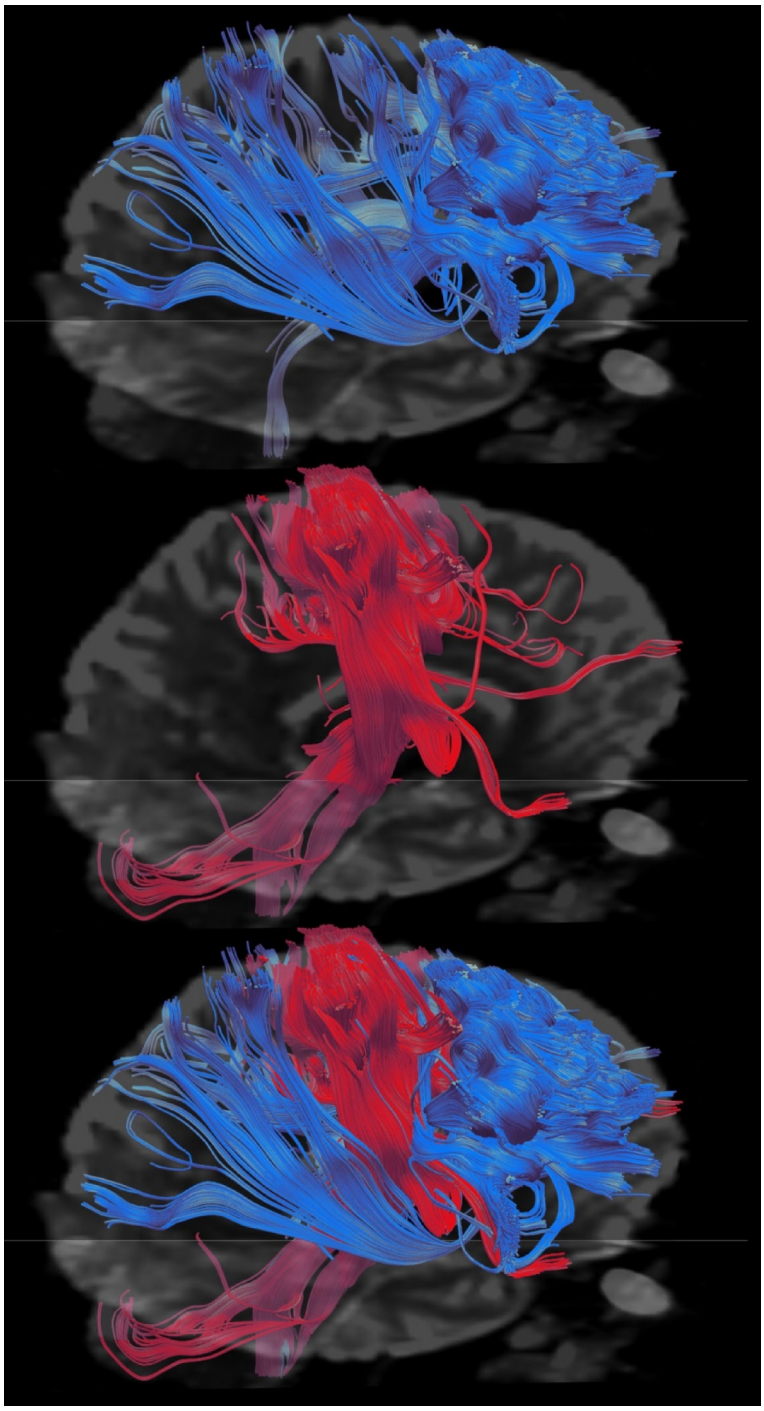

Figure 5.6 Deterministic tracking from the SMA and pre-SMA.

Lateral view on a 3D-rendering of deterministic streamline tracking from the SMA (red) and from the pre-SMA (blue) cluster, for a single healthy control.

5.3.6 Group differences

Voxel-wise comparison of the two connectivity maps from SMA and pre-SMA revealed a number of differences between JME patients and healthy controls which are summarised in Figure 5.7 A.

In patients with JME, the pre-SMA cluster showed:

- reduced connectivity to the adjacent pre-frontal and fronto-polar areas (Figure 5.7 B);
- increased connectivity to the mesial central region (Figure 5.7 C); and
- increased connectivity to the descending motor pathways (Figure 5.7 D).

The SMA cluster showed

- decreased connectivity to the primary motor cortex (Figure 5.7 E);
- increased connectivity to the occipital lobe (Figure 5.7 F); and
- increased connectivity to the lateral temporal neocortex (Figure 5.7 G).

The sectional images in Figure 5.7 show the group differences as overlay thresholded at $p<0.05$ (uncorrected). After correction for multiple comparisons using the false discovery rate, the peak voxels of all group differences were significant, at $p<0.05$ (2-tailed T test).

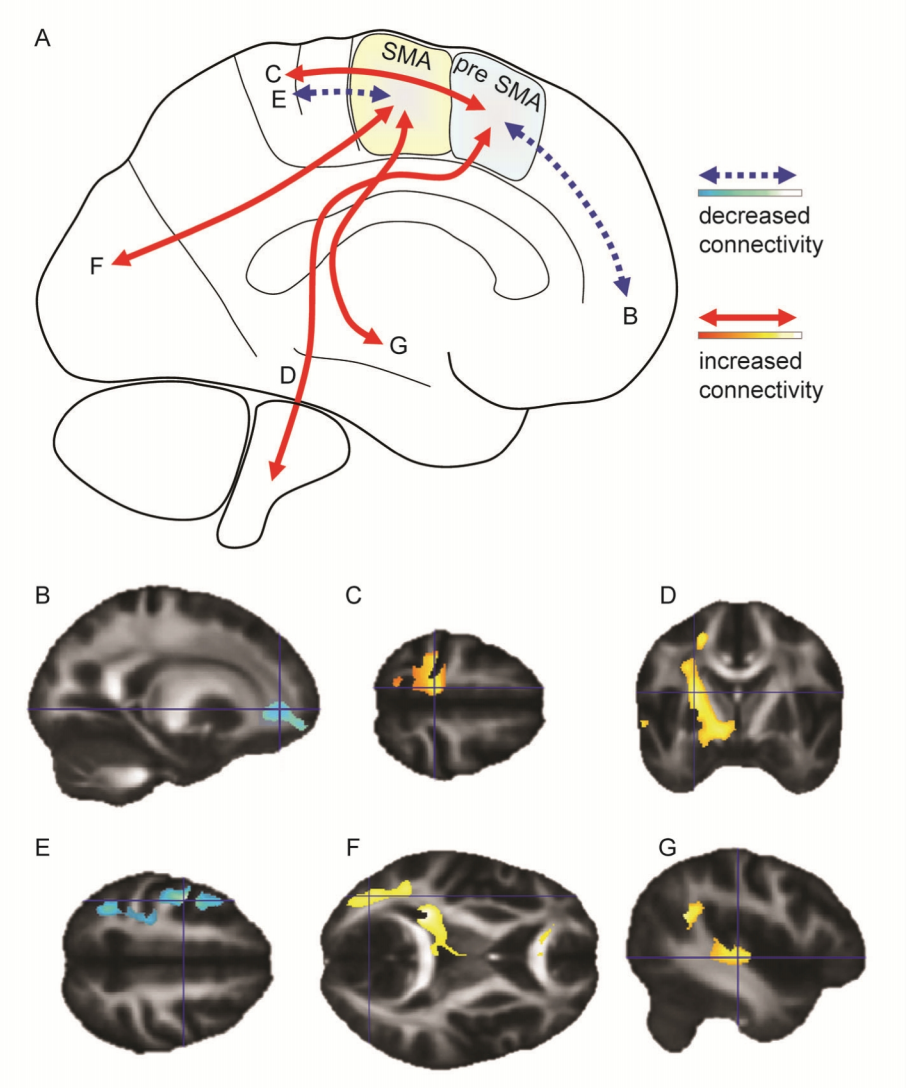

Figure 5.7 Alterations of structural connectivity in JME patients.

Schematic summary of alterations in JME (A). The anterior pre-SMA cluster showed reduced connectivity to anterior frontopolar regions (B), and increased connectivity to the mesial central region (C) and descending motor pathways (D). The posterior SMA cluster showed reduced connectivity to the central region (E), but increased connectivity to the occipital cortex (F) and temporal neocortex (G).

5.3.7 Correlations

In JME, the structural connectivity measure from the pre-SMA cluster to the mesial central region correlated positively with the functional connectivity between the adjacent dorso-lateral pre-frontal cortex and the mesial central region, as shown by fMRI (Figure 5.8 A, Pearson's correlation coefficient R=0.47, p=0.01).

The shorter the interval since last seizure, the higher connectivity was found between pre-SMA and central region (Figure 5.8 B, correlation coefficient R=-0.56, p=0.001). There was no correlation between connectivity measures and cognitive performance. In patients with photosensitivity, connectivity between the SMA and the occipital cortex was stronger (n=5, not statistically significant) and this subgroup alone did not show increased connectivity of the pre-SMA.

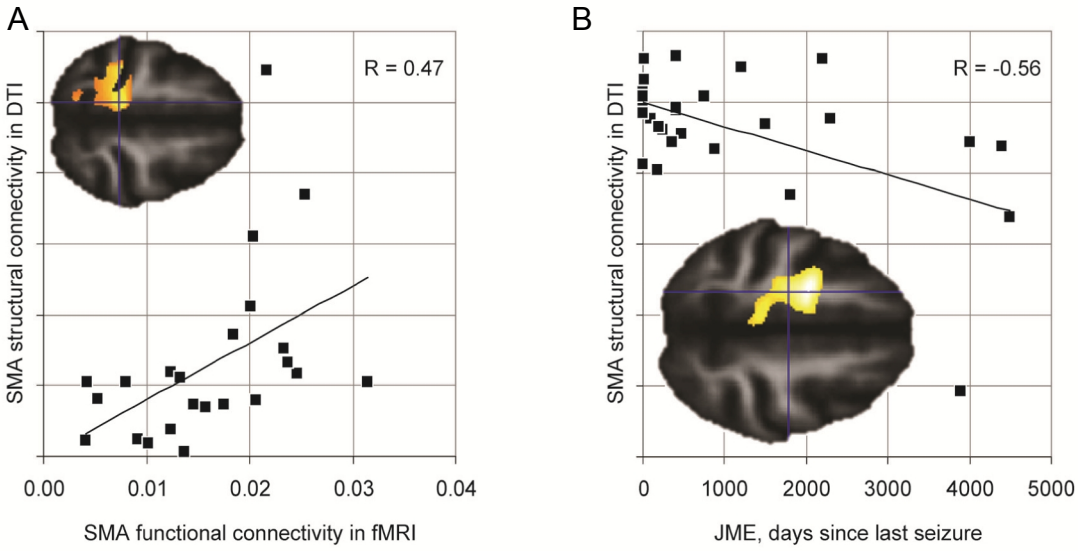

Figure 5.8 Correlation of structural connectivity measures.

Functional connectivity between the pre-frontal cortex and SMA found with fMRI, correlated significantly with the structural connectivity shown with DTI (A). Connectivity of the SMA also correlated with disease activity (B).

5.4 Discussion

In this DTI study, I used connectivity fingerprinting to automatically parcellate the mesial frontal region and compare the connectivity profiles of SMA and pre- SMA in patients with JME and healthy controls.

5.4.1 Alterations of structural connectivity

I showed an increased measure of micro-structural connectivity between the pre-frontal cognitive network (pre-SMA), and the motor system in JME and this correlated positively with functional connectivity between these two systems, which was described to also be increased in the previous chapter (Vollmar et al., 2011). These findings suggest that structural alterations in the mesial frontal region underlie the functional hyperconnectivity and may be crucial in the pathophysiology of JME. Although our patient numbers were too small for detailed subgroup analyses, this structural-functional connectivity profile of the mesial frontal region provides a framework to explain several characteristic features of JME:

1) Increased connectivity between pre-frontal cortex and the central region enables a pathway for cognitive activity to affect the hyperexcitable motor system, where increasing co-activation can elicit epileptiform discharges (Matsuoka et al., 2000) and trigger myoclonic jerks (Inoue et al., 1994). The increased connectivity between temporal neocortex and SMA provides an additional pathway for increased cognitive effects on the motor system in JME.

2) Reduced connectivity between the pre-SMA region and the frontopolar cortex may be the anatomical basis for impairment of frontal lobe function in JME (Wandschneider et al., 2010). The absence of a linear correlation between intra-frontal connectivity and neuropsychological performance in our cohort may be a limitation of the relatively good performing patient group and could be more accessible in a population with a broader range of cognitive performance.

3) Increased connectivity between SMA and occipital cortex, which was stronger in photosensitive patients, may represent a pathway for the provocative effect of photic stimulation to elicit fronto-central discharges and seizures.

These findings also link some previously reported imaging abnormalities in JME patients that will be summarised and discussed on the following section.

Unfortunately a large number of studies were performed in "IGE" without further differentiation between JME and other generalised epilepsy syndromes. This limits comparability with our data and some specific effects of JME may have been missed in such studies on mixed IGE.

5.4.2 Fractional anisotropy and tractography

Diffusion tensor imaging provides detailed information about degree and directionality of water diffusivity in white matter, where the anatomy of axonal bundles restricts free water diffusivity across fibres. This can be summarised in condensed measures like mean diffusivity or fractional anisotropy (FA) which are helpful for voxel-wise analysis of the data. But these measures do not fully utilize the available information within a

DTI dataset and care must be taken when inferences are made on the biological mechanisms underlying alterations of such measures (Jones et al., 2013). Reductions of FA are usually interpreted as reduced connectivity, due to a loss of fibre density or integrity, representing neuronal loss or neuronal damage. In our previous study, we also found a reduced FA in the mesial frontal cortex connecting to the SMA in patients with JME (O'Muircheartaigh et al., 2011), However, to interpret this as "reduced connectivity" would contradict our finding of an increased functional connectivity of the SMA (Vollmar et al., 2011).

In this DTI study, I used voxel-wise diffusion tensor tractography and connectivity-based fingerprinting of the mesial frontal lobe. These advanced DTI analysis techniques provide much more detailed information about the microstructural anatomy of brain regions.

In the SMA, the main afferent and efferent fibres run in a superior-inferior direction, descending to motor pathways, running alongside the corticospinal tract from the precentral gyrus. (Figure 5.9) Here we could show that JME patients have a higher probability of connection between the pre-SMA and the central region, i.e. a higher proportion of fibres travelling in an anterior-posterior direction from the pre-SMA to the central region – thereby crossing the descending fibres from the SMA. Such an increased proportion of crossing fibres in JME perfectly explains a reduced FA in this white matter region: Intersecting neuronal bundles of different spatial orientations allow diffusion of water in multiple directions. This reduced constraint will be reflected as reduced FA, even if all fibres are structurally and functionally intact and the total number of fibres remains unchanged or even has increased.

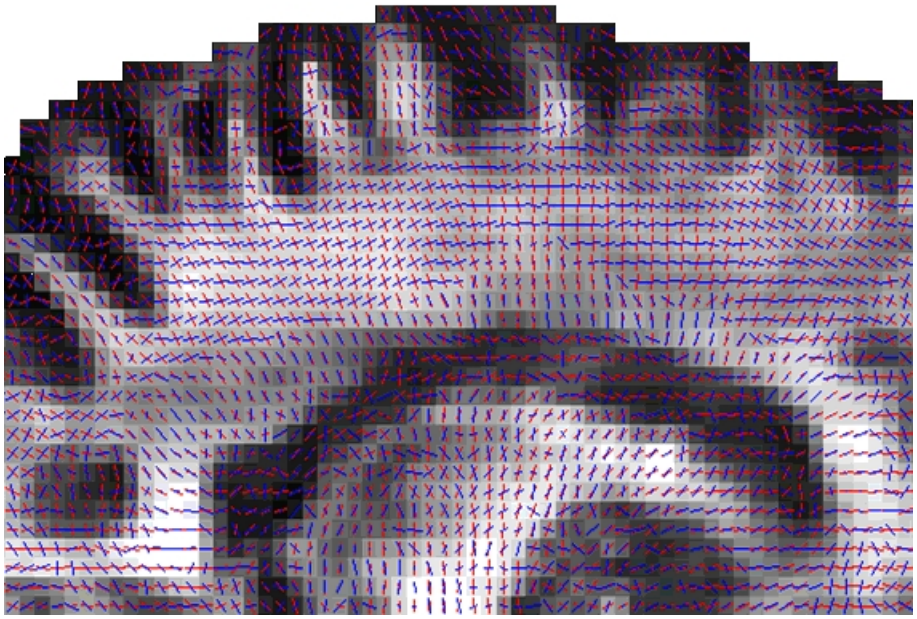

Figure 5.9 Crossing fibres.

This parasagittal slice through the central region and SMA shows the predominant direction of descending fibres (red) however, the second most likely fibre orientation travel in an anterior – posterior direction (blue). We could show that these fibres are increased in patients with JME, resulting in a higher proportion of crossing fibres, explaining a reduced FA in the mesial frontal lobe.

5.4.3 Morphometric studies of T1-weighted images in JME

Subtle morphometric abnormalities of mesial frontal gray matter have been the first focal structural alterations described in JME patients (Woermann et al., 1999b), and these initial findings have been replicated several times.

There were, however, discrepancies between different morphometric studies. Some described increases in frontal gray matter volume (Kim et al., 2007) (Betting et al., 2006) (Lin et al., 2009b) which have been interpreted as microdysgenesis with ectopic neurons, while other studies reported reduced frontal gray matter volume (O'Muircheartaigh et al., 2011) (Tae et al., 2006), which is usually interpreted as regional neuronal loss. Some of these discrepancies may be explained by methodological differences in the

processing and analysis of T1-weighted images, or by differences in the patient cohorts, but they also illustrate, that the exact nature of alterations is not entirely clear yet.

One morphometric study additionally reported reduced bilateral occipital gray matter volume only in photosensitive JME patients, but not in JME who were not photosensitive (Lin et al., 2009b). This suggests specific structural alterations in certain subgroups of JME, similar to the indication from our data, where increased connectivity between the occipital lobe and the motor system was stronger in photosensitive patients.

Several morphometric studies have described reduced gray matter volume in the thalamus of JME patients ((Mory et al., 2011) (Lin et al., 2009b) (Kim et al., 2014) (Saini et al., 2013) (Pulsipher et al., 2009).

A meta-analysis (Cao et al., 2013) has identified two common findings from seven morphometric studies in JME patients: 1) an increased gray matter volume in the SMA and mesial frontoorbital cortex and 2) a bilateral decrease of gray matter volume in the thalamus.

To date the only histopathological report on JME patients is the study by Meencke and Janz (Meencke and Janz, 1984) which included two patients with JME. Both patients had frequent seizures, insufficient response to anticonvulsive mediation and psychiatric comorbidities. In spite of this clinically severe form of JME, there was no evidence for major neuronal loss in neuropathology, except for selective neuronal loss in the nucleus mesialis of the thalamus in one patient.

5.4.4 Other functional imaging studies in JME

In a recent EEG-fMRI study, JME patients and controls were exposed to intermittent photic stimulation during a simultaneous EEG - fMRI scan. Both groups showed the expected BOLD response to photic stimulation in the visual cortex, but patients with JME additionally showed a stronger negative BOLD response in the sensorimotor cortex and in regions representing the default mode network (Bartolini et al., 2014). The increased functional effect of occipital activation on the sensorimotor system correlates well with the increased measures for structural connectivity between the supplementary motor area and the occipital lobe that we described here. Although we had too few patients with known photosensitivity for a direct group comparison or correlation analysis, this connectivity alteration was stronger in photosensitive patients in our cohort. The increased functional coupling between the occipital cortex and the default mode network, described by Bartolini et al, matches our finding from fMRI with an impaired default mode deactivation during the cognitive task (chapter 4.4.9 page 167)(Vollmar et al., 2011). In summary, their study (Bartolini et al., 2014) confirms an altered interaction between the motor system and other neuronal networks in JME patients as we have described in the previous chapter

Using FDG-PET to quantify regional brain glucose metabolism, Swartz et al reported an decreased frontal glucose utilisation in JME patients (Swartz et al., 1996). This effect was seen at the resting baseline, and there was an impaired activation during a working memory paradigm. The degree of hypometabolism correlated with poor performance in the working memory task in JME patients.

A similar correlation of reduced frontal glucose uptake with impaired executive functioning was later replicated in another PET study in patients with JME (McDonald et al., 2006)

Other PET imaging studies in JME patients showed additional alterations in neurotransmission, such as reduced serotonin receptor binding in the frontal lobe (Meschaks et al., 2005) and also alterations of the dopamine transporter capacity in the midbrain (Ciumas et al., 2008) and dopamine receptor binding in the posterior putamen (Landvogt et al., 2010).

Magnetic resonance spectroscopy studies have investigated metabolic alterations in JME patients and have reported reduced levels of N-acetyl-aspartate in the thalamus (Mory et al., 2003). Studies in IGE patients also reported decreased N-acetyl-aspartate levels and increased glutamate / glutamine levels, probably indicating increased excitability (Simister et al., 2003). A more recent magnetic resonance spectroscopy study has shown additional alterations of Gamma-aminobutyric acid (GABA) transmission, which was decreased in the thalamus and increased in the frontal lobe (Hattingen et al., 2014).

Most MRS studies use rather large volumes within the frontal lobe, and typically use regions in the dorsolateral pre-frontal cortex. None of the above studies has specifically investigated the mesial frontal region and SMA, where we found most alterations of functional and structural connectivity.

5.4.5 Thalamo-cortical connectivity

Several recent studies showed alterations of thalamo-cortical connectivity in patients with JME and in mixed cohorts of patients with different IGE syndromes. This is relevant, when interpreting alterations of functional connectivity. Functional effects between two cortical regions can be based on direct cortico-cortical effects, or they can be facilitated via the thalamus exerting effects on both cortical regions.

Here I showed evidence for an increase of direct cortico-cortical structural connectivity between the pre-frontal cognitive system and the motor cortex in JME. However, given the heterogeneity of JME and given the multitude of clinical, imaging, electrophysiological and genetic findings in this disease, most likely several mechanisms are involved.

In our cohort, we have also investigated structural and functional thalamo-cortical connectivity in JME patients (O'Muircheartaigh et al., 2012).
We found a reduced structural connection probability between the anterior thalamus and the SMA and motor cortex. We have also investigated functional connectivity and its psychophysiological modulation by a verbal fluency task. Healthy controls showed a task induced reduction of functional connectivity between the thalamus and bilateral SMA and motor cortex. This effect was absent in JME patients, indicating a failed negative feedback mechanism of cognitive activity on thalamo-motor cortex connectivity.
In relation to the increased functional connectivity between pre-frontal cognitive areas and the motor system we described before (Chapter 4, page 134)(Vollmar et al., 2011), this indicates that at least part of the increased functional connectivity is facilitated via impaired thalamic inhibition of the motor system.

A recent study, in 49 IGE patients (31 of which had JME), combined T1 morphometry and resting state fMRI (Kim et al., 2014). The authors showed a reduced functional connectivity of the anterior thalamus to the mesial pre-frontal cortex and mesial precuneus in IGE patients, similar to our findings. In their study, reduced functional thalamic connectivity correlated with longer disease duration, indicating a progressive decline over the course of the disease.

Using DTI data in 10 patients with JME, Deppe et al showed a reduced FA in the anterior limb of the internal capsule, connecting the anterior thalamus to the pre-frontal cortex (Deppe et al., 2008). This FA reduction seems to reflect an impaired structural connectivity between the thalamus and the frontal lobe, matching the structural connectivity findings from our study (O'Muircheartaigh et al., 2012) and the reduced functional connectivity reported by Kim (Kim et al., 2014).

The fact that some morphometric studies have found a correlation between both frontal and thalamic volume changes with neuropsychological performance suggests an impact of this altered circuitry on cognitive performance (Hutchinson et al., 2010). This is further strengthened by anti-correlated metabolic effects in GABA-ergic neurotransmission reported from magnetic resonance spectroscopy in JME (Hattingen et al., 2014).

In summary, there is convincing evidence from different independent modalities that alterations in thalamo-cortical connectivity contribute to the pathophysiology of JME. Impaired thalamic inhibition of the motor system in response to pre-frontal cognitive activation may play a key role.

5.5 Conclusion

The findings from this connectivity fingerprinting study link several clinical observations in JME.

An increased structural connectivity between the pre-SMA and the motor system provides an explanation for the specific effect in JME, where cognitive effort and praxis can trigger motor seizures in the central region.

The impaired intra-frontal connectivity may represent the structural basis of frontal lobe dysfunction, frequently seen in JME.

Increased connectivity between the motor system and the occipital lobe may reflect the structural basis of photosensitivity.

JME is “the most common” generalised epilepsy syndrome, probably because the syndrome currently includes patients with a wide spectrum of clinical manifestation. There are huge differences between JME patients with regard to seizure frequency, specific, trigger mechanisms, type and degree of cognitive impairment, psychiatric comorbidities, response to treatment and also genetic findings. Most likely this diversity represents different subsyndromes of JME, where different aspects of the multifactorial pathophysiology contribute differently to ictogenesis. As indicated by the results from this study, we hypothesise that individual functional and structural connectivity profiles in JME can identify such subsyndromes via specific alterations in different neuronal systems, supporting the recent concept of “system epilepsies”.

The presence of clear structural alterations in our well controlled cohort with many seizure free patients strongly argues for these alterations to be a pre-existing determining factor rather than a secondary effect of seizures.

We could show evidence for two different mechanisms of connectivity alterations: 1) direct cortico-cortical connectivity changes and 2) alterations of functional connectivity via changed cortico-thalamo-cortical feedback circuits. Given the heterogeneity of JME described above, these different mechanisms are in no way mutually exclusive, but most likely are both involved to different degrees in the different subsyndromes within the JME population.

Methodologically this DTI study shows that the truth behind reduced FA can be more complex - and much more interesting - than just “neuronal loss”.

6. Frontal lobe epilepsy – functional effects

6.1 Background

The aim of our fMRI analyses from patients with frontal lobe epilepsy (FLE) was to identify common correlates of specific cognitive impairments, often observed in patients with FLE. While our patient population has shown significant cognitive deficits, there were only few and weak consistent fMRI findings across the group of patients. This is partially explained by the heterogeneity of the FLE patient population, comprising different underlying pathologies, different clinical and neurophysiological findings. This heterogeneity reflects to some degree the different underlying pathologies, ranging from a small circumscribed lesion of 1 cm to a diffuse pathology, involving a whole hemisphere. Furthermore cognitive processes, such as the ones studied by our paradigms, are often carried out by complex neuronal networks, with different possible strategies, which might vary between patients with different functional deficits. Given the huge variability of individual findings, a number of FLE patients can hardly be considered a "group". Therefore I have carried out only few traditional group analyses in these patients, but rather focussed on a new methodological approach, to analyse results from a single individual patient by statistical comparison against the healthy control population.

6.2 Individual patient results

The analysis of individual FLE patient's fMRI paradigms revealed an extremely heterogeneous pattern of activation. While some patients showed an entirely normal distribution of activation, some showed no activation at all and had to be excluded from further analyses. The majority of patients in between these two extremes showed a very wide spectrum of spatial distribution of their activation.

Two examples are shown here to illustrate possible effects in FLE patients.

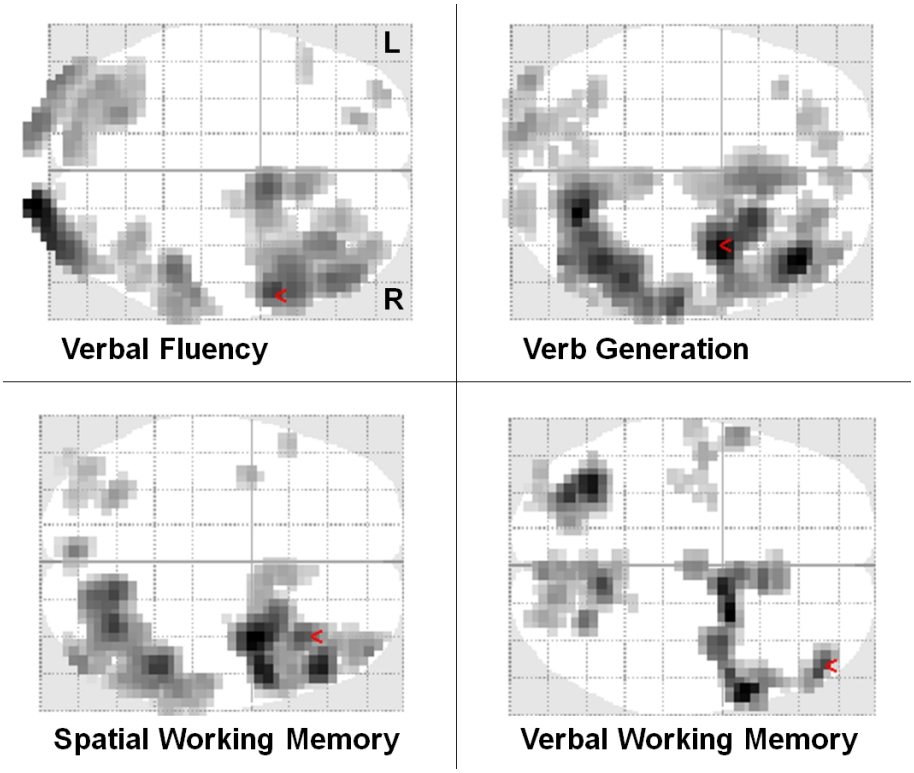

Figure 6.1 Single FLE patient fMRI, example 1. SPM glassbrain seen from top

The patient shown in Figure 6.1 had FLE with early childhood onset which was clinically not clearly lateralized. All four paradigms which usually activate the left frontal lobe in healthy controls, did not elicit any left frontal activation in this patient. This indicates consistent dysfunction of the left frontal lobe.

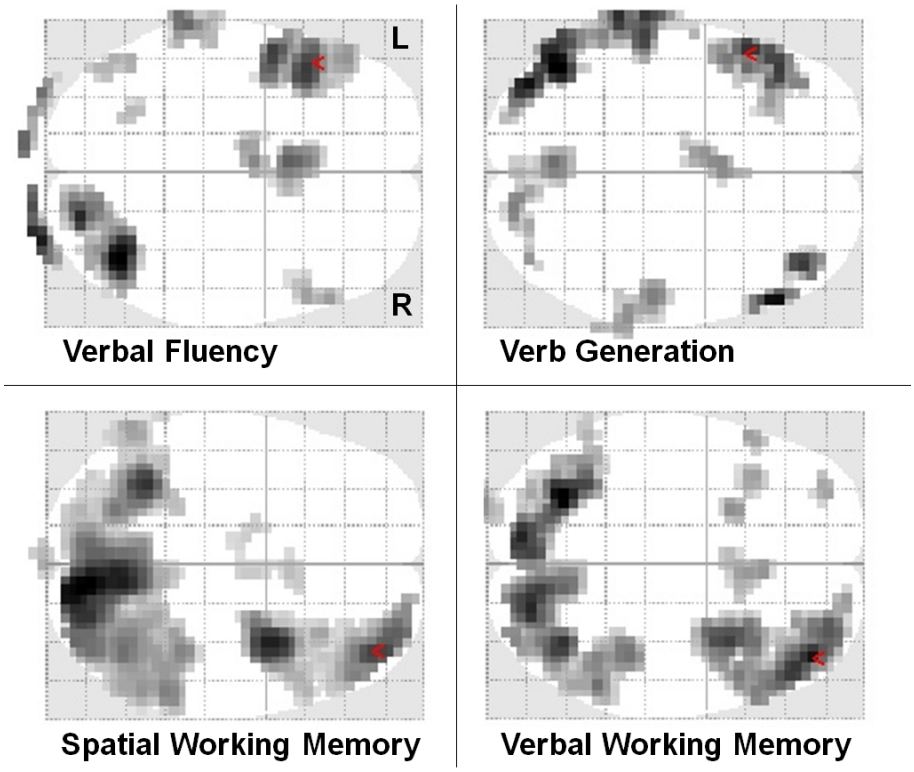

Figure 6.2 Single FLE patient fMRI, example 2. SPM glassbrain seen from top

The patient shown in Figure 6.2 also had left FLE, but with onset at the age of 8. He did show clear left language dominance, indicated consistently by both language paradigms. The two working memory paradigms, however, showed no left frontal activation, indicating reorganisation of executive functions to the right frontal lobe, while language function still remains in the epileptic left frontal lobe.

The specific activation pattern in these two cases might be visually easy to appreciate, and indeed allow inferences for these two individual cases. However, these examples also show, how such effects are difficult to describe other than qualitatively.

6.3 Group analyses

In the group analysis patients with frontal lobe epilepsy generally showed a diffusely reduced activation in all fMRI paradigms, affecting both hemispheres.

Group analysis of the activation from the dot-back paradigm showed bilateral frontal and parietal activation in healthy controls (red in Figure 6.3), and diffuse bilateral reduction in both, left and right FLE patients (blue).

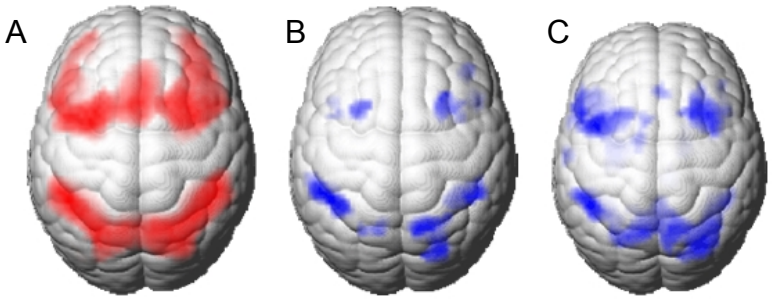

Figure 6.3 Bilaterally reduced activation in left and right FLE

Bilateral frontal and parietal activation ("2-back minus 0-back" contrast) in healthy controls (A, p<0,001 FDR). Left and right FLE patients showed decreased activation compared to healthy controls (B and C, group differences shown, p<0.05 FDR)

6.4 Functional connectivity

We performed functional connectivity analysis of language fMRI data in controls and patients with FLE. For this purpose a seed region was defined in the left inferior frontal gyrus of the left hemisphere, and functional connectivity analysis was carried out to identify voxels with a signal time course correlated to the seed region in the temporal lobe.

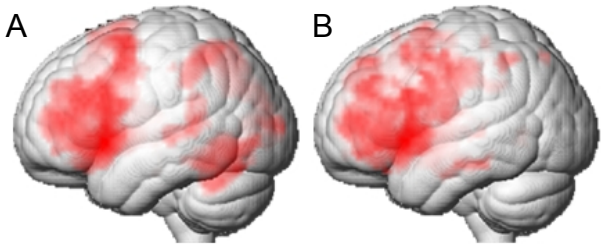

Figure 6.4 Functional connectivity of the language network in controls (A) and FLE patients (B)

In healthy controls this resembled the known language network of the left hemisphere, including the left inferior frontal gyrus, parietal lobe and posterior temporal neocortex (Figure 6.4, left) In FLE patients we saw a reduced functional connectivity to the temporal lobe, indicating disruption of the regular language network. However, at the same time, increased and a more widespread functional connectivity within the left frontal lobe was seen, reflecting individual reorganization within the left frontal lobe.

6.5 Quantification of Dysfunction

6.5.1 Background

Given the challenges with group comparisons in such a heterogeneous group, we rather focussed on the possibility to use fMRI as complementary diagnostic tool to quantitatively identify dysfunctional cortex in individual patients.

We investigate the usefulness of a battery of four cognitive fMRI tasks and a novel optimized analysis approach to identify areas of cortical dysfunction and provide clinically relevant lateralizing and localizing information about the functional deficit zone in individual patients. This new analysis methodology was applied in a cohort of FLE patients with no visible lesion in MRI or with one small single lesion in a frontal lobe with the aim to provide evidence on the epileptogenic zone.

6.5.2 Subjects and Methods

6.5.2.1 Study population

A total of 62 patients with FLE were identified and scanned for this study. For this quantitative fMRI analysis we wanted to separate the effect of chronic epilepsy from the effect of structural lesions, and only included patients with non-lesional FLE, or lesions smaller than 15mm. This left 58 patients with pharmacoresistant FLE for quantification: 52 (90%) from the National Hospital for Neurology and Neurosurgery, London and six patients (10%) from King's College London. Fifty-six of these patients (97%) underwent presurgical epilepsy evaluation including prolonged EEG-Video monitoring; two patients had only ambulatory EEG but unequivocal history of FLE.

Thirteen patients and four controls were excluded from the final analysis for the following reasons:

a) because one or more of the four fMRI paradigms failed to elicit activation (mostly the dot-back task), b) because subjects fell asleep during one of the paradigms, c) because subjects were unable to perform the cognitive tasks despite prior training, or d) because of excessive movement during the fMRI acquisition (more than 5 mm once, or more than 3 mm repeatedly, or synchronized with the switch between active and resting condition)

Forty-five patients with FLE, (24 female, mean age 33.2, SD 9.7 years) and 20 healthy controls (same population as for the JME study, 12 female, mean age 31.4, SD 8.6 years) successfully completed all four fMRI paradigms and were included in the final analysis.

In this final group of 45 FLE patients, 33 (73%) had no visible lesion in clinical 3-Tesla MRI after review by an experienced neuroradiologist and epileptologist. The other 12 patients had small lesions of less than 15mm diameter: focal cortical dysplasia (FCD, n=9), cavernoma (n=2) or glioma (n=1).

Based on the review of all available clinical data, 25 (56%) had left FLE and 20 (44%) had right FLE.

6.5.2.2 fMRI paradigms

All participants performed a total of four block designed cognitive fMRI paradigms, which comprised of two language and two working memory paradigms, as previously described (Stretton et al., 2012). All blocks had 30 seconds of duration, alternating active task with resting blocks. In the Verbal fluency paradigm, single letters were presented to the subject, with the instruction to think of words starting with that letter.

In the Verb generation tasks, series of single words were presented, with the instruction to mentally repeat the presented word (control condition) or to think of an associated verb. The spatial working memory paradigm consisted of randomly appearing dots, where subjects had to indicate the position of previously presented dots with a joystick. During the Verbal working memory task, series of words were presented and subjects had to indicate, when a word was repeated. For all paradigms, subjects were specifically instructed for the rest period, to maintain fixation but not to think about the previous or upcoming tasks.

6.5.2.3 fMRI analysis

The fMRI analysis was performed using SPM 5 software (http://www.fil.ion.ucl.ac.uk/spm/). Images were realigned for movement correction, spatially normalised to an acquisition-specific EPI template in Montréal Neurological Institute (MNI)-space, re-sampled to isotropic 3x3x3mm voxels, and finally smoothed with an 8x8x8 mm kernel. First-level statistical analysis was performed using the general linear model and included Realignment parameters as multiple regressors to model subject head movement during the experiment. Contrasts were defined by comparing active conditions against the resting period and also against a control task.

Single-subject activation - visual inspection

The individual activation pattern from each cognitive task was visually inspected for each patient, using a threshold of $p<0.01$ (uncorrected) and a cluster extend threshold of 20 voxels. Patients who did not show any activation in one or more paradigms at this

threshold, and patients where the activation patterns were suspicious of artifactual activation, e.g. from movement, were excluded from further analysis.

Single-subject activation – statistical analysis

As we compared individual patients against a group of healthy controls, this resulted in an extremely small group comprised of only one subject. In SPM, the statistics are optimized for comparison between similarly sized groups of subjects and are usually overly conservative for very small groups and for single subjects. Consequently, and considering the heterogeneity of clinical findings, we considered each individual patient as a single subject and followed recommendations by R. Henson for statistical analysis of single subjects using difference images (in: http://www.mrc-cbu.cam.ac.uk/people/rik.henson/personal/Henson_Singlecase_06.pdf). For every patient, 20 difference images were created for every fMRI task, subtracting the patient's activation contrast from every single control's activation contrast. The 80 resulting difference contrast images for one patient were then analysed using one sample T-tests, with the null hypothesis, that these differences show a random distribution and average to zero. Contrasts were defined, identifying areas which were significantly different from the control population. Reduced activation, compared to controls was defined as dysfunction, whereas areas of increased activation were defined as reorganization. To improve reliability, the two language tasks and the two working memory tasks were combined for analysis of dysfunction and reorganization in language and in working memory. To identify areas consistently dysfunctional across both cognitive domains, a global dysfunction contrast was defined, testing for reduced activation across all four cognitive tasks.

6.5.2.4 Regions of interest and quantification

To identify the spatial distribution of cognitive networks involved in the fMRI tasks in healthy controls, a combined group activation map from all four tasks was defined as "taskmap". The left and right frontal and extra-frontal regions were each divided in regions within and outside this task map, separating findings within the normal cognitive networks from those outside. The resulting eight regions of interest (ROI) were used for quantification of dysfunction maps from individual patients by determining the number of voxels within each ROI, deviating from the activation pattern seen in healthy controls, with a T-score greater than eight.

This quantification provides for every patient eight values for dysfunction and reorganization. These were calculated for the three difference contrasts mentioned above, based on 1) language, 2) working memory and 3) the combination of all cognitive tasks.

To define the range of normal variation of individual activation patterns, the same analysis was applied to healthy controls, comparing every single control against all other subjects from the control group.

6.5.3 Results

6.5.3.1 Activation patterns in healthy controls

Healthy controls showed activation of the left middle and inferior frontal gyrus and superior temporal gyrus during the language tasks. The working memory tasks elicited bilateral activation of the middle frontal gyrus and superior parietal lobe. A thresholded outline of this group activation map was used to define the taskmap.

Healthy controls also showed "dysfunctional" voxels in all examined ROI, according to our definition of "less activation than in all other controls" . This deviation from the group average represents the range of variability of individual activation patterns in a healthy control population. Allowing for a 5% false positive rate amongst the 20 controls, the second highest dysfunction score for every region was chosen as threshold to define "dysfunction" in FLE patients.

6.5.3.2 Overall dysfunction in FLE patients

Twelve of 25 patients with left FLE (48%) and 11 of the 20 patients with right FLE (55%) showed values of global dysfunction beyond the range of variation observed in healthy controls, i.e. more than 789 dysfunctional voxels.

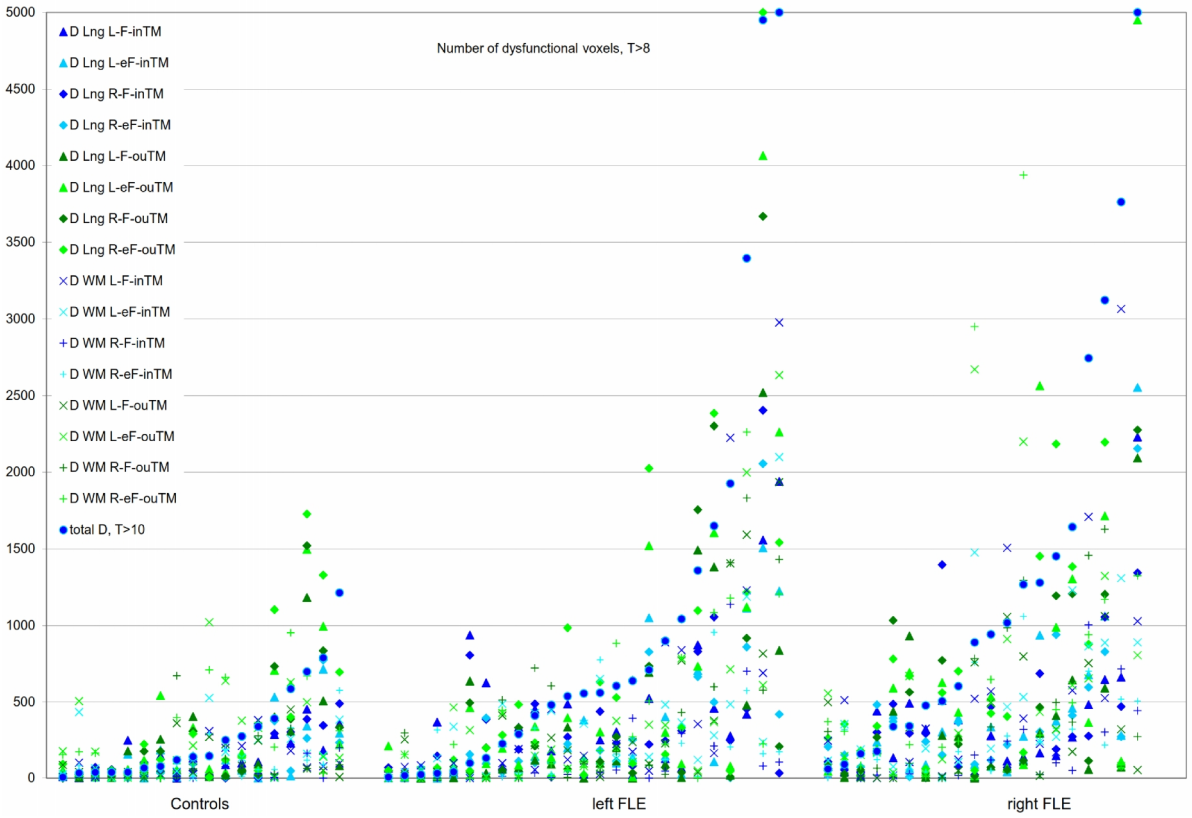

Figure 6.5 Quantitative dysfunction in healthycontrols, left FLE and right FLE

Figure 6.5 shows the distribution of cortical dysfunction, measured as number of voxels with T-score > 8 for each region of interest (ROI), derived from the language tasks (Lng) and from the working memory tasks (WM). Healthy controls and FLE patients are sorted in ascending order of the total dysfunction score.

6.5.3.3 Dysfunction within and outside the taskmap

Comparing dysfunction in1 individual ROI, when including ROI within and outside the taskmap, healthy controls showed a much higher range of "dysfunction" outside the core taskmap, representing bigger individual differences in the activation pattern. Consequently only few patients (7 of 25 left FLE, 11 of 20 right FLE) reached dysfunction values beyond the range seen in healthy controls.

Restricting the analysis to ROI within the taskmap, i.e. to the main areas usually activated during the cognitive tasks, 12 of 25 left FLE (48%) and 12 of 20 right FLE (60%) showed dysfunction values larger than in controls.

6.5.3.4 Lateralization of dysfunction

From the 12 left FLE with supra-threshold dysfunction, the maximum dysfunction was located on the left side (n=5), bilateral (n=4) or on the right side (n=3). From the 12 right FLE patients, the maximum supra-threshold dysfunction was right-sided (n=6), bilateral (n=3) or left-sided (n=3).

6.5.3.5 Language and working memory specific dysfunction

In the 12 left FLE, the maximum dysfunction was detected in the language paradigms in 6 and in the working memory paradigms in the other 6 patients. From the 12 right FLE, the maximum dysfunction was observed in the language paradigms in 5 and in the working memory paradigms in 7 patients.

6.5.3.6 Frontal and extra-frontal dysfunction:

From the 12 left FLE, the maximum dysfunction was detected in frontal ROI in 10 and in extra-frontal ROI in 2 patients. In the group of 12 patients with right FLE, maximum dysfunction was found in frontal ROI in only 4 and in extra-frontal ROI in 8 patients.

6.5.3.7 Correlation with Neuropsychology

We assessed correlation of our fMRI quantification findings with neuropsychological performance based on our a-priori hypotheses of material-specific effects across groups (left and right) and tasks (verbal versus non-verbal). The following correlations were observed for the two groups of fMRI tasks (language and working memory):

Language fMRI: only in patients with left FLE, there was a correlation between language fMRI and language performance scores: the greater the fMRI dysfunction, the lower the Verbal Fluency scores. There was also an association between increased frontal recruitment and a higher error score, i.e. intrusions and repetitions in the verbal fluency tests.

Working memory fMRI: only in right FLE patients, there was a correlation between working memory fMRI and memory performance. The greater the right frontal and extra-frontal dysfunction, the lower the design and list learning scores.

None of the other neuropsychological measured showed a significant correlation with any of the quantitative measures of dysfunction or reorganization.

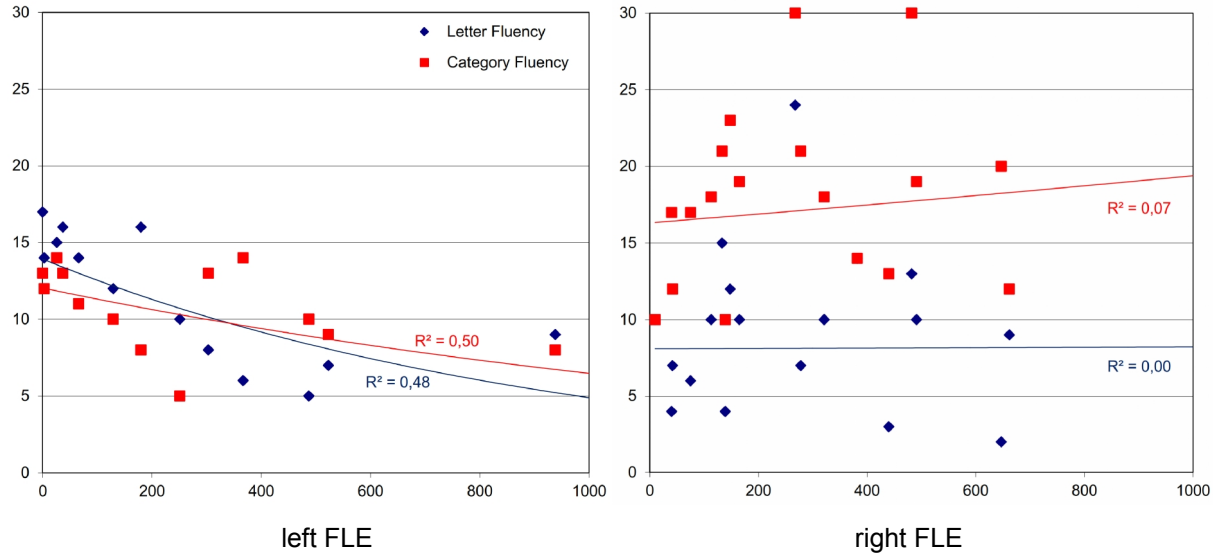

Figure 6.6 Dysfunction in language fMRI correlates with reduced verbal fluency in left FLE

The achieved verbal fluency score (y-axis) of left FLE patients was lower for patients with a higher number of dysfunctional voxels (x-axis), i.e. voxels with significantly reduced activation during language fMRI, compared with healthy controls. No such correlation was seen in right FLE patients, who on average achieved higher verbal fluency scores.

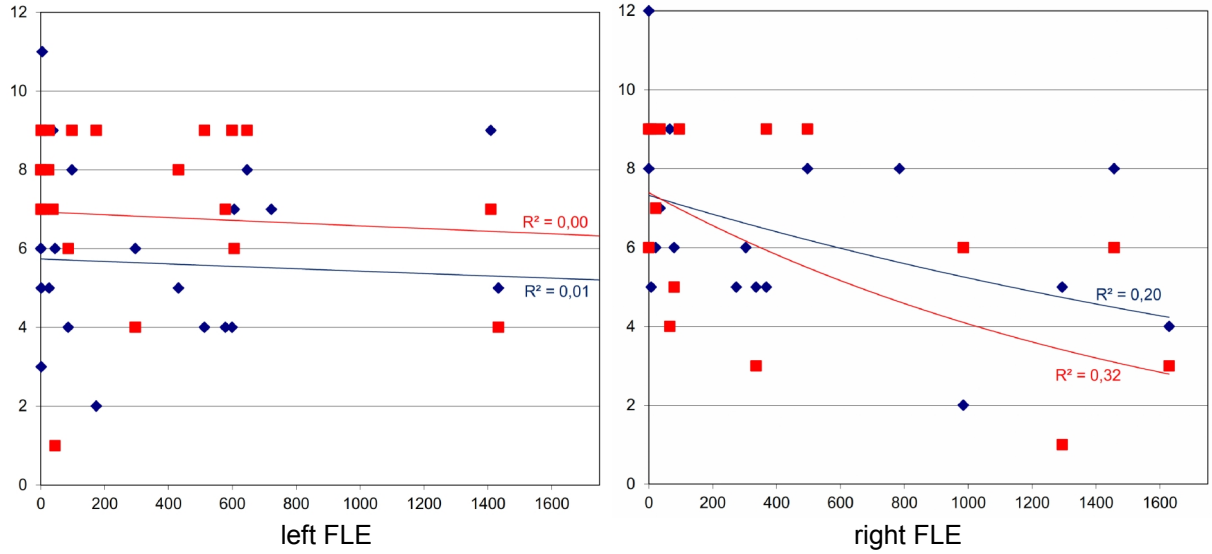

Figure 6.7 Dysfunction in working memory fMRI correlates with reduced learning scores in right FLE

The achieved list learning and design learning scores (y-axis) of right FLE patients was lower for patients with a higher number of dysfunctional voxels (x-axis), i.e. voxels with significantly reduced activation during working memory fMRI, compared with healthy controls. No such correlation was seen in left FLE patients.

6.5.3.8 Correlation of Reorganization with Neuropsychology

Similar to the way we defined "dysfunctional" voxels as those, less activated than in healthy controls, we have also defined "reorganized" voxels as those that are more active in an individual patient, than usually seen in controls. Such reorganized voxels represent brain areas recruited by patients, probably trying to compensate for some deficits caused by dysfunctional voxels elsewhere.

Looking into the correlation of reorganized voxels with neuropsychological parameters, there were two noteworthy observations, only found in the group of patients with left FLE :

Reorganization, i.e. the additional recruitment of neuronal resources in brain areas outside the seizure onset zone was correlated with a better verbal fluency score. The more voxels were recruited, the higher the verbal fluency score.

Interestingly, this correlation was stronger between voxels recruited in the right frontal lobe and the letter fluency score, probably indicating, that this not very specific task can be successfully "taken over" by right frontal cortical areas.

On the other hand, the number of recruited voxels in the left extrafrontal region showed a stronger correlation with an improved category fluency score, probably indicating, that this semantically more demanding task is better compensated by left hemispheric cortical areas within the language dominant hemisphere, but outside the diseased frontal lobe.

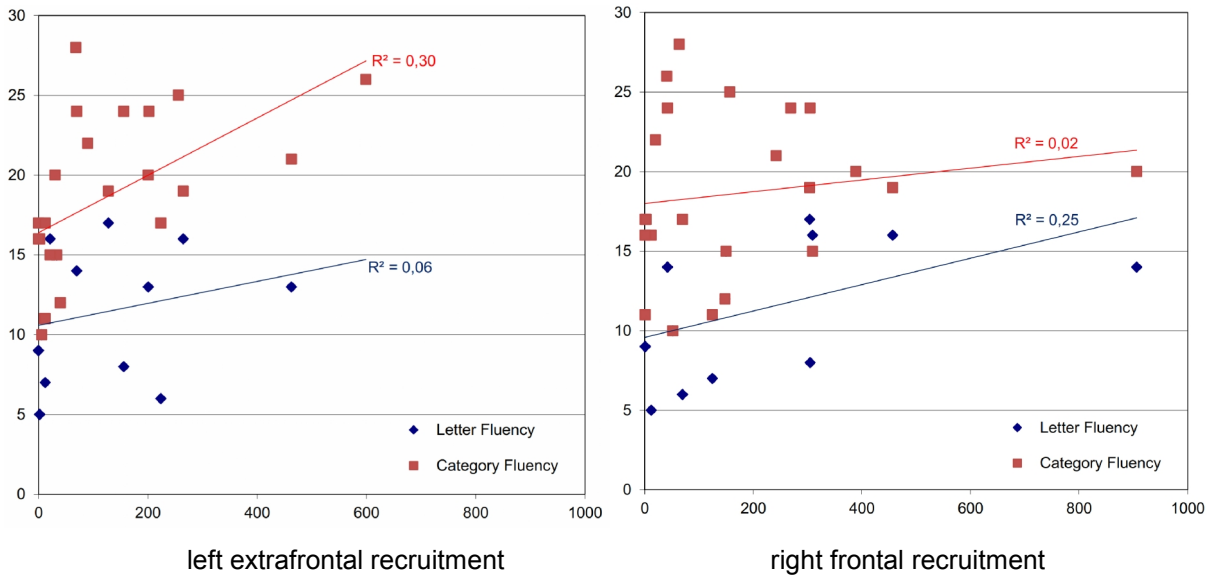

Figure 6.8 Reorganisation in Language fMRI correlates with improved verbal fluency in left FLE

The achieved verbal fluency scores (y-axis) of left FLE patients increased with a higher number of reorganized voxels (x-axis), i.e. voxels with significantly higher activation during language fMRI, than usually seen in healthy controls. This correlation was stronger between left extrafrontal recruitment and an improved category fluency score. Right frontal recruitment, contralateral to the seizure onset, showed a stronger correlation with improved letter fluency performance.

The third correlation we observed was between the number of reorganized voxels within the left frontal lobe and a higher number of errors made during the test. The more voxels were increasingly activated in the left frontal lobe, the more repetitions and intrusions occurred during the verbal fluency test. Even though this correlation was partially driven by one patient and we had data only from some patients, it is still interesting because it provides indirect evidence for the “dysfunction” in the left frontal lobe: recruiting voxels there does not actually improve performance, but rather introduces mistakes.

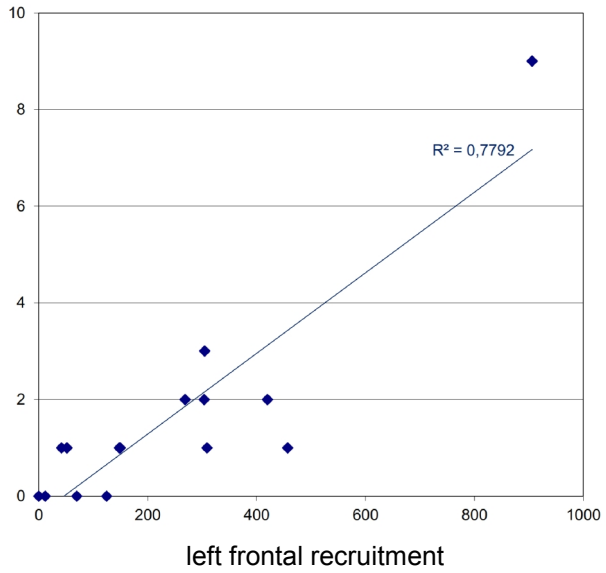

Figure 6.9 Reorganisation within the diseased left frontal lobe correlates with increased mistakes

A higher number of recruited voxels within the left frontal lobe (x-axis), i.e. voxels with significantly higher activation during language fMRI, than in healthy controls was correlated with more mistakes (y-axis: number of repetitions + intrusions) in the verbal fluency assessment.

6.5.4 Discussion

We present a novel diagnostic approach using cognitive fMRI to provide localizing information in the clinically challenging group of patients with FLE through the identification of dysfunctional cortex.

The combined analysis of all four cognitive fMRI tasks revealed cortical areas of reduced activation, i.e. dysfunction, in about half of our patient cohort.

Four patients had a complete absence of activation in one frontal lobe or in one brain hemisphere during all fMRI tasks, indicating significant, widespread cortical dysfunction. Twenty-one patients showed an activation pattern, for all fMRI tasks, not significantly different from healthy controls. The remaining 20 patients showed other patterns of reduced activation with a variable distribution of their individual dysfunction. Most clusters of dysfunctional voxels were consistent with the electro-clinical lateralizing and localizing information. Only six patients showed areas of maximum dysfunction in the contralateral hemisphere.

The heterogeneity of our fMRI results is not surprising, given the heterogeneity of the clinical, electrophysiology, neurophysiology and structural imaging findings in FLE, also reflected in our patient cohort.

FLE is a heterogeneous group of disorders, both congenital and acquired, with varied and often unknown location and extension of the epileptogenic zone and underlying histopathological changes.

The specific nature of the underlying pathology for each FLE patient is likely to have a different impact on cognition. Duration of epilepsy, age at seizure onset, seizure frequency are other factors likely influencing the changes in cognitive networks over time. The re-organization process varies widely between patients, further reflecting the different individual pre-existing cognitive networks, the different functional relevance of the affected areas, and the different compensation capacity and strategies of each patient.

Functional MRI studies have advanced our knowledge of the effects of refractory seizures, lesions and surgery in cohorts of patients with temporal lobe epilepsy (TLE) with a limited number of well-defined pathologies, such as hippocampal sclerosis or dysembrioplastic neuroepithelial tumour (DNT) and treated usually with standardized operations (anterior 2/3 temporal lobectomy, or selective amygdalo-hippocampectomy). Even in the more homogeneous and better characterized TLE patient group, the current value of fMRI is limited for the individual patients. The heterogeneity of the seizure-onset zone localization within the frontal lobe, the underlying aetiology and the proposed surgical interventions precludes any group analysis in FLE, we focus on the interpretation of results in single patients.

fMRI is not a quantitative method. Hence, it is used primarily for lateralization of language and memory functions in unilateral pathologies, rather than for quantification. In the case of cryptogenic epilepsies arising in the frontal lobe, lateralization of function is not necessarily sufficient and localization has to be compared with the individual variability of activations in healthy controls. There are several constellations, where our approach has shown benefit for the individual patient:

In 12 patients, fMRI showed a predominant cluster of "dysfunction" in the presumed epileptic frontal lobe. Here, the findings from fMRI increase the confidence in the clinical diagnosis and predict a low risk of cognitive side-effects from resective epilepsy surgery.

In 15 patients with clearly lateralised, but more widespread alteration of the activation pattern, fMRI may indicate the presence of a more widespread epileptogenic network, probably indicating reduced chances for seizure freedom after a frontal lobe resection.

In two left FLE patients , our quantification showed a single left parietal cluster of dysfunction, without alterations of frontal activation pattern, possibly indicating a left parietal focal pathology not previously detected. Parietal lobe epilepsy has been shown to often propagate rapidly to the frontal lobe, mimicking symptoms and diagnostic findings of FLE.

In half of the patients, activation maps were not significantly different from those in healthy controls, suggesting either a very small, circumscribed lesion, or a lesion outside the cognitive networks covered by our set of paradigms.

Our approach of "dysfunctional MRI" seems particularly capable to identify patients with diffuse, widespread pathologies, who may require extensive invasive recordings and who may prove to have multifocal seizure onset and less favourable surgical outcome.

6.5.4.1 Comparison between left and right frontal lobe

Memory and language performance are influenced by many factors, including attention and motivation, which are known to comprise frontal and more complex networks than language or specific memory functions itself. A lack of correlation between fMRI and

neuropsychological findings is not surprising, as “damage” may be located anywhere in the frontal lobe, which is well connected with fast spread of seizure activity within and across both frontal lobes.

On a group level, the most obvious differences between patients and healthy controls were:

6.5.4.2 Dysfunction correlates negatively with verbal fluency only in left FLE

Language fMRI mainly activated the left frontal lobes in both, patients and controls. In FLE patients, however, the comparison against the healthy control population revealed significant right frontal dysfunction. It is known that language processing is a bilateral task, even though activation is usually much stronger on the left. Apparently the language tasks do involve right hemispheric activation that may be weaker than on the left, but seems to be a relevant part of the language processing network. This is consistent with previous reports on right-sided language processing. Interestingly, this right frontal dysfunction in language fMRI showed an association with memory measures from the neuropsychology assessment performed before scanning the patient/ out of the scanner. This may reflect the influence of higher order frontal lobe functions such as attention or motivation that are supportive for language tasks.

Our observations may be representative of the more widespread functional networks of the right frontal lobe. Whereas the language dominant left frontal lobe is more specialized and involved within the left-hemispheric language network, the right frontal lobe is typically more involved in complex higher cognitive functions that require widespread bilateral cortical activation. Whereas left FLE appears to cause dysfunction

in rather enclosed, highly specialized functional subsystems, which need immediate compensatory recruitment in neighbouring or contralateral homolog areas, right FLE causes more widespread, extra-frontal dysfunction, which does not seem to require equivalent recruitment of compensatory areas.

6.5.4.3 Increased extra-frontal dysfunction in right compared to left FLE patients

Right FLE patients showed increased dysfunction within and beyond the affected right frontal lobe, which may indicate an effect of a right-sided focus on higher order cognitive systems, including remote areas in the right parietal and temporal lobes.

Interestingly these patients did not show a lower neuropsychological performance level, possibly indicating the intrinsic redundancy of such higher order functions. The absence of compensatory recruitment, as well as the similar performance level may indicate less functional relevance of their dysfunction. It is known that the more widespread higher order cognitive systems show greater plasticity and also, that lesions within such systems do not necessarily cause a deficit.

This is different from the more hard-wired primary language relevant areas such as the left inferior frontal gyrus, or even more so, the primary motor cortex, where a defined lesion will typically cause a very stereotyped deficit (e.g. accessory language areas in the basal temporal lobe can be resected without permanent deficit). In line with this explanation, our left FLE patients recruited widespread additional areas, activated by cognitive tasks, to compensate for the dysfunction within the “strategically more relevant” left frontal lobe.

6.5.4.4 Left FLE is associated with more widespread, contralateral frontal dysfunction than right FLE

Patients with left FLE on the other hand showed a more widespread, bilateral dysfunction with almost equal dysfunction scores on either side. In contrast, right FLE showed a highly lateralised dysfunction with the average right frontal dysfunction score being three times higher than the contra-lateral, left frontal dysfunction score. This difference most likely reflects the crucial role of the dominant hemisphere, where pathology does not only cause a local dysfunction, but also has remote effects on contralateral brain regions.

The most striking difference between left and right FLE patients was seen in the working memory paradigms. Whereas left FLE patients showed significant bilateral dysfunction on the working memory composite score, very little dysfunction was seen in patients with right FLE. This may reflect the higher potential for reorganization of executive functions like the working memory paradigms. The local effects of a right frontal pathology can be accounted for by reorganization, resulting in a well-functioning network of executive functioning, whereas the more severe impact of a left frontal pathology disrupts the bilateral cognitive network. This is consistent with the more severe neuropsychological impairment in left compared to right FLE.

6.5.4.5 Methodological considerations & Limitations

The application of dysfunction maps from combined analysis of a battery of cognitive fMRI tasks is novel. Our approach, not to rely on a single fMRI task, is in keeping with previous studies showing that a combination of several language fMRI tasks improves concordance with results from intracarotid amobarbital tests (IAT) (Gaillard, Balsamo et al. 2002). Additionally the combined statistical analysis of several language tasks in

one common model was shown to also increase the concordance with IAT results (Rutten, Ramsey et al. 2002). However, there is no established processing pipeline for the combination of fMRI paradigms from different domains, and no established criteria on thresholds of significance. The gross dysfunctional score, the number of dysfunctional voxels with a T-score > 10, showed a total range of 7 to 5415 voxels in patients and from 6 to 1214 voxels in controls, and the regional dysfunctional scores for every ROI showed a similarly increased range in patients. Allowing for a typical 5% false positive rate, we defined the cut-off for dysfunction scores at the second highest level seen in a healthy control, i.e. the one control with the highest dysfunction score would be wrongly diagnosed to be "dysfunctional".

Applying this threshold we have identified regional dysfunction in the frontal lobes in 28-48% of the patients, depending on the tasks analysed and on the side of presumed seizure onset. This relatively high yield is encouraging, as the majority of our patients had cryptogenic, non-lesional focal epilepsy and any localizing information is clinically beneficial in these patients. Also this yield is similar to other more invasive and more expensive diagnostic methods, such as FDG-PET and SPECT.

Our current battery of fMRI tasks has a clear bias towards the left hemisphere, which was activated by all four tasks, while the right hemisphere was only active during the two working memory tasks. Furthermore, FLE patients may have very different strategies to compensate for their dysfunction. A patient with right hemispheric disease and deficits in the visuo-spatial domain may use a more verbal strategy to complete a certain task.

One major limitation of our approach is that identifying dysfunction will only work in "functional" areas. Our method is limited to detect functional alterations in areas

activated by the performed tasks. The effect of focal epilepsy on other cortical areas cannot be assessed. Certain areas such as the fronto-orbital or fronto-polar cortex are difficult to investigate with common fMRI paradigms, and even a combination of more fMRI paradigms will be leaving some cortical areas uncovered. Focal pathologies in such regions would only alter activation maps, if secondary effects result in more widespread functional reorganization. Particularly the right frontal lobe contains large cortical areas which are "silent" at least to the rather coarse assessment from fMRI paradigms. Subtle higher functions such as appropriate social interaction are almost impossible to be activated by an fMRI task, and therefore a dysfunction in such areas would remain undetected.

Another limitation is of course the heterogeneity of activation patterns, depending on pre-existing cognitive networks, permanent and temporary effects of disease, seizures and medication, and different cognitive strategies applied to perform a certain task, that might vary between subjects and even within one subject. This is reflected in the detection of some significantly altered voxels in every healthy control, illustrating this inter-individual variability. This huge variability weakens statistical power to reliably detect abnormalities, particularly when the control population is rather small, as in our case. To have a better representation of "normal" activation patterns, it would be beneficial to have a larger control population for comparison.

For the correlation of quantitative fMRI measures with neuropsychological scores, the average performance in each group should be similar, which was not the case in our FLE cohort. The relatively low performance of this patient group might have hindered the identification of other correlations, and this might be possible in future studies, including higher performing patients.

Given these limitations, this approach, in its current implementation, is certainly not a recommended clinical test, but rather shows the potential of optimizing this approach, to develop a more sensitive and more specific test battery and analysis strategy, which might then be useful in selected clinical cases, where other imaging modalities fail to identify the underlying abnormality.

6.5.4.6 Future work

Our new approach, combining language and memory tasks, paves the way towards a more comprehensive "whole-brain activation map", including a variety of functional tasks, with increased sensitivity to detect dysfunctional areas in other parts of the brain.

A more comprehensive set of tasks and a bigger control population, providing more statistical power, might then also allow to make more inferences on the functional relevance of decreased or increased fMRI activation, particularly when controls are better matched to patients performance.

Another possibility to assess the relevance of fMRI activation alterations would be to compare pre-and post-operative activation maps with pre- and post-operative performance in individual patients. Preserved cognitive performance in spite of an altered postoperative activation pattern would indicate a less efficient or less relevant pre-operative strategy, whereas a postoperative cognitive decline would indicate a functionally relevant pre-operative activation pattern . Identical pre- and post-operative activation patterns on the other hand would indicate a full functional reorganization before surgery, with no need to further adjust after a resection.

7. Conclusions and Outlook

7.1 Conclusions DTI Test-Retest

Initially, the same DTI acquisition scheme, with 32 diffusion weighted directions was used at the two identical 3 Tesla MRI scanners on both study sites, UCL and King's College. This would have allowed to acquire DTI data of some subjects on one site and from other subjects on the other site. For such a distributed data acquisition, comparability of data had to be ensured before any group analyses of mixed data samples. Our results showed that although not identical, the inter-site variability between DTI data from both scanners was only slightly larger than the intra-site, test-retest variability on one scanner. Both were significantly lower than for DTI data acquired at 1.5 Tesla, ranging from approximately 1% to 2% coefficient of variation for measures from FA maps. This would have allowed for a combined analysis of data acquired at both sites.

Later on, a new DTI acquisition scheme was established at UCL, based on 52 diffusion weighted directions, with multiple interleaved B0 images. Also scan time availability allowed acquiring DTI data on both sites independently, so that ultimately two different DTI acquisitions were recorded for each subject, maximizing data compatibility with other research projects on each site. This has eliminated the need to pool DTI data from both sites, so our inter-site reliability assessment was not needed any more for further analyses of DTI data from this study.

However, the confirmation of a good inter-site reliability still holds true and might be useful for later projects, where large recruitment numbers and limited scan time raise the need to pool DTI data from two sites.

7.2 Conclusions JME

The initial aim of this study was to identify common areas of cortical dysfunction, underlying the cognitive impairment often seen in JME patients. However it turned out, our patient population simply didn't have a significant cognitive impairment, in most neuropsychological tests they performed similar to healthy controls. I assume, this reflects some recruitment bias, where well-functioning patients, many of them seizure free for years, are more willing to participate in a research study, than more affected patients with ongoing seizures and cognitive challenges. However, this allowed for the unexpected opportunity to study a sample of high performing JME patients and actually led to the discovery of a maybe even more interesting phenomenon, which might not have been seen in more impaired and underperforming patients.

In summary, our findings from fMRI in JME have shown an increased co-activation of the motor cortex during cognitive tasks with increasing task difficulty, on the basis of an increased functional connectivity between cognitive cortical areas and the motor system. During simpler tasks, JME patients usually showed the same cortical activation as healthy controls.

Rather than a simple 'loss of function' there appears to be a threshold of cognitive demand, beyond which cognitive activation is associated with excessive regional activation, across the borders of different functional networks. Such an excessive activation of large neuronal populations seems to be less efficient, as patients do still perform slightly below average. This excessive activation could also explain why many patients with JME find it particularly 'tiring' to focus on a demanding task like reading.

However, the most interesting aspect of this finding is that this load dependent co-activation of the motor cortex most likely directly shows the mechanism of cognitively triggered seizures in these patients: a functional short circuit between cognitive systems and the motor system.

The observed alterations of micro-structural connectivity of the mesial frontal region correlated strongly with the increased functional connectivity and may represent the anatomical basis for cognitive triggering of motor seizures in JME. Changes in the mesial frontal connectivity profile provide an explanatory framework for several other clinical observations in JME and may be the link between seizure semiology, neurophysiology, neuropsychology and imaging findings in JME.

Future imaging studies in JME should aim to further disentangle the relative contribution of cortico-cortical and thalamo-cortical connectivity changes. Studies on JME patients with specific prominent seizure triggers might allow to define JME subsyndromes, where a specific connectivity profile predicts certain clinical characteristics. The proof of microstructural connectivity alterations in well controlled, high performing JME patients indicates a genetic basis of some of these altertaions, and this should be investigated further in studies on siblings and families of JME patients as well as in studies combining neuroimaging and genetic testing.

7.3 Conclusions FLE

Cognitive fMRI has proven difficult for group analyses in FLE, given the huge heterogeneity of this patient group.

However, focussing on single subject analyses, cognitive fMRI was able to identify dysfunctional cortex in some patients with frontal lobe epilepsy and previously normal conventional structural MRI.

This novel method still requires optimization, to improve sensitivity and specificity, but has potential to provide complementary lateralizing and localizing information in patients with “non-lesional” FLE in the future.

.

8. References

Akgun, Y., Soysal, A., Atakli, D., Yuksel, B., Dayan, C., Arpaci, B., 2009. Cortical excitability in juvenile myoclonic epileptic patients and their asymptomatic siblings: a transcranial magnetic stimulation study. Seizure 18, 387–91. doi:10.1016/j.seizure.2009.02.002

Alexander, A.L., Lee, J.E., Wu, Y.-C., Field, A.S., 2006. Comparison of diffusion tensor imaging measurements at 3.0 T versus 1.5 T with and without parallel imaging. Neuroimaging Clin. N. Am. 16, 299–309, xi. doi:10.1016/j.nic.2006.02.006

Aliberti, V., Grünewald, R.A., Panayiotopoulos, C.P., Chroni, E., 1994. Focal electroencephalographic abnormalities in juvenile myoclonic epilepsy. Epilepsia 35, 297–301.

Appleton, R., Beirne, M., Acomb, B., 2000. Photosensitivity in juvenile myoclonic epilepsy. Seizure 9, 108–11. doi:10.1053/seiz.1999.0376

Archer, J.S., Briellmann, R.S., Syngeniotis, A., Abbott, D.F., Jackson, G.D., 2003. Spike-triggered fMRI in reading epilepsy: Involvement of left frontal cortex working memory area. Neurology 60, 415–421. doi:10.1212/WNL.60.3.415

Ardekani, S., Selva, L., Sayre, J., Sinha, U., 2006. Quantitative metrics for evaluating parallel acquisition techniques in diffusion tensor imaging at 3 Tesla. Invest. Radiol. 41, 806–14. doi:10.1097/01.rli.0000242859.75922.be

Arnold, S., Schlaug, G., Niemann, H., Ebner, A., Lüders, H., Witte, O.W., Seitz, R.J., 1996. Topography of interictal glucose hypometabolism in unilateral mesiotemporal epilepsy. Neurology 46, 1422–30. doi:10.1212/WNL.46.5.1422

Ashburner, J., Andersson, J.L.R., Fristen, K.J., 2000. Image registration using a symmetric prior - In three dimensions. Hum. Brain Mapp. 9, 212–225. doi:10.1002/(SICI)1097-0193(200004)9:4<212::AID-HBM3>3.0.CO;2-#

Avanzini, G., Manganotti, P., Meletti, S., Moshé, S.L., Panzica, F., Wolf, P., Capovilla, G., 2012. The system epilepsies: a pathophysiological hypothesis. Epilepsia 53, 771–8. doi:10.1111/j.1528-1167.2012.03462.x

Badawy, R. a B., Curatolo, J.M., Newton, M., Berkovic, S.F., Macdonell, R. a L., 2006. Sleep deprivation increases cortical excitability in epilepsy: syndrome-specific effects. Neurology 67, 1018–22. doi:10.1212/01.wnl.0000237392.64230.f7

Badawy, R. a B., Curatolo, J.M., Newton, M., Berkovic, S.F., Macdonell, R. a L., 2007. Changes in cortical excitability differentiate generalized and focal epilepsy. Ann. Neurol. 61, 324–31. doi:10.1002/ana.21087

Badawy, R. a B., Harvey, A.S., Macdonell, R. a L., 2009a. Cortical hyperexcitability and epileptogenesis: Mechanisms of epilepsy - 2. J. Clin. Neurosci. 16, 485–500. doi:10.1016/j.jocn.2008.10.001

Badawy, R. a B., Macdonell, R. a L., Jackson, G.D., Berkovic, S.F., 2009b. Why do seizures in generalized epilepsy often occur in the morning? Neurology 73, 218–22. doi:10.1212/WNL.0b013e3181ae7ca6

Badawy, R. a B., Macdonell, R. a L., Jackson, G.D., Berkovic, S.F., 2010. Can changes in cortical excitability distinguish progressive from juvenile myoclonic epilepsy? Epilepsia 51, 2084–8. doi:10.1111/j.1528-1167.2010.02557.x

Badawy, R.A.B., Vogrin, S.J., Lai, A., Cook, M.J., 2013. Capturing the epileptic trait: cortical excitability measures in patients and their unaffected siblings. Brain 136, 1177–91. doi:10.1093/brain/awt047

Bartolini, E., Pesaresi, I., Fabbri, S., Cecchi, P., Giorgi, F.S., Sartucci, F., Bonuccelli, U., Cosottini, M., 2014. Abnormal response to photic stimulation in Juvenile Myoclonic Epilepsy: An EEG-fMRI study. Epilepsia 55, 1038–47. doi:10.1111/epi.12634

Basser, P.J., Mattiello, J., LeBihan, D., 1994. MR diffusion tensor spectroscopy and imaging. Biophys. J. 66, 259–67. doi:10.1016/S0006-3495(94)80775-1

Basser, P.J., Pierpaoli, C., 1996. Microstructural and physiological features of tissues elucidated by quantitative-diffusion-tensor MRI. J. Magn. Reson. B 111, 209–19.

Baykan, B., Altindag, E.A., Bebek, N., Ozturk, A.Y., Aslantas, B., Gurses, C., Baral-Kulaksizoglu, I., Gokyigit, A., 2008. Myoclonic seizures subside in the fourth decade in juvenile myoclonic epilepsy. Neurology 70, 2123–2129. doi:10.1212/01.wnl.0000313148.34629.1d

Baykan, B., Martínez-Juárez, I.E., Altindag, E. a, Camfield, C.S., Camfield, P.R., 2013. Lifetime prognosis of juvenile myoclonic epilepsy. Epilepsy Behav. 28 Suppl 1, S18–24. doi:10.1016/j.yebeh.2012.06.036

Beckmann, C.F., Smith, S.M., 2004. Probabilistic independent component analysis for functional magnetic resonance imaging. IEEE Trans. Med. Imaging 23, 137–52. doi:10.1109/TMI.2003.822821

Behrens, T.E.J., Berg, H.J., Jbabdi, S., Rushworth, M.F.S., Woolrich, M.W., 2007. Probabilistic diffusion tractography with multiple fibre orientations: What can we gain? Neuroimage 34, 144–55. doi:10.1016/j.neuroimage.2006.09.018

Behrens, T.E.J., Woolrich, M.W., Jenkinson, M., Johansen-Berg, H., Nunes, R.G., Clare, S., Matthews, P.M., Brady, J.M., Smith, S.M., 2003. Characterization and propagation of uncertainty in diffusion-weighted MR imaging. Magn. Reson. Med. 50, 1077–88. doi:10.1002/mrm.10609

Berl, M.M., Zimmaro, L.A., Khan, O.I., Dustin, I., Ritzl, E., Duke, E.S., Sepeta, L.N., Sato, S., Theodore, W.H., Gaillard, W.D., 2014. Characterization of atypical

language activation patterns in focal epilepsy. Ann. Neurol. 75, 33–42. doi:10.1002/ana.24015

Bernasconi, A., Bernasconi, N., Bernhardt, B.C., Schrader, D., 2011. Advances in MRI for "cryptogenic" epilepsies. Nat. Rev. Neurol. 7, 99–108. doi:10.1038/nrneurol.2010.199

Bernhardt, B.C., Rozen, D. a., Worsley, K.J., Evans, A.C., Bernasconi, N., Bernasconi, A., 2009. Thalamo–cortical network pathology in idiopathic generalized epilepsy: Insights from MRI-based morphometric correlation analysis. Neuroimage 46, 373–381. doi:10.1016/j.neuroimage.2009.01.055

Betting, L.E., Mory, S.B., Li, L.M., Lopes-Cendes, I., Guerreiro, M.M., Guerreiro, C.A.M., Cendes, F., 2006. Voxel-based morphometry in patients with idiopathic generalized epilepsies. Neuroimage 32, 498–502. doi:10.1016/j.neuroimage.2006.04.174

Bettus, G., Guedj, E., Joyeux, F., Confort-Gouny, S., Soulier, E., Laguitton, V., Cozzone, P.J., Chauvel, P., Ranjeva, J.-P., Bartolomei, F., Guye, M., 2009. Decreased basal fMRI functional connectivity in epileptogenic networks and contralateral compensatory mechanisms. Hum. Brain Mapp. 30, 1580–91. doi:10.1002/hbm.20625

Bien, C.G., Raabe, A.L., Schramm, J., Becker, A., Urbach, H., Elger, C.E., 2013. Trends in presurgical evaluation and surgical treatment of epilepsy at one centre from 1988-2009. J. Neurol. Neurosurg. Psychiatry 84, 54–61. doi:10.1136/jnnp-2011-301763

Bien, C.G., Szinay, M., Wagner, J., Clusmann, H., Becker, A.J., Urbach, H., 2009. Characteristics and surgical outcomes of patients with refractory magnetic resonance imaging-negative epilepsies. Arch. Neurol. 66, 1491–9. doi:10.1001/archneurol.2009.283

Bisdas, S., Bohning, D.E., Besenski, N., Nicholas, J.S., Rumboldt, Z., 2008. Reproducibility, interrater agreement, and age-related changes of fractional anisotropy measures at 3T in healthy subjects: effect of the applied b-value. AJNR. Am. J. Neuroradiol. 29, 1128–33. doi:10.3174/ajnr.A1044

Biswal, B., Zerrin Yetkin, F., Haughton, V.M., Hyde, J.S., 1995. Functional connectivity in the motor cortex of resting human brain using echo-planar mri. Magn. Reson. Med. 34, 537–541. doi:10.1002/mrm.1910340409

Bonekamp, D., Nagae, L.M., Degaonkar, M., Matson, M., Abdalla, W.M. a, Barker, P.B., Mori, S., Horská, A., 2007. Diffusion tensor imaging in children and adolescents: reproducibility, hemispheric, and age-related differences. Neuroimage 34, 733–42. doi:10.1016/j.neuroimage.2006.09.020

Bonelli, S.B., Thompson, P.J., Yogarajah, M., Vollmar, C., Powell, R.H.W., Symms, M.R., McEvoy, A.W., Micallef, C., Koepp, M.J., Duncan, J.S., 2012. Imaging language networks before and after anterior temporal lobe resection: results of a

longitudinal fMRI study. Epilepsia 53, 639–50. doi:10.1111/j.1528-1167.2012.03433.x

Brown, P., Day, B.L., Rothwell, J.C., Thompson, P.D., Marsden, C.D., 1991. Intrahemispheric and interhemispheric spread of cerebral cortical myoclonic activity and its relevance to epilepsy. Brain 114 (Pt 5, 2333–51.

Broyd, S.J., Demanuele, C., Debener, S., Helps, S.K., James, C.J., Sonuga-Barke, E.J.S., 2009. Default-mode brain dysfunction in mental disorders: a systematic review. Neurosci. Biobehav. Rev. 33, 279–96. doi:10.1016/j.neubiorev.2008.09.002

Bush, G., 2010. Attention-deficit/hyperactivity disorder and attention networks. Neuropsychopharmacology 35, 278–300. doi:10.1038/npp.2009.120

Calhoun, V.D., Maciejewski, P.K., Pearlson, G.D., Kiehl, K. a, 2008. Temporal lobe and "default" hemodynamic brain modes discriminate between schizophrenia and bipolar disorder. Hum. Brain Mapp. 29, 1265–75. doi:10.1002/hbm.20463

Camfield, C.S., Camfield, P.R., 2009. Juvenile myoclonic epilepsy 25 years after seizure onset: a population-based study. Neurology 73, 1041–5. doi:10.1212/WNL.0b013e3181b9c86f

Cao, B., Tang, Y., Li, J., Zhang, X., Shang, H.-F., Zhou, D., 2013. A meta-analysis of voxel-based morphometry studies on gray matter volume alteration in juvenile myoclonic epilepsy. Epilepsy Res. 106, 370–7. doi:10.1016/j.eplepsyres.2013.07.003

Caramia, M.D., Gigli, G., Iani, C., Desiato, M.T., Diomedi, M., Palmieri, M.G., Bernardi, G., 1996. Distinguishing forms of generalized epilepsy using magnetic brain stimulation. Electroencephalogr. Clin. Neurophysiol. 98, 14–9. doi:10.1016/0013-4694(95)00150-6

Casey, B.J., Giedd, J.N., Thomas, K.M., 2000. Structural and functional brain development and its relation to cognitive development. Biol. Psychol. 54, 241–57. doi:S0301051100000582

Catarino, C.B., Vollmar, C., Noachtar, S., 2012. Paradoxical lateralization of non-invasive electroencephalographic ictal patterns in extra-temporal epilepsies. Epilepsy Res. 99, 147–55. doi:10.1016/j.eplepsyres.2011.11.002

Cercignani, M., Bammer, R., Sormani, M.P., Fazekas, F., Filippi, M., 2003. Inter-sequence and inter-imaging unit variability of diffusion tensor MR imaging histogram-derived metrics of the brain in healthy volunteers. AJNR. Am. J. Neuroradiol. 24, 638–43.

Chassoux, F., Landré, E., Mellerio, C., Turak, B., Mann, M.W., Daumas-Duport, C., Chiron, C., Devaux, B., 2012. Type II focal cortical dysplasia: electroclinical phenotype and surgical outcome related to imaging. Epilepsia 53, 349–58. doi:10.1111/j.1528-1167.2011.03363.x

Chouinard, P. a, Paus, T., 2006. The primary motor and premotor areas of the human cerebral cortex. Neurosci. 12, 143–52. doi:10.1177/1073858405284255

Chung, S., Courcot, B., Sdika, M., Moffat, K., Rae, C., Henry, R.G., 2010. Bootstrap quantification of cardiac pulsation artifact in DTI. Neuroimage 49, 631–40. doi:10.1016/j.neuroimage.2009.06.067

Ciccarelli, O., Parker, G.J.M., Toosy, A.T., Wheeler-Kingshott, C.A.M., Barker, G.J., Boulby, P.A., Miller, D.H., Thompson, A.J., 2003. From diffusion tractography to quantitative white matter tract measures: a reproducibility study. Neuroimage 18, 348–359. doi:10.1016/S1053-8119(02)00042-3

Ciumas, C., Wahlin, T.B.R., Jucaite, A., Lindstrom, P., Halldin, C., Savic, I., 2008. Reduced dopamine transporter binding in patients with juvenile myoclonic epilepsy. Neurology 71, 788–794. doi:10.1212/01.wnl.0000316120.70504.d5

Cook, P. a, Symms, M., Boulby, P. a, Alexander, D.C., 2007. Optimal acquisition orders of diffusion-weighted MRI measurements. J. Magn. Reson. imaging 25, 1051–8. doi:10.1002/jmri.20905

Cook, P.A., Bai, Y., Nedjati-Gilani, S., Seunarine, K.K., Hall, M.G., Parker, G.J., Alexander, D.C., 2006. Camino: Open-Source Diffusion-MRI Reconstruction and Processing, in: 14th Scientific Meeting of the International Society for Magnetic Resonance in Medicine. p. 2759.

Craiu, D., 2013. What is special about the adolescent (JME) brain? Epilepsy Behav. 28 Suppl 1, S45–51. doi:10.1016/j.yebeh.2012.12.008

Crespel, A., Gelisse, P., Reed, R.C., Ferlazzo, E., Jerney, J., Schmitz, B., Genton, P., 2013. Management of juvenile myoclonic epilepsy. Epilepsy Behav. 28 Suppl 1, S81–6. doi:10.1016/j.yebeh.2013.01.001

Da Silva Sousa, P., Lin, K., Garzon, E., Ceiki Sakamoto, A., Yacubian, E.M.T., 2005a. Language- and praxis-induced jerks in patients with juvenile myoclonic epilepsy. Epileptic Disord. 7, 115–21.

Da Silva Sousa, P., Lin, K., Garzon, E., Sakamoto, A.C., Yacubian, E.M.T., 2005b. Self-perception of factors that precipitate or inhibit seizures in juvenile myoclonic epilepsy. Seizure 14, 340–6. doi:10.1016/j.seizure.2005.04.007

David, O., Blauwblomme, T., Job, A.-S., Chabardès, S., Hoffmann, D., Minotti, L., Kahane, P., 2011. Imaging the seizure onset zone with stereo-electroencephalography. Brain 134, 2898–911. doi:10.1093/brain/awr238

De Araujo Filho, G.M., Yacubian, E.M.T., 2013. Juvenile myoclonic epilepsy: psychiatric comorbidity and impact on outcome. Epilepsy Behav. 28 Suppl 1, S74–80. doi:10.1016/j.yebeh.2013.03.026

De Nijs, L., Wolkoff, N., Coumans, B., Delgado-Escueta, A. V, Grisar, T., Lakaye, B., 2012. Mutations of EFHC1, linked to juvenile myoclonic epilepsy, disrupt radial

and tangential migrations during brain development. Hum. Mol. Genet. 21, 5106–17. doi:10.1093/hmg/dds356

De Tisi, J., Bell, G.S., Peacock, J.L., McEvoy, A.W., Harkness, W.F.J., Sander, J.W., Duncan, J.S., 2011. The long-term outcome of adult epilepsy surgery, patterns of seizure remission, and relapse: a cohort study. Lancet 378, 1388–95. doi:10.1016/S0140-6736(11)60890-8

Dejanovic, B., Lal, D., Catarino, C.B., Arjune, S., Belaidi, A.A., Trucks, H., Vollmar, C., Surges, R., Kunz, W.S., Motameny, S., Altmüller, J., Köhler, A., Neubauer, B.A., Epicure Consortium, Nürnberg, P., Noachtar, S., Schwarz, G., Sander, T., 2014. Exonic microdeletions of the gephyrin gene impair GABAergic synaptic inhibition in patients with idiopathic generalized epilepsy. Neurobiol. Dis. 67, 88–96. doi:10.1016/j.nbd.2014.02.001

Delgado-Escueta, A. V, 2007. Advances in genetics of juvenile myoclonic epilepsies. Epilepsy Curr. 7, 61–7. doi:10.1111/j.1535-7511.2007.00171.x

Delgado-Escueta, A. V, Enrile-Bacsal, F., 1984. Juvenile myoclonic epilepsy of Janz. Neurology 34, 285–94. doi:10.1212/WNL.34.3.285

Delgado-Escueta, A. V, Koeleman, B.P.C., Bailey, J.N., Medina, M.T., Durón, R.M., 2013. The quest for juvenile myoclonic epilepsy genes. Epilepsy Behav. 28 Suppl 1, S52–7. doi:10.1016/j.yebeh.2012.06.033

Deppe, M., Kellinghaus, C., Duning, T., Möddel, G., Mohammadi, S., Deppe, K., Schiffbauer, H., Kugel, H., Keller, S.S., Ringelstein, E.B., Knecht, S., 2008. Nerve fiber impairment of anterior thalamocortical circuitry in juvenile myoclonic epilepsy. Neurology 71, 1981–5. doi:10.1212/01.wnl.0000336969.98241.17

Devinsky, O., Gershengorn, J., Brown, E., Perrine, K., Vazquez, B., Luciano, D., 1997. Frontal functions in juvenile myoclonic epilepsy. Neuropsychiatry. Neuropsychol. Behav. Neurol. 10, 243–6.

Dodson, W.E., 2004. Definitions and Classification of Epilepsy, in: Shorvon, S.D., Fish, D.R., Perruca, E., Dodson, W.E. (Eds.), The Treatment of Epilepsy. Blackwell Science Ltd, Oxford, pp. 3–20.

Doose, H., Gerken, H., Kiefer, R., Völzke, E., 1977. Genetic factors in childhood epilepsy with focal sharp waves. II. EEG findings in patients and siblings. Neuropadiatrie 8, 10–20. doi:10.1055/s-0028-1091500

Engel, J., 2001. A Proposed Diagnostic Scheme for People with Epileptic Seizures and with Epilepsy: Report of the ILAE Task Force on Classification and Terminology. Epilepsia 42, 796–803. doi:10.1046/j.1528-1157.2001.10401.x

Engel, J., 2002. So what can we conclude--do seizures damage the brain? Prog. Brain Res. 135, 509–12. doi:10.1016/S0079-6123(02)35048-9

Fair, D.A., Dosenbach, N.U.F., Church, J.A., Cohen, A.L., Brahmbhatt, S., Miezin, F.M., Barch, D.M., Raichle, M.E., Petersen, S.E., Schlaggar, B.L., 2007.

Development of distinct control networks through segregation and integration. Proc. Natl. Acad. Sci. U. S. A. 104, 13507–12. doi:10.1073/pnas.0705843104

Filho, G.M. de A., Rosa, V.P., Lin, K., Caboclo, L.O.S.F., Sakamoto, A.C., Yacubian, E.M.T., 2008. Psychiatric comorbidity in epilepsy: a study comparing patients with mesial temporal sclerosis and juvenile myoclonic epilepsy. Epilepsy Behav. 13, 196–201. doi:10.1016/j.yebeh.2008.01.008

Fink, G.R., Frackowiak, R.S., Pietrzyk, U., Passingham, R.E., 1997. Multiple nonprimary motor areas in the human cortex. J. Neurophysiol. 77, 2164–74.

Focke, N.K., Yogarajah, M., Bonelli, S.B., Bartlett, P. a, Symms, M.R., Duncan, J.S., 2008. Voxel-based diffusion tensor imaging in patients with mesial temporal lobe epilepsy and hippocampal sclerosis. Neuroimage 40, 728–37. doi:10.1016/j.neuroimage.2007.12.031

Fransson, P., 2006. How default is the default mode of brain function? Further evidence from intrinsic BOLD signal fluctuations. Neuropsychologia 44, 2836–45. doi:10.1016/j.neuropsychologia.2006.06.017

Friston, K.J., 2005. Models of brain function in neuroimaging. Annu. Rev. Psychol. 56, 57–87. doi:10.1146/annurev.psych.56.091103.070311

Friston, K.J., Josephs, O., Zarahn, E., Holmes, A.P., Rouquette, S., Poline, J., 2000. To smooth or not to smooth? Bias and efficiency in fMRI time-series analysis. Neuroimage 12, 196–208. doi:10.1006/nimg.2000.0609

Gastaut, H., 1973. Dictionary of epilepsy. Geneva : World Health Organization.

Ge, Y., Law, M., Grossman, R.I., 2005. Applications of diffusion tensor MR imaging in multiple sclerosis. Ann. N. Y. Acad. Sci. 1064, 202–19. doi:10.1196/annals.1340.039

Gelisse, P., Genton, P., Raybaud, C., Thomas, P., Dravet, C., 2000. Structural brain lesions do not influence the prognosis of juvenile myoclonic epilepsy. Acta Neurol. Scand. 102, 188–91.

Gelisse, P., Genton, P., Thomas, P., Rey, M., Samuelian, J.C., Dravet, C., 2001. Clinical factors of drug resistance in juvenile myoclonic epilepsy. J. Neurol. Neurosurg. Psychiatry 70, 240–3.

Genton, P., Thomas, P., Kasteleijn-Nolst Trenité, D.G. a, Medina, M.T., Salas-Puig, J., 2013. Clinical aspects of juvenile myoclonic epilepsy. Epilepsy Behav. 28 Suppl 1, S8–14. doi:10.1016/j.yebeh.2012.10.034

Guaranha, M.S.B., da Silva Sousa, P., de Araújo-Filho, G.M., Lin, K., Guilhoto, L.M.F.F., Caboclo, L.O.S.F., Yacubian, E.M.T., 2009. Provocative and inhibitory effects of a video-EEG neuropsychologic protocol in juvenile myoclonic epilepsy. Epilepsia 50, 2446–55. doi:10.1111/j.1528-1167.2009.02126.x

Gui, M., Tamhane, A. a, Arfanakis, K., 2008. Contribution of cardiac-induced brain pulsation to the noise of the diffusion tensor in Turboprop diffusion tensor imaging (DTI). J. Magn. Reson. imaging 27, 1164–8. doi:10.1002/jmri.21335

Hader, W.J., Tellez-Zenteno, J., Metcalfe, A., Hernandez-Ronquillo, L., Wiebe, S., Kwon, C.-S., Jette, N., 2013. Complications of epilepsy surgery: a systematic review of focal surgical resections and invasive EEG monitoring. Epilepsia 54, 840–7. doi:10.1111/epi.12161

Hattingen, E., Lückerath, C., Pellikan, S., Vronski, D., Roth, C., Knake, S., Kieslich, M., Pilatus, U., 2014. Frontal and thalamic changes of GABA concentration indicate dysfunction of thalamofrontal networks in juvenile myoclonic epilepsy. Epilepsia 55, 1030–7. doi:10.1111/epi.12656

Heiervang, E., Behrens, T.E.J., Mackay, C.E., Robson, M.D., Johansen-Berg, H., 2006. Between session reproducibility and between subject variability of diffusion MR and tractography measures. Neuroimage 33, 867–77. doi:10.1016/j.neuroimage.2006.07.037

Helmstaedter, C., 2001. Behavioral Aspects of Frontal Lobe Epilepsy. Epilepsy Behav. 2, 384–395. doi:10.1006/ebeh.2001.0259

Hutchinson, E., Pulsipher, D., Dabbs, K., Myers y Gutierrez, A., Sheth, R., Jones, J., Seidenberg, M., Meyerand, E., Hermann, B., 2010. Children with new-onset epilepsy exhibit diffusion abnormalities in cerebral white matter in the absence of volumetric differences. Epilepsy Res. 88, 208–14. doi:10.1016/j.eplepsyres.2009.11.011

Inoue, Y., Seino, M., Kubota, H., Yamakaku, K., Tanaka, M., Yagi, K., 1994. Epilepsy with praxisinduced seizures, in: Wolf, P. (Ed.), Epileptic Seizures and Syndromes. John Libbey, London, p. 81—91.

Iqbal, N., Caswell, H.L., Hare, D.J., Pilkington, O., Mercer, S., Duncan, S., 2009. Neuropsychological profiles of patients with juvenile myoclonic epilepsy and their siblings: a preliminary controlled experimental video-EEG case series. Epilepsy Behav. 14, 516–21. doi:10.1016/j.yebeh.2008.12.025

Jack, C.R., Rydberg, C.H., Krecke, K.N., Trenerry, M.R., Parisi, J.E., Rydberg, J.N., Cascino, G.D., Riederer, S.J., 1996. Mesial temporal sclerosis: diagnosis with fluid-attenuated inversion-recovery versus spin-echo MR imaging. Radiology 199, 367–73. doi:10.1148/radiology.199.2.8668780

Jackson, J.H., 1873. On the anatomical, physiological and pathological investigation of epilepsies. West Rid. Lunatic Asylum Med Reports 3, 315–339.

Jäger, L., Werhahn, K.J., Hoffmann, A., Berthold, S., Scholz, V., Weber, J., Noachtar, S., Reiser, M., 2002. Focal epileptiform activity in the brain: detection with spike-related functional MR imaging--preliminary results. Radiology 223, 860–9. doi:10.1148/radiol.2233010360

Jallon, P., Latour, P., 2005. Epidemiology of idiopathic generalized epilepsies. Epilepsia 46 Suppl 9, 10–4. doi:10.1111/j.1528-1167.2005.00309.x

Jansen, J.F.A., Kooi, M.E., Kessels, A.G.H., Nicolay, K., Backes, W.H., 2007. Reproducibility of quantitative cerebral T2 relaxometry, diffusion tensor imaging, and 1H magnetic resonance spectroscopy at 3.0 Tesla. Invest. Radiol. 42, 327–37. doi:10.1097/01.rli.0000262757.10271.e5

Janz, D., 1985. Epilepsy with impulsive petit mal (juvenile myoclonic epilepsy). Acta Neurol. Scand. 72, 449–59.

Janz, D., Christian, W., 1957. Impulsive Petit mal. Dtsch Z Nervenheilk 176, 348–386.

Jeha, L.E., Najm, I., Bingaman, W., Dinner, D., Widdess-Walsh, P., Lüders, H., 2007. Surgical outcome and prognostic factors of frontal lobe epilepsy surgery. Brain 130, 574–84. doi:10.1093/brain/awl364

Jette, N., Wiebe, S., 2013. Update on the surgical treatment of epilepsy. Curr. Opin. Neurol. 26, 201–7. doi:10.1097/WCO.0b013e32835ef345

Johansen-Berg, H., Behrens, T.E.J., Robson, M.D., Drobnjak, I., Rushworth, M.F.S., Brady, J.M., Smith, S.M., Higham, D.J., Matthews, P.M., 2004. Changes in connectivity profiles define functionally distinct regions in human medial frontal cortex. Proc. Natl. Acad. Sci. U. S. A. 101, 13335–40. doi:10.1073/pnas.0403743101

Jones, D.K., 2004. The effect of gradient sampling schemes on measures derived from diffusion tensor MRI: a Monte Carlo study. Magn. Reson. Med. 51, 807–15. doi:10.1002/mrm.20033

Jones, D.K., 2014. Gaussian Modeling of the Diffusion Signal, in: Johansen-Berg, H., Behrens, T.E.J. (Eds.), Diffusion MRI. Elsevier, pp. 87–104. doi:10.1016/B978-0-12-396460-1.00005-6

Jones, D.K., Knösche, T.R., Turner, R., 2013. White matter integrity, fiber count, and other fallacies: the do's and don'ts of diffusion MRI. Neuroimage 73, 239–54. doi:10.1016/j.neuroimage.2012.06.081

Jones, D.K., Williams, S.C.R., Gasston, D., Horsfield, M.A., Simmons, A., Howard, R., 2002. Isotropic resolution diffusion tensor imaging with whole brain acquisition in a clinically acceptable time. Hum. Brain Mapp. 15, 216–30.

Kasteleijn-Nolst Trenité, D.G. a, de Weerd, A., Beniczky, S., 2013a. Chronodependency and provocative factors in juvenile myoclonic epilepsy. Epilepsy Behav. 28 Suppl 1, S25–9. doi:10.1016/j.yebeh.2012.11.045

Kasteleijn-Nolst Trenité, D.G. a, Schmitz, B., Janz, D., Delgado-Escueta, A. V, Thomas, P., Hirsch, E., Lerche, H., Camfield, C., Baykan, B., Feucht, M., Martínez-Juárez, I.E., Duron, R.M., Medina, M.T., Rubboli, G., Jerney, J., Hermann, B., Yacubian, E., Koutroumanidis, M., Stephani, U., Salas-Puig, J., Reed, R.C., Woermann, F., Wandschneider, B., Bureau, M., Gambardella, A.,

Koepp, M.J., Gelisse, P., Gurses, C., Crespel, A., Nguyen-Michel, V.H., Ferlazzo, E., Grisar, T., Helbig, I., Koeleman, B.P.C., Striano, P., Trimble, M., Buono, R., Cossette, P., Represa, A., Dravet, C., Serafini, A., Berglund, I.S.-, Sisodiya, S.M., Yamakawa, K., Genton, P., 2013b. Consensus on diagnosis and management of JME: From founder's observations to current trends. Epilepsy Behav. 28 Suppl 1, S87–90. doi:10.1016/j.yebeh.2012.11.051

Kim, J. Bin, Suh, S.-I., Seo, W.-K., Oh, K., Koh, S.-B., Kim, J.H., 2014. Altered thalamocortical functional connectivity in idiopathic generalized epilepsy. Epilepsia 55, 592–600. doi:10.1111/epi.12580

Kim, J.H., Lee, J.K.J.-M., Koh, S.-B., Lee, S.-A., Kim, S.I., Kang, J.K., 2007. Regional grey matter abnormalities in juvenile myoclonic epilepsy: a voxel-based morphometry study. Neuroimage 37, 1132–7. doi:10.1016/j.neuroimage.2007.06.025

Koepp, M.J., 2005. Juvenile myoclonic epilepsy--a generalized epilepsy syndrome? Acta Neurol. Scand. Suppl. 181, 57–62. doi:10.1111/j.1600-0404.2005.00511.x

Koepp, M.J., Woermann, F.G., 2005. Imaging structure and function in refractory focal epilepsy. Lancet Neurol. 4, 42–53. doi:10.1016/S1474-4422(04)00965-2

Kullmann, D.M., 2002. The neuronal channelopathies. Brain 125, 1177–1195. doi:10.1093/brain/awf130

Kuzniecky, R.I., Knowlton, R.C., 2002. Neuroimaging of epilepsy. Semin. Neurol. 22, 279–88. doi:10.1055/s-2002-36647

Labate, A., Ambrosio, R., Gambardella, A., Sturniolo, M., Pucci, F., Quattrone, A., 2007. Usefulness of a morning routine EEG recording in patients with juvenile myoclonic epilepsy. Epilepsy Res. 77, 17–21. doi:10.1016/j.eplepsyres.2007.07.010

Landman, B. a, Farrell, J. a D., Jones, C.K., Smith, S. a, Prince, J.L., Mori, S., 2007. Effects of diffusion weighting schemes on the reproducibility of DTI-derived fractional anisotropy, mean diffusivity, and principal eigenvector measurements at 1.5T. Neuroimage 36, 1123–38. doi:10.1016/j.neuroimage.2007.02.056

Landvogt, C., Buchholz, H.-G., Bernedo, V., Schreckenberger, M., Werhahn, K.J., 2010. Alteration of dopamine D2/D3 receptor binding in patients with juvenile myoclonic epilepsy. Epilepsia 51, 1699–706. doi:10.1111/j.1528-1167.2010.02569.x

Lee, J.J., Lee, S.-Y.S.K.S.-Y.S.K., Park, K.-I., Kim, D.W., Lee, D.S., Chung, C.K., Nam, H.W., 2008. Frontal lobe epilepsy: clinical characteristics, surgical outcomes and diagnostic modalities. Seizure 17, 514–23. doi:10.1016/j.seizure.2008.01.007

Lin, K., Carrete, H., Lin, J., Peruchi, M.M., de Araújo Filho, G.M., Guaranha, M.S.B., Guilhoto, L.M.F.F., Sakamoto, A.C., Yacubian, E.M.T., 2009a. Magnetic resonance spectroscopy reveals an epileptic network in juvenile myoclonic epilepsy. Epilepsia 50, 1191–200. doi:10.1111/j.1528-1167.2008.01948.x

Lin, K., Jackowski, A.P., Carrete, H., de Araújo Filho, G.M., Silva, H.H., Guaranha, M.S.B., Guilhoto, L.M.F.F., Bressan, R.A., Yacubian, E.M.T., 2009b. Voxel-based morphometry evaluation of patients with photosensitive juvenile myoclonic epilepsy. Epilepsy Res. 86, 138–45. doi:10.1016/j.eplepsyres.2009.05.016

Logothetis, N.K., 2008. What we can do and what we cannot do with fMRI. Nature 453, 869–78. doi:10.1038/nature06976

Lüders, H., Acharya, J., Baumgartner, C., Benbadis, S., Bleasel, A., Burgess, R., Dinner, D.S., Ebner, A., Foldvary, N., Geller, E., Hamer, H., Holthausen, H., Kotagal, P., Morris, H., Meencke, H.J., Noachtar, S., Rosenow, F., Sakamoto, A., Steinhoff, B.J., Tuxhorn, I., Wyllie, E., 1999. A new epileptic seizure classification based exclusively on ictal semiology. Acta Neurol. Scand. 99, 137–41.

MacDonald, B.K., Cockerell, O.C., Sander, J.W., Shorvon, S.D., 2000. The incidence and lifetime prevalence of neurological disorders in a prospective community-based study in the UK. Brain 123 (Pt 4, 665–76. doi:10.1093/brain/123.4.665

Manganotti, P., Bongiovanni, L.G., Fuggetta, G., Zanette, G., Fiaschi, a, 2006. Effects of sleep deprivation on cortical excitability in patients affected by juvenile myoclonic epilepsy: a combined transcranial magnetic stimulation and EEG study. J. Neurol. Neurosurg. Psychiatry 77, 56–60. doi:10.1136/jnnp.2004.041137

Manganotti, P., Bongiovanni, L.G., Zanette, G., Fiaschi, a, 2000. Early and late intracortical inhibition in juvenile myoclonic epilepsy. Epilepsia 41, 1129–38.

Manganotti, P., Tamburin, S., Bongiovanni, L.G., Zanette, G., Fiaschi, A., 2004. Motor responses to afferent stimulation in juvenile myoclonic epilepsy. Epilepsia 45, 77–80.

Martínez-Juárez, I.E., Alonso, M.E., Medina, M.T., Durón, R.M., Bailey, J.N., López-Ruiz, M., Ramos-Ramírez, R., León, L., Pineda, G., Castroviejo, I.P., Silva, R., Mija, L., Perez-Gosiengfiao, K., Machado-Salas, J., Delgado-Escueta, A. V, 2006. Juvenile myoclonic epilepsy subsyndromes: family studies and long-term follow-up. Brain 129, 1269–80. doi:10.1093/brain/awl048

Matsuoka, H., Nakamura, M., Ohno, T., Shimabukuro, J., Suzuki, T., Numachi, Y., Awata, S., 2005. The role of cognitive-motor function in precipitation and inhibition of epileptic seizures. Epilepsia 46 Suppl 1, 17–20. doi:10.1111/j.0013-9580.2005.461006.x

Matsuoka, H., Takahashi, T., Sasaki, M., Matsumoto, K., Yoshida, S., Numachi, Y., Saito, H., Ueno, T., Sato, M., 2000. Neuropsychological EEG activation in patients with epilepsy. Brain 123 (Pt 2, 318–30.

Matsuoka, H., Takahashi, T., Sasaki, M., Yoshida, S., Numachi, Y., Sato, M., 2002. The long-term course of seizure susceptibility in two patients with juvenile myoclonic epilepsy. Seizure 11, 126–30. doi:10.1053/seiz.2002.0591

Mayer, T. a, Schroeder, F., May, T.W., Wolf, P.T., 2006. Perioral reflex myoclonias: a controlled study in patients with JME and focal epilepsies. Epilepsia 47, 1059–67. doi:10.1111/j.1528-1167.2006.00575.x

McDonald, C.R., Delis, D.C., Norman, M. a, Wetter, S.R., Tecoma, E.S., Iragui, V.J., 2005. Response inhibition and set shifting in patients with frontal lobe epilepsy or temporal lobe epilepsy. Epilepsy Behav. 7, 438–46. doi:10.1016/j.yebeh.2005.05.005

McDonald, C.R., Swartz, B.E., Halgren, E., Patell, A., Daimes, R., Mandelkern, M., 2006. The relationship of regional frontal hypometabolism to executive function: a resting fluorodeoxyglucose PET study of patients with epilepsy and healthy controls. Epilepsy Behav. 9, 58–67. doi:10.1016/j.yebeh.2006.04.007

Meencke, H.J., Janz, D., 1984. Neuropathological findings in primary generalized epilepsy: a study of eight cases. Epilepsia 25, 8–21.

Meschaks, A., Lindstrom, P., Halldin, C., Farde, L., Savic, I., 2005. Regional reductions in serotonin 1A receptor binding in juvenile myoclonic epilepsy. Arch. Neurol. 62, 946–50. doi:10.1001/archneur.62.6.946

Moeller, F., Siebner, H.R., Ahlgrimm, N., Wolff, S., Muhle, H., Granert, O., Boor, R., Jansen, O., Gotman, J., Stephani, U., Siniatchkin, M., 2009. fMRI activation during spike and wave discharges evoked by photic stimulation. Neuroimage 48, 682–95. doi:10.1016/j.neuroimage.2009.07.019

Mory, S.B., Betting, L.E., Fernandes, P.T., Lopes-Cendes, I., Guerreiro, M.M., Guerreiro, C. a M., Cendes, F., Li, L.M., 2011. Structural abnormalities of the thalamus in juvenile myoclonic epilepsy. Epilepsy Behav. 21, 407–11. doi:10.1016/j.yebeh.2011.05.018

Mory, S.B., Li, L.M., Guerreiro, C.A.M., Cendes, F., 2003. Thalamic dysfunction in juvenile myoclonic epilepsy: a proton MRS study. Epilepsia 44, 1402–5. doi:10.1046/j.1528-1157.2003.67702.x

Nagy, Z., Weiskopf, N., Alexander, D.C., Deichmann, R., 2007. A method for improving the performance of gradient systems for diffusion-weighted MRI. Magn. Reson. Med. 58, 763–8. doi:10.1002/mrm.21379

Ni, H., Kavcic, V., Zhu, T., Ekholm, S., Zhong, J., 2006. Effects of number of diffusion gradient directions on derived diffusion tensor imaging indices in human brain. AJNR. Am. J. Neuroradiol. 27, 1776–81. doi:27/8/1776 [pii]

Noachtar, S., Arnold, S., Yousry, T.A., Bartenstein, P., Werhahn, K.J., Tatsch, K., 1998. Ictal technetium-99m ethyl cysteinate dimer single-photon emission tomographic findings and propagation of epileptic seizure activity in patients with extratemporal epilepsies. Eur. J. Nucl. Med. Mol. Imaging 25, 166–172. doi:10.1007/s002590050210

O'Dwyer, R., Silva Cunha, J.P., Vollmar, C., Mauerer, C., Feddersen, B., Burgess, R.C., Ebner, A., Noachtar, S., 2007. Lateralizing significance of quantitative

analysis of head movements before secondary generalization of seizures of patients with temporal lobe epilepsy. Epilepsia 48, 524–30. doi:10.1111/j.1528-1167.2006.00967.x

O'Muircheartaigh, J., Vollmar, C., Barker, G.J., Kumari, V., Symms, M.R., Thompson, P., Duncan, J.S., Koepp, M.J., Richardson, M.P., 2011. Focal structural changes and cognitive dysfunction in juvenile myoclonic epilepsy. Neurology 76, 34–40. doi:10.1212/WNL.0b013e318203e93d

O'Muircheartaigh, J., Vollmar, C., Barker, G.J., Kumari, V., Symms, M.R., Thompson, P., Duncan, J.S., Koepp, M.J., Richardson, M.P., 2012. Abnormal thalamocortical structural and functional connectivity in juvenile myoclonic epilepsy. Brain 135, 3635–44. doi:10.1093/brain/aws296

Ottman, R., Annegers, J.F., Risch, N., Hauser, W.A., Susser, M., 1996. Relations of genetic and environmental factors in the etiology of epilepsy. Ann. Neurol. 39, 442–9. doi:10.1002/ana.410390406

Panayiotopoulos, C.P., 2007. The significance of the syndromic diagnosis of the epilepsies, in: Sander, J.W., Walker, M.C., Smalls, J.E. (Eds.), Epilepsy 2007 - From Cell to Community. International League Against Epilepsy, Uk Chapter, pp. 105–110.

Panayiotopoulos, C.P., Obeid, T., Tahan, A.R., 1994. Juvenile myoclonic epilepsy: a 5-year prospective study. Epilepsia 35, 285–96.

Panayiotopoulos, C.P., Tahan, R., Obeid, T., 1991. Juvenile myoclonic epilepsy: factors of error involved in the diagnosis and treatment. Epilepsia 32, 672–6.

Panzica, F., Rubboli, G., Franceschetti, S., Avanzini, G., Meletti, S., Pozzi, A., Tassinari, C. a, 2001. Cortical myoclonus in Janz syndrome. Clin. Neurophysiol. 112, 1803–9.

Papadakis, N.G., Xing, D., Huang, C.L., Hall, L.D., Carpenter, T. a, 1999. A comparative study of acquisition schemes for diffusion tensor imaging using MRI. J. Magn. Reson. 137, 67–82. doi:10.1006/jmre.1998.1673

Papanicolaou, a C., Loring, D.W., Deutsch, G., Eisenberg, H.M., 1986. Task-related EEG asymmetries: a comparison of alpha blocking and beta enhancement. Int. J. Neurosci. 30, 81–5.

Pascalicchio, T.F., de Araujo Filho, G.M., da Silva Noffs, M.H., Lin, K., Caboclo, L.O.S.F., Vidal-Dourado, M., Ferreira Guilhoto, L.M.F., Yacubian, E.M.T., 2007. Neuropsychological profile of patients with juvenile myoclonic epilepsy: a controlled study of 50 patients. Epilepsy Behav. 10, 263–7. doi:10.1016/j.yebeh.2006.11.012

Pfefferbaum, A., Adalsteinsson, E., Sullivan, E. V, 2003. Replicability of diffusion tensor imaging measurements of fractional anisotropy and trace in brain. J. Magn. Reson. imaging 18, 427–33. doi:10.1002/jmri.10377

Piazzini, A., Turner, K., Vignoli, A., Canger, R., Canevini, M.P., 2008. Frontal cognitive dysfunction in juvenile myoclonic epilepsy. Epilepsia 49, 657–62. doi:10.1111/j.1528-1167.2007.01482.x

Pierpaoli, C., Jezzard, P., Basser, P.J., Barnett, A.S., Di Chiro, G., 1996. Diffusion tensor MR imaging of the human brain. Radiology 201, 637–648. doi:10.1148/radiology.201.3.8939209

Pondal-Sordo, M., Diosy, D., Téllez-Zenteno, J.F., Sahjpaul, R., Wiebe, S., 2007. Usefulness of intracranial EEG in the decision process for epilepsy surgery. Epilepsy Res. 74, 176–82. doi:10.1016/j.eplepsyres.2007.03.011

Powell, H.W.R., Guye, M., Parker, G.J.M., Symms, M.R., Boulby, P., Koepp, M.J., Barker, G.J., Duncan, J.S., 2004. Noninvasive in vivo demonstration of the connections of the human parahippocampal gyrus. Neuroimage 22, 740–7. doi:10.1016/j.neuroimage.2004.01.011

Pulsipher, D.T., Seidenberg, M., Guidotti, L., Tuchscherer, V.N., Morton, J., Sheth, R.D., Hermann, B., 2009. Thalamofrontal circuitry and executive dysfunction in recent-onset juvenile myoclonic epilepsy. Epilepsia 50, 1210–9. doi:10.1111/j.1528-1167.2008.01952.x

Rémi, J., Vollmar, C., de Marinis, A., Heinlin, J., Peraud, A., Noachtar, S., 2011. Congruence and discrepancy of interictal and ictal EEG with MRI lesions in focal epilepsies. Neurology 77, 1383–90. doi:10.1212/WNL.0b013e31823152c3

Risse, G.L., 2006. Cognitive outcomes in patients with frontal lobe epilepsy. Epilepsia 47 Suppl 2, 87–9. doi:10.1111/j.1528-1167.2006.00699.x

Riva, D., Avanzini, G., Franceschetti, S., Nichelli, F., Saletti, V., Vago, C., Pantaleoni, C., D'Arrigo, S., Andreucci, E., Aggio, F., Paruta, N., Bulgheroni, S., 2005. Unilateral frontal lobe epilepsy affects executive functions in children. Neurol. Sci. 26, 263–70. doi:10.1007/s10072-005-0469-7

Robinson, R.A., Gardiner, R.M., Johnson, M., 2009. Molecular genetics of the epilepsies, in: Sander, J.W., Rugg-Gunn, F.J., Smalls, J.E. (Eds.), Epilepsy 2009 International League Against Epilepsy, Uk Chapter.

Rodin, E., Ancheta, O., 1987. Cerebral electrical fields during petit mal absences. Electroencephalogr. Clin. Neurophysiol. 66, 457–66.

Roebling, R., Scheerer, N., Uttner, I., Gruber, O., Kraft, E., Lerche, H., 2009. Evaluation of cognition, structural, and functional MRI in juvenile myoclonic epilepsy. Epilepsia 50, 2456–65. doi:10.1111/j.1528-1167.2009.02127.x

Rorden, C., Brett, M., 2000. Stereotaxic display of brain lesions. Behav. Neurol. 12, 191–200.

Saini, J., Sinha, S., Bagepally, B.S., Ramchandraiah, C.T., Thennarasu, K., Prasad, C., Taly, a B., Satishchandra, P., 2013. Subcortical structural abnormalities in juvenile

myoclonic epilepsy (JME): MR volumetry and vertex based analysis. Seizure 22, 230–5. doi:10.1016/j.seizure.2013.01.001

Salek-Haddadi, A., Mayer, T., Hamandi, K., Symms, M., Josephs, O., Fluegel, D., Woermann, F., Richardson, M.P., Noppeney, U., Wolf, P., Koepp, M.J., 2009. Imaging seizure activity: a combined EEG/EMG-fMRI study in reading epilepsy. Epilepsia 50, 256–64. doi:10.1111/j.1528-1167.2008.01737.x

Sander, J.W., 2007. The incidence and prevalence of epilepsy, in: Sander, J.W., Walker, M.C., Smalls, J.E. (Eds.), Epilepsy 2007 - From Cell to Community. International League Against Epilepsy, Uk Chapter, pp. 1–6.

Sander, J.W., Hart, Y.M., Johnson, A.L., Shorvon, S.D., 1990. National General Practice Study of Epilepsy: newly diagnosed epileptic seizures in a general population. Lancet 336, 1267–71.

Sander, J.W., Shorvon, S.D., 1996. Epidemiology of the epilepsies. J. Neurol. Neurosurg. Psychiatry 61, 433–43.

Schankin, C.J., Rémi, J., Klaus, I., Sostak, P., Reinisch, V.M., Noachtar, S., Straube, A., 2011. Headache in juvenile myoclonic epilepsy. J. Headache Pain 12, 227–233. doi:10.1007/s10194-011-0332-6

Schneider-von Podewils, F., Gasse, C., Geithner, J., Wang, Z.I., Bombach, P., Berneiser, J., Herzer, R., Kessler, C., Runge, U., 2014. Clinical predictors of the long-term social outcome and quality of life in juvenile myoclonic epilepsy: 20-65 years of follow-up. Epilepsia 55, 322–30. doi:10.1111/epi.12491

Seneviratne, U., Cook, M., D'Souza, W., 2014. Focal abnormalities in idiopathic generalized epilepsy: A critical review of the literature. Epilepsia 55, 1157–69. doi:10.1111/epi.12688

Serafini, A., Rubboli, G., Gigli, G.L., Koutroumanidis, M., Gelisse, P., 2013. Neurophysiology of juvenile myoclonic epilepsy. Epilepsy Behav. 28 Suppl 1, S30–9. doi:10.1016/j.yebeh.2012.11.042

Simasathien, T., Vadera, S., Najm, I., Gupta, A., Bingaman, W., Jehi, L., 2013. Improved outcomes with earlier surgery for intractable frontal lobe epilepsy. Ann. Neurol. 73, 646–54. doi:10.1002/ana.23862

Simister, R.J., McLean, M.A., Barker, G.J., Duncan, J.S., 2003. Proton MRS reveals frontal lobe metabolite abnormalities in idiopathic generalized epilepsy., Neurology. doi:10.1212/01.WNL.0000086903.69738.DC

Skare, S., Andersson, J.L., 2001. On the effects of gating in diffusion imaging of the brain using single shot EPI. Magn. Reson. Imaging 19, 1125–8.

Smith, S.M., 2002. Fast robust automated brain extraction. Hum. Brain Mapp. 17, 143–55. doi:10.1002/hbm.10062

So, E.L., Lee, R.W., 2014. Epilepsy surgery in MRI-negative epilepsies. Curr. Opin. Neurol. 27, 206–12. doi:10.1097/WCO.0000000000000078

Sonmez, F., Atakli, D., Sari, H., Atay, T., Arpaci, B., 2004. Cognitive function in juvenile myoclonic epilepsy. Epilepsy Behav. 5, 329–36. doi:10.1016/j.yebeh.2004.01.007

Sonuga-Barke, E.J.S., Castellanos, F.X., 2007. Spontaneous attentional fluctuations in impaired states and pathological conditions: a neurobiological hypothesis. Neurosci. Biobehav. Rev. 31, 977–86. doi:10.1016/j.neubiorev.2007.02.005

Stefan, H., Hummel, C., Scheler, G., Genow, A., Druschky, K., Tilz, C., Kaltenhäuser, M., Hopfengärtner, R., Buchfelder, M., Romstöck, J., 2003. Magnetic brain source imaging of focal epileptic activity: a synopsis of 455 cases. Brain 126, 2396–405. doi:10.1093/brain/awg239

Sullivan, E. V, Pfefferbaum, A., 2006. Diffusion tensor imaging and aging. Neurosci. Biobehav. Rev. 30, 749–61. doi:10.1016/j.neubiorev.2006.06.002

Swartz, B.E., Simpkins, F., Halgren, E., Mandelkern, M., Brown, C., Krisdakumtorn, T., Gee, M., 1996. Visual working memory in primary generalized epilepsy: an 18FDG-PET study. Neurology 47, 1203–12.

Szaflarski, J.P., Kay, B., Gotman, J., Privitera, M.D., Holland, S.K., 2013. The relationship between the localization of the generalized spike and wave discharge generators and the response to valproate. Epilepsia 54, 471–80. doi:10.1111/epi.12062

Tae, W.S., Hong, S.B., Joo, E.Y., Han, S.J., Cho, J.-W., Seo, D.W., Lee, J.-M., Kim, I.Y., Byun, H.S., Kim, S.I., 2006. Structural Brain Abnormalities in Juvenile Myoclonic Epilepsy Patients: Volumetry and Voxel-Based Morphometry. Korean J. Radiol. 7, 162. doi:10.3348/kjr.2006.7.3.162

Tau, G.Z., Peterson, B.S., 2010. Normal development of brain circuits. Neuropsychopharmacology 35, 147–68. doi:10.1038/npp.2009.115

Thomas, R.H., Walsh, J., Church, C., Marson, A.G., Baker, G.A., Rees, M.I., 2014. A comprehensive neuropsychological description of cognition in drug-refractory juvenile myoclonic epilepsy. Epilepsy Behav. 36, 124–129. doi:10.1016/j.yebeh.2014.04.027

Trebuchon, A., Bartolomei, F., McGonigal, A., Laguitton, V., Chauvel, P., 2013. Reversible antisocial behavior in ventromedial prefrontal lobe epilepsy. Epilepsy Behav. 29, 367–73. doi:10.1016/j.yebeh.2013.08.007

Trinka, E., Kienpointner, G., Unterberger, I., Luef, G., Bauer, G., Doering, L.B., Doering, S., 2006. Psychiatric comorbidity in juvenile myoclonic epilepsy. Epilepsia 47, 2086–91. doi:10.1111/j.1528-1167.2006.00828.x

Upton, D., Thompson, P.J., 1997. Age at onset and neuropsychological function in frontal lobe epilepsy. Epilepsia 38, 1103–13.

Van Buren, J.M., 1987. Complications of surgical precedures in the diagnosis and treatment of epilepsy, in: Engel, J.J. (Ed.), Surgical Treatment of the Epilepsies. Raven Press, New York, pp. 465–475.

Vingerhoets, G., Deblaere, K., Backes, W.H., Achten, E., Boon, P., Boon, P.J., Hofman, P., Vermeulen, J., Vonck, K., Wilmink, J., Aldenkamp, A.P., 2004. Lessons for neuropsychology from functional MRI in patients with epilepsy. Epilepsy Behav. 5 Suppl 1, S81–9. doi:10.1016/j.yebeh.2003.11.011

Vollmar, C., O'Muircheartaigh, J., Barker, G.J., Symms, M.R., Thompson, P., Kumari, V., Duncan, J.S., Janz, D., Richardson, M.P., Koepp, M.J., 2011. Motor system hyperconnectivity in juvenile myoclonic epilepsy: a cognitive functional magnetic resonance imaging study. Brain 134, 1710–9. doi:10.1093/brain/awr098

Vollmar, C., O'Muircheartaigh, J., Barker, G.J., Symms, M.R., Thompson, P., Kumari, V., Duncan, J.S., Richardson, M.P., Koepp, M.J., 2010. Identical, but not the same: intra-site and inter-site reproducibility of fractional anisotropy measures on two 3.0T scanners. Neuroimage 51, 1384–94. doi:10.1016/j.neuroimage.2010.03.046

Vollmar, C., O'Muircheartaigh, J., Symms, M.R., Barker, G.J., Thompson, P., Kumari, V., Stretton, J., Duncan, J.S., Richardson, M.P., Koepp, M.J., 2012. Altered microstructural connectivity in juvenile myoclonic epilepsy: the missing link. Neurology 78, 1555–9. doi:10.1212/WNL.0b013e3182563b44

Von Oertzen, J., Urbach, H., Jungbluth, S., Kurthen, M., Reuber, M., Fernández, G., Elger, C.E., 2002. Standard magnetic resonance imaging is inadequate for patients with refractory focal epilepsy. J. Neurol. Neurosurg. Psychiatry 73, 643–7. doi:10.1136/jnnp.73.6.643

Voon, V., Brezing, C., Gallea, C., Ameli, R., Roelofs, K., LaFrance, W.C., Hallett, M., 2010. Emotional stimuli and motor conversion disorder. Brain 133, 1526–36. doi:10.1093/brain/awq054

Vulliemoz, S., Vollmar, C., Koepp, M.J., Yogarajah, M., O'Muircheartaigh, J., Carmichael, D.W., Stretton, J., Richardson, M.P., Symms, M.R., Duncan, J.S., 2011. Connectivity of the supplementary motor area in juvenile myoclonic epilepsy and frontal lobe epilepsy. Epilepsia 52, 507–14. doi:10.1111/j.1528-1167.2010.02770.x

Wandschneider, B., Centeno, M., Vollmar, C., Stretton, J., O'Muircheartaigh, J., Thompson, P.J., Kumari, V., Symms, M., Barker, G.J., Duncan, J.S., Richardson, M.P., Koepp, M.J., 2013. Risk-taking behavior in juvenile myoclonic epilepsy. Epilepsia 54, 2158–65. doi:10.1111/epi.12413

Wandschneider, B., Centeno, M., Vollmar, C., Symms, M., Thompson, P.J., Duncan, J.S., Koepp, M.J., 2014. Motor co-activation in siblings of patients with juvenile myoclonic epilepsy: an imaging endophenotype? Brain 1–11. doi:10.1093/brain/awu175

Wandschneider, B., Kopp, U. a, Kliegel, M., Stephani, U., Kurlemann, G., Janz, D., Schmitz, B., 2010. Prospective memory in patients with juvenile myoclonic

epilepsy and their healthy siblings. Neurology 75, 2161–7. doi:10.1212/WNL.0b013e318202010a

Wang, Z.I., Alexopoulos, A. V, Jones, S.E., Jaisani, Z., Najm, I.M., Prayson, R. a, 2013. The pathology of magnetic-resonance-imaging-negative epilepsy. Mod. Pathol. 26, 1051–8. doi:10.1038/modpathol.2013.52

Wheeler-Kingshott, C.A.M., Hickman, S.J., Parker, G.J.M., Ciccarelli, O., Symms, M.R., Miller, D.H., Barker, G.J., 2002. Investigating cervical spinal cord structure using axial diffusion tensor imaging. Neuroimage 16, 93–102. doi:10.1006/nimg.2001.1022

Whitfield-Gabrieli, S., Thermenos, H.W., Milanovic, S., Tsuang, M.T., Faraone, S. V, McCarley, R.W., Shenton, M.E., Green, A.I., Nieto-Castanon, A., LaViolette, P., Wojcik, J., Gabrieli, J.D.E., Seidman, L.J., 2009. Hyperactivity and hyperconnectivity of the default network in schizophrenia and in first-degree relatives of persons with schizophrenia. Proc. Natl. Acad. Sci. U. S. A. 106, 1279–84. doi:10.1073/pnas.0809141106

Wiebe, S., Blume, W.T., Girvin, J.P., Eliasziw, M., 2001. A randomized, controlled trial of surgery for temporal-lobe epilepsy. N. Engl. J. Med. 345, 311–8. doi:10.1056/NEJM200108023450501

Wieshmann, U.C., 2003. Clinical application of neuroimaging in epilepsy. J. Neurol. Neurosurg. Psychiatry 74, 466–70. doi:10.1136/jnnp.74.4.466

Wieshmann, U.C., Barker, G.J., Symms, M.R., Bartlett, P.A., Stevens, J.M., Shorvon, S.D., 1998. Fast fluid-attenuated inversion-recovery imaging: first experience with a 3D version in epilepsy. Neuroradiology 40, 483–489. doi:10.1007/s002340050630

Winston, G.P., Yogarajah, M., Symms, M.R., McEvoy, A.W., Micallef, C., Duncan, J.S., 2011. Diffusion tensor imaging tractography to visualize the relationship of the optic radiation to epileptogenic lesions prior to neurosurgery. Epilepsia 52, 1430–8. doi:10.1111/j.1528-1167.2011.03088.x

Woermann, F.G., Free, S.L., Koepp, M.J., Ashburner, J., Duncan, J.S., 1999a. Voxel-by-voxel comparison of automatically segmented cerebral gray matter--A rater-independent comparison of structural MRI in patients with epilepsy. Neuroimage 10, 373–84. doi:10.1006/nimg.1999.0481

Woermann, F.G., Free, S.L., Koepp, M.J., Sisodiya, S.M., Duncan, J.S., 1999b. Abnormal cerebral structure in juvenile myoclonic epilepsy demonstrated with voxel-based analysis of MRI. Brain 122 (Pt 1, 2101–8.

Woermann, F.G., Vollmar, C., 2009. Clinical MRI in children and adults with focal epilepsy: a critical review. Epilepsy Behav. 15, 40–9. doi:10.1016/j.yebeh.2009.02.032

Yacubian, E.M., Wolf, P., 2014. Praxis induction. Definition, relation to epilepsy syndromes, nosological and prognostic significance. A focused review. Seizure 23, 247–251. doi:10.1016/j.seizure.2014.01.011

Yogarajah, M., Focke, N.K., Bonelli, S.B., Thompson, P., Vollmar, C., McEvoy, A.W., Alexander, D.C., Symms, M.R., Koepp, M.J., Duncan, J.S., 2010. The structural plasticity of white matter networks following anterior temporal lobe resection. Brain 133, 2348–64. doi:10.1093/brain/awq175

Zhang, Z., Lu, G., Zhong, Y., Tan, Q., Yang, Z., Liao, W., Chen, Z., Shi, J., Liu, Y., 2009. Impaired attention network in temporal lobe epilepsy: a resting FMRI study. Neurosci. Lett. 458, 97–101. doi:10.1016/j.neulet.2009.04.040

Zilles, K., Schlaug, G., Matelli, M., Luppino, G., Schleicher, a, Qü, M., Dabringhaus, a, Seitz, R., Roland, P.E., 1995. Mapping of human and macaque sensorimotor areas by integrating architectonic, transmitter receptor, MRI and PET data. J. Anat. 187 (Pt 3, 515–37.